Synthesis of Novel PB-*b*-PS-*b*-PEO and PE-*b*-PS-*b*-PEO Triblock Terpolymers, their Morphological Characterization and Crystallization Kinetics of the Corresponding Crystallizable Blocks

Dissertation

zur Erlangung des akademischen Grades
Doktor der Naturwissenschaften
(Dr. rer. nat.)
der Technischen Fakultät
der Christian-Albrechts-Universität zu Kiel

Adriana Boschetti-de-Fierro

Kiel

2007

1. Gutachter   Prof. Dr. Volker Abetz

2. Gutachter   Prof. Dr. Franz Faupel

3. Gutachter   Prof. Dr. Stephan Förster

Datum der mündlichen Prüfung 28.06.07

Table of Contents

List of Tables

List of Figures

Chapter 1. Introduction

Block copolymers are macromolecules that consist of at least two polymers with different properties. These polymers are covalently linked, and the block copolymer properties combine the individual properties of the different blocks. In this way, it is possible to design materials with given or desirable properties. Equally interesting is the self-assembly ability presented by block copolymers. Since the combined blocks have different properties, they are usually immiscible, but the macrophase separation is prevented by the covalent bond. Therefore, the blocks separate into microphases (or microdomains), which dimensions are usually in the nanometer range, and the overall sample presents, in the best case, long-range order of these microdomains in crystal-like lattices.

The self-assembly ability and the tailor-made-properties capability have made block copolymers very interesting for diverse applications, such as drug delivery, nanopatterning, nanolithography and templates, among others. Since the applications are based on the microphase morphology (microstructure), a lot of investigative efforts have been oriented to understand the process of morphology generation, the variables that affect the generated microstructure, and the possibility to control it, among others.

One factor that is known to affect the microphase separation is polymer crystallization. The crystallinity in polymers is an attractive property, since it gives very good mechanical properties to the material below the crystallization temperature, and allows processing above the melting temperature. Therefore, block copolymers with crystallizable blocks are of special interest. However, crystallization is known to compete with microphase separation during the morphology generation process. In that way, a crystallizable block in a block copolymer can break-out from the previously generated morphology, template the morphology generation or crystallize in a confined manner inside the preformed microdomain.

Confined crystallization is particularly appealing, since the microdomain dimensions are comparable to the polymer crystal thickness, and the nucleation and diffusion steps of the crystallization process are influenced by this restriction in space. The development of crystallization studies where the process is somehow controlled is very relevant, mainly because polymer crystallization so far is only a mildly understood process. The continuous advances in experimental techniques have allowed detailed studies, for instance in the early stages of crystallization, which results cannot be fully explained by the polymer crystallization theory proposed by Lauritzen and Hoffman in the 1960s. Also, the improvements in simulation packages have allowed very detailed computer simulations of the crystallization process, and those results are also not completely described by the LH model. This has generated the proposal of new polymer crystallization theories (i.e., the multistage model proposed by Strobl) and the corresponding debate in the polymer crystallization community.

Polymer crystallization in block copolymers has attracted attention starting from 1990s with works from the groups of R.E. Cohen (MIT, Boston), R.A. Register (Princeton University), and A.J. Ryan (University of Sheffield). Latter, the groups of L. Zhu (The University of Connecticut, Storrs-Mansfield), W.J. de Jeu (FOM-Institute AMOLF, Amsterdam), I.W. Hamley (then at University of Leeds), G. Reiter (Institut de Chimie des Surfaces et Interfaces, Mulhouse) and A.J. Müller (Universidad Simón Bolívar, Caracas) have joint to the research in the area.

The crystallization kinetics of a crystallizable block in a block copolymer has been found to be affected by manifold variables, besides those well known for homopolymers such as molecular weight. Most of the published works have dealt with crystallization of one block in diblock copolymers (weakly and strongly segregated systems) and studied the competition between microphase separation and polymer crystallization. Break-out,

2

template and confined crystallization have been identified, and the latter has been studied under soft- and hard-confinement (according to the physical state of the amorphous second block, which is either rubbery or glassy). Besides the system itself that describes the segregation strength and the confinement type if any, the second most important variable that has been identified to affect the crystallization kinetics is the morphology. Whether the crystallization takes place within spheres, cylinders, gyroids or lamellae as well as the connectivity between those microphases have been topics of the mentioned works. The studies of block copolymers with two crystallizable blocks are fewer and the effect of the block with highest crystallization temperature on the crystallization kinetics of the block with lowest crystallization temperature is still not completely known.

A systematic study of confined crystallization starts with the selection of the system, which should be formed by polymers that produce a strongly segregated system. Since the possibility of variations in the composition is desirable for the analysis of the effect of morphology on the crystallization kinetics, the synthesis with a well-controlled technique such as anionic polymerization is a great advantage. Once the appropriate system has been chosen and diverse compositions are available, the required bulk morphology characterization is conventionally carried out by transmission electron microscopy (TEM) or small angle X-ray scattering (SAXS), and could be supplemented by thin film characterization conducted by atomic force microscopy (AFM). Thermal properties could be determined by differential scanning calorimetry (DSC) and the competition between microphase separation and crystallization can be analyzed by the results of the afore-mentioned methods. Crystallization kinetics can be then followed by different techniques, among which DSC, SAXS and wide angle X-ray diffraction (WAXD) are the most common.

It is the motivation of this doctoral work to contribute to the understanding of polymer crystallization by analyzing the crystallization kinetics in confined microphases, as well as to gain insight into the competition process of morphology generation in block copolymers with crystallizable blocks. The strategy employed is to synthesize tailor-made triblock terpolymers with up to two crystallizable blocks, characterize their morphological properties and analyze the crystallization kinetics in systems where the domains of the crystallizable blocks are under hard-confinement (i.e., being neighbored by a glassy block). The main questions around this proposal are: How is the interplay between two crystallization processes and microphase separation in triblock terpolymers? Is it possible to find confined crystallization for the two crystallizable blocks simultaneously? How and when are the crystallization processes independent? If the crystallizable blocks are the end blocks, a rubbery middle block might "pass" information from one end block to another, but could a glassy middle block also do so? In terms of a polymer crystal, what are the influential surroundings, just the immediate neighbor? or is there also a "long range" effect?

This doctoral thesis is organized in the following way: in Chapter 2, a general theoretical background on block copolymer self-assembly and polymer crystallization is given. The materials and experimental methods and apparatus employed during the experimental work are summarized in Chapter 3. The results and discussions are presented in Chapters 4 to 7. Those chapters have been organized by topic, and an introduction of the specific chapter subject has been included in each case, together with the corresponding experimental details. The particular conclusions are as well summarized at the end of each chapter. The distribution is as follows: (i) Chapter 4 deals with the triblock terpolymer synthesis and basic morphological and thermal characterization. (ii) Chapter 5 is a short chapter on specific morphological characterization of some triblock terpolymers as a function of a

thermal protocol. (iii) The topic of Chapter 6 is the morphology in thin films, and (iv) Chapter 7 portrays the isothermal crystallization DSC experiments, the derived studies of the crystallization kinetics and further thermal characterization. Finally, the work is summarized in Chapter 8.

Chapter 2. Theoretical Background

2.1. Block Copolymers
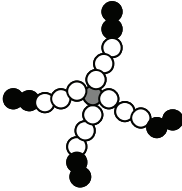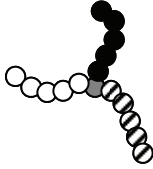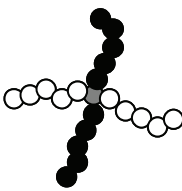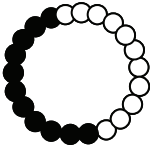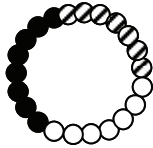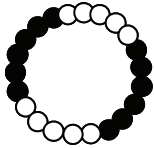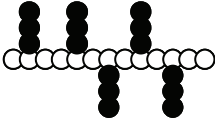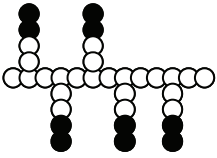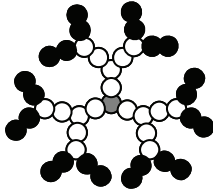
2.1.1. General Aspects

Block copolymers consist of two or more chemically linked homopolymers. According to the copolymer chain topology, different types of block copolymers are obtained, such as linear, star and branched, as depicted in Table 2.1. The wide range of possible block copolymers presented in Table 2.1 has become accessible due to advances in controlled polymerization techniques, especially anionic polymerization. Different monomers have also been polymerized thanks to reversible addition fragmentation chain transfer polymerization (RAFT), atom transfer radical polymerization (ATRP) or cationic polymerization. The combination of two techniques, i. e., the transfer from one technique to another, completes the polymer design task.

The first attractive characteristic of block copolymers is the combination of desired properties just as in polymer blends. For example, one could think of a block copolymer where a minority block has a high melting temperature (T_m) and the majority one a low glass transition temperature (T_g), resulting in a thermoplastic elastomer. Another example is the combination of a stiff block modified with a minority of a rubbery one, in order to improve the overall mechanical and impact properties; or hydrophobic and hydrophilic polymers combined as a block copolymer surfactant.

The second and more important characteristic of block copolymers is their self-assembling ability.[1, 2] The constituent blocks are usually immiscible and tend to separate driven by this nonspecific interaction. However, the macrophase separation is prevented by the covalent bond(s) that links the different blocks. Therefore, they are only able to separate in microphases which size corresponds to the chain dimensions, with the intersegmental

7

Table 2.1.   Different types of block copolymers.

Type	Copolymer	Terpolymer
Linear	AB	ABC
	ABA	
	A-A-*grad*-B-B	
	AB-multiblock	
Star	AB-star A$_2$B$_2$-miktoarm	ABC-miktoarm
Cyclic	Cyclic-AB Cyclic-AB-multiblock	Cyclic-ABC
Branched	A-*graft*-B A-*graft*-AB	
Dendrimer-like	AB-dendrimer	

bonds forming the interphase. This phenomenon creates microphases in the mesoscale, which are also known as domains and are composed by a majority of one block (this composition is usually close to 100 %). Since the size of the domains depends on the chain

dimensions it is very regular in the case of uniform macromolecules, and that generates a long-range order of these domains in the so-called morphologies.

Thermodynamically speaking, the microphase separation occurs because the immiscible blocks tend to reduce their repulsive interaction. By doing so, their conformational entropy (which is lower in an ordered structure) should not be reduced to a great extend. It can be then said that the microphase formation is a competition between the repulsive interactions and the conformational entropy.[3]

2.1.2. Amorphous Diblock Copolymers

The domain type and its arrangement in a specific morphology is determined by the block copolymer type and composition. The simplest case is that of a linear diblock copolymer A_nB_m. The case where the repetitive lengths (Kuhn lengths) of the two blocks are the same is usually employed as a model system for theoretical calculations.[4-10]

The morphologies formed by diblock copolymers as a function of the volume fraction ϕ_A are shown in Figure 2.1. When the content of A is small in the copolymer, the A block forms spherical phases arranged in BCC lattices into a matrix of B. By increasing the ϕ_A, the formed morphology changes to cylinders of A which are hexagonally arranged. The gyroid phase is formed by two continuous interpenetrating phases of A in a B matrix. The lattice of such a gyroid phase is complex and more than one type is possible (for instance, two interpenetrating tripod lattices with mirror symmetry).[11-13] The symmetric situation generates a lamellar morphology. The reverse morphologies are obtained for $\phi_A > \phi_B$ ($\phi_A >$ 0.5).
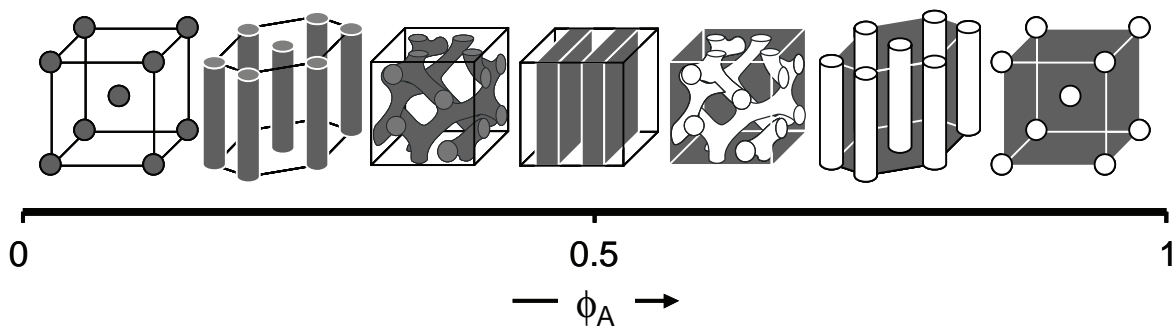
Figure 2.1. Morphologies formed by a linear diblock copolymer (AB) as function of the volume fraction of the A block.

The miscibility of two polymer blocks can be expressed as a function of its thermodynamic repulsion (described as the Flory-Huggings-Staverman interaction parameter, χ_{ij}), the block volume fraction ϕ_A and the copolymer total degree of polymerization, N_c. This implies that every block copolymer is in a disordered state below a given χN_c. Above that value, the most energetically favorable morphology will be formed, as depicted in the phase diagram in Figure 2.2. This phase diagram (sometimes called phase map since experimentally it can only be achieved by studying block copolymers with different compositions) was developed using numerical self consistent field theory (NSCFT), an approximation first used by Helfand[14-16] for strong segregated systems (SSL), and followed in parallel by Leibler[17] and Erukhimovich[18] for weak segregated systems (WSL). The stability phases initially described for an amorphous block copolymer were disordered, lamellar, hexagonal, and cubic phases. The gyroid phase, which is only stable in a small composition region, was discovered[13] and theoretically described later.[19]

Depending on the incompatibility between the blocks, the segregation strength may be weak or strong. In the weak segregation regime, the interphases are broad and have variable density since they are composed of a local mixture of the two phases. The interphase of strongly segregated blocks is sharp and narrow. Symmetric diblock copolymers are described to microphase separate, i.e., to undergo order-disorder transition,

10
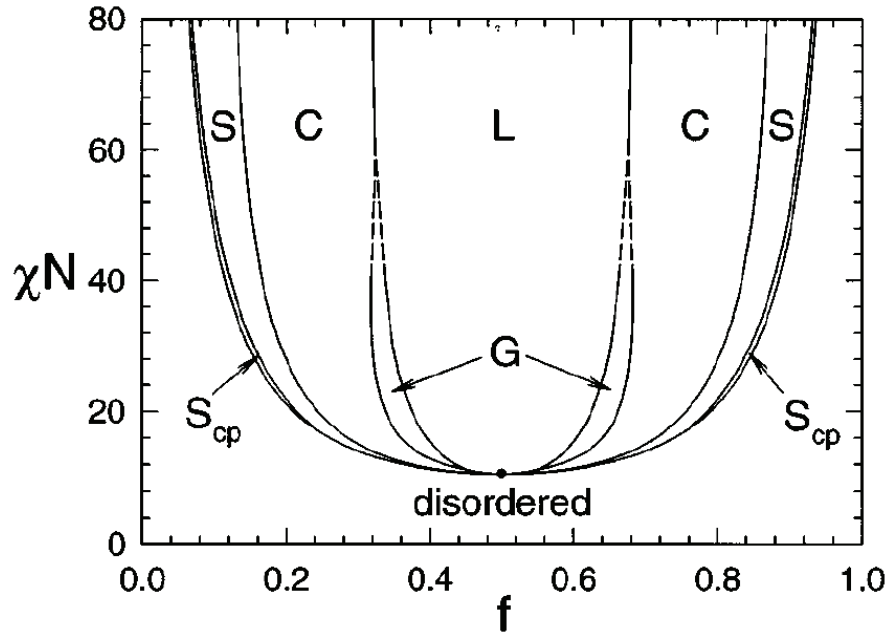
Figure 2.2. Phase diagram for conformationally symmetric diblock melts. The regions of stability for the lamellar, gyroid, cylindrical, spherical and close-packed spherical phases are denoted L, G, C, S and S_{cp}, respectively. All transitions are first order except for the mean-field critical point which is marked by a dot. Dashed lines are extrapolated phase boundaries. Figure taken from references 8 and 19.

at values of $\chi N_c \approx 10.5$.[17] The lamellar spacing d is often employed in order to interpret the segregation regimes. d is proportional to $N_c^{1/2}$ in the disordered state, and the dependence is associated with the absence of segregation.[8] The weak segregation regime will appear at values of $10.5 < \chi N_c < 16$, and it is usually assumed that the lamellar spacing relationship from the disordered state continues into the weak segregation regime. However, the exponent has been calculated as 0.994,[8] and experimental data has been fitted to an exponent of $\sim 4/5$.[8] For $\chi N_c > 16$, the system was said to be in the strong segregation regime, and the domain periodicity is directly proportional to $\chi^{1/6} N_c^{2/3}$.[3] The relationship shows the dependence to the interaction parameter and the fact that the dependence to the molecular weight becomes stronger. Matsen described the intermediate segregation regime,[19] in order to explain the complex structures and develop a phase diagram, as the region of $\chi N_c \approx 15\text{-}60$, locating the strong segregation regime at values of

χN_c higher than 60, which is also better described by the strong segregation theory and therefore commonly accepted.

Experimental phase diagrams have been found to be in very good agreement with the theoretical predictions. When the characteristic lengths of the blocks are different, which is a more realistic case, the order-order phase transition boundaries are shifted and therefore the symmetry of the diagram has been found to be affected.[3, 20] One important experimental finding is the influence of the solvent used during the casting film procedure. When a selective solvent for the block A is employed, then the apparent volume fraction of A in the block copolymer will be higher than the actual volume fraction. This could influence notably the originated morphology.[21-24]

2.1.3. Amorphous Triblock Terpolymers

The addition of a third, chemically different block introduces new variables into the microphase separation process. Besides the interaction parameters χ_{AB}, χ_{BC} and χ_{AC}, there is the experimental impossibility to find a solvent equally favorable for the three blocks. This implies that the solvent employed will always be selective, and the resultant morphology might be then influenced.

Therefore, in triblock terpolymer structures with complex lattices are formed. An example of a phase diagram for a linear polystyrene-*block*-poly(2-vinylpyridine)-*block*-poly(*tert*-butyl methacrylate), PS-*b*-P2VP-*b*-PtBMA, is presented in Figure 2.3.[25] The synthesis of different compositions was achieved by increasing the PtBMA content and keeping the other two blocks constant. The complexity of the morphologies in experimental diagram is obvious, once it is compared to the diblock copolymer case presented in Figure 2.1.
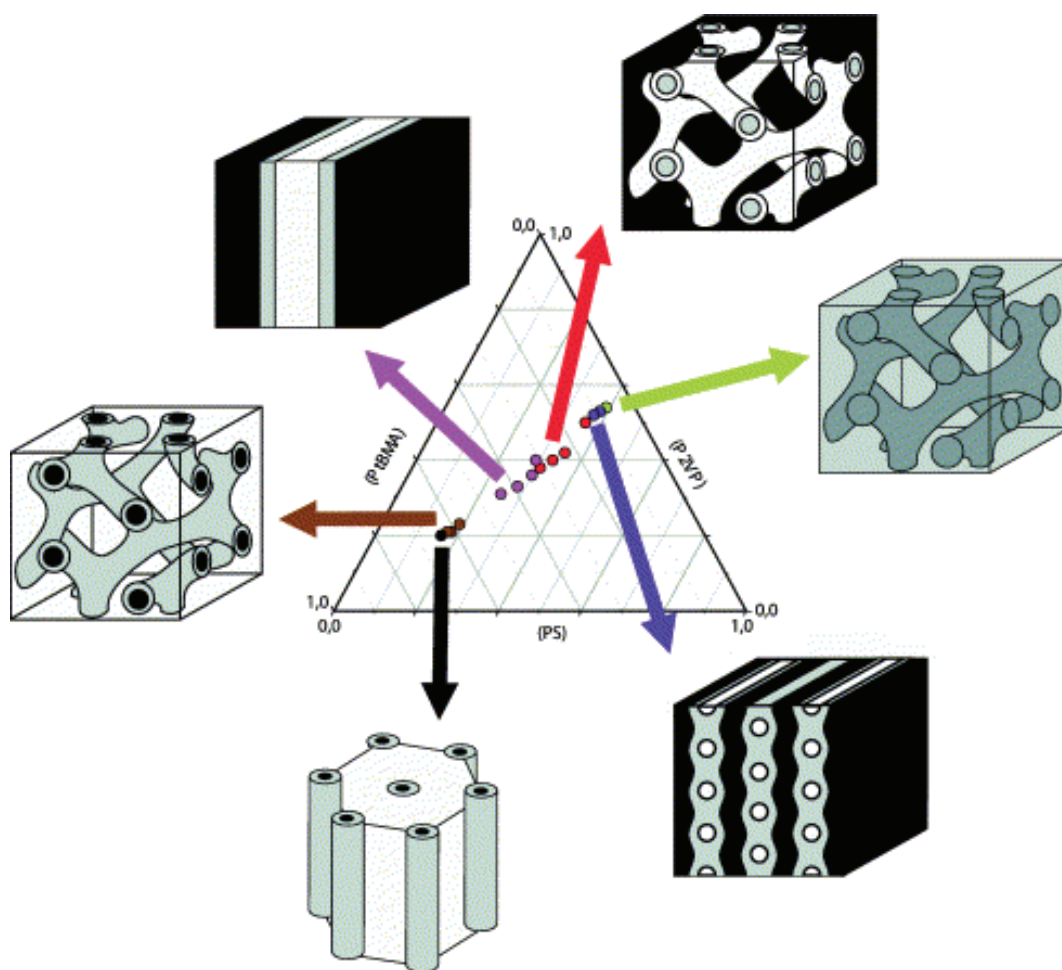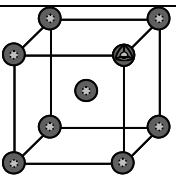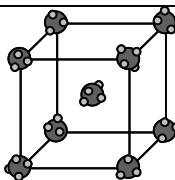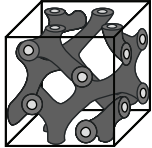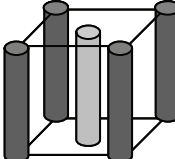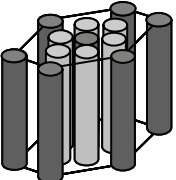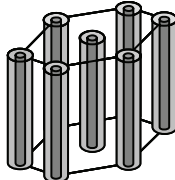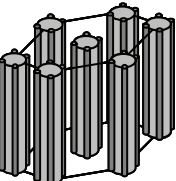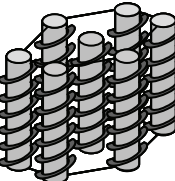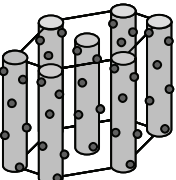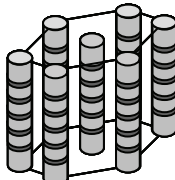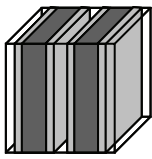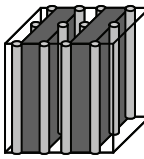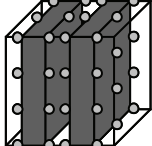
Figure 2.3. Phase diagram of linear polystyrene-*block*-poly(2-vinylpyridine)-*block*-poly(*tert*-butyl methacrylate), PS-*b*-P2VP-*b*-PtBMA, with increasing PtBMA content and constant PS and P2VP blocks. Figure taken from reference 25.

The expected thermodynamically stable structures have increased in amount, and it is commonly believed that many interesting structures are to be yet discovered. In the phase diagram for PS-*b*-P2VP-*b*-PtBMA presented in Figure 2.3, only some of the possible morphologies are depicted. Many works had given insight into the fascinating morphologies formed by amorphous triblock terpolymers, such as tricontinuous morphology,[26] "banana morphology",[27] and "knitting-pattern".[23, 28] Some of the schematic morphologies are summarized in Table 2.2.

Table 2.2. Summary of some of the morphologies formed by amorphous triblock terpolymers experimentally found.

Morphology	Cartoon	Morphology	Cartoon
Core-shell spheres[21]		Spheres-on-spheres[29]	
Core-shell double gyroid[30]		Tetragonal cylindrical morphology[31, 32]	
Hexagonally packed cylinders[33]		Core-shell-cylinder[22, 34, 35]	
Cylinders-at-cylinder[36]		Helices-around-cylinder[36]	
Spheres-on-cylinders[35]		Rings-around-cylinder[36-38]	
Lamellae[21, 37]		Cylinders between lamellae[37-39]	
Spheres between lamellae[38, 40]			

The self-assembly ability of block copolymers both in solution (in selective solvents) and in bulk, due to their multiple possible morphologies, makes them appropriate for multiple applications. Some examples are thermoplastic elastomers, information storage, drug

delivery, nanoreactors, carriers, photonic materials, (multi)functional sensors, nanopatterning and nanolithography.

2.1.4. Competition between Microphase Separation and Crystallization in Block Copolymers

So far, the microphase separation of amorphous block copolymers has been described. When at least one of the blocks forming a block copolymer is able to crystallize, the observed morphology will be the result of a competition between microphase separation and crystallization. Three different cases are generally possible, and are illustrated as the processes occur during a slow cooling of the sample from the disordered state.[41-44]

The listed cases consider the presence of one crystallizable block. Some studies have dealt with two crystallizable blocks in a diblock copolymer or as constituents of a triblock terpolymer.[45-59] In these cases, the morphology formation is affected by the already complex microphase separation process, and by each one of the crystallization processes. Additionally, the crystallization of the block crystallizing at lower temperature is also influenced by the previously grown crystalline phase.

When the crystallization temperature is higher than the order-disorder transition temperature ($T_c > T_{ODT}$), the crystallizable block will crystallize from the homogeneous melt. The resultant morphology will be alternating lamellae of crystalline and amorphous phases.

In the case of a higher order-disorder transition ($T_c < T_{ODT}$), the block copolymer is expected to microphase separate in the molten state. The effect of the crystallization on the generated structure will depend on the properties of the other blocks.

When the crystallization temperature is higher than the glass transition temperature of the other block ($T_{cA} > T_{gB}$), the crystallization will take place by disrupting the previously

formed morphology. The resultant morphology, as in the former case, will be alternating lamellae. This case is known as break-out crystallization.

If the crystallization occurs below the glass transition of the other block ($T_{cA} < T_{gB}$), then the structure generated by microphase separation will prevail over crystallization. The crystals will grow inside the domains. If the crystallizable block is not forming a matrix in the structure, then the crystallization is considered to take place in a confined way.

Experimentally, it has been observed that the structure can be modified by the occurrence of confined crystallization. These modifications are basically related to the domain size and shape. They have been attributed to the volume reduction produced by the increase of density in the crystalline domains. As an example, Balsamo et al.[57] found deformed cylinders of poly(ε-caprolactone) in polystyrene-*block*-polybutadiene-*block*-poly(ε-caprolactone). Also a deformation was found by Schmalz et al.[59] for the poly(ethylene oxide) cylinders in polybutadiene-*block*-polystyrene-*block*-poly(ethylene oxide) triblock terpolymers.

The occurrence of the crystallization process inside a block copolymer microphase is very attractive. The size of a microphase is in the mesoscale, which implies that the final size of the crystal will be comparable to the crystalline lamellae dimensions. Due to the reduced dimensions, the diffusion process looses importance and the probability of finding an appropriate heterogeneous nucleus decreases. Therefore, the crystallization process can be studied under conditions rarely encountered in other systems, and that simplification helps to understand the complete phenomenon.[42, 43, 60]

2.2. Polymer Crystallization

Crystallization could be described as the phase transition process from the disordered molten state to the ordered crystalline one. The disordered state is characterized by the

randomly coiled chains, while the ordered state is distinguished by the crystalline lamellae. Polymer crystals are formed by folded polymer chains, which give the lamella the particularity of the amorphous interfaces. Those interfaces are formed by entanglements, end-groups, bulky substituent groups and chain defects, all of which cannot be included into the crystalline array. Those amorphous interfaces are linked to the crystal, and constitute the nature of the semicrystalline state of polymer crystals.[61, 62]

The most characteristic dimension of the crystalline lamella is its thickness, since the other two dimensions are usually very large. The lamellar thickness depends on the temperature at which it was created. That means that the polymer crystallization process is kinetically defined, instead of thermodynamically. The crystal grown at a given temperature is the crystal with the highest generation rate, not necessarily the structure with the lowest free energy.

Another indication of the kinetic character of polymer crystallization is the supercooling ΔT, defined as expressed in Equation 2.1. It is always necessary to apply a supercooling in order to induce crystallization in a crystallizable polymer, and the crystallization rate is directly proportional to the applied supercooling. This characteristic is quite unique, compared to the thermodynamically defined liquid-solid phase change in low molar mass compounds.

$$\Delta T = T_m^0 - T_c \quad\quad\quad\quad\quad\quad\quad\quad\quad\quad \text{(Equation 2.1)}$$

One of the most important conclusions from the previously stated observations is the metastability of the polymer crystals. Since they are non-equilibrium structures, they continuously rearrange and can modify their structure over time. Many variables affect the metastable crystal, such as temperature, stress or solvent vapor. This gives great importance to the history of a crystal, i.e., how it was generated, under which conditions and how it has been kept.

2.2.1. Crystallization Process

The crystallization starts by a nucleation process and it continues by growth.[63, 64] Only under very large supercoolings, the spinodal decomposition can occur. The nucleation process is still under extensive investigation, since the advances in experimental techniques are facilitating the study of the early stages of crystallization. Many of the present research is dedicated to the study of melt organization prior crystallization.[65-70] Computer simulations are also been extensively discussed, especially those by Muthukumar.[67, 71] Strobl[72] has proposed a new crystallization theory in order to explain the results of organization in the molten state obtained by different groups. A sketch of the mechanism, also known as the multistage model, is presented in Figure 2.4.
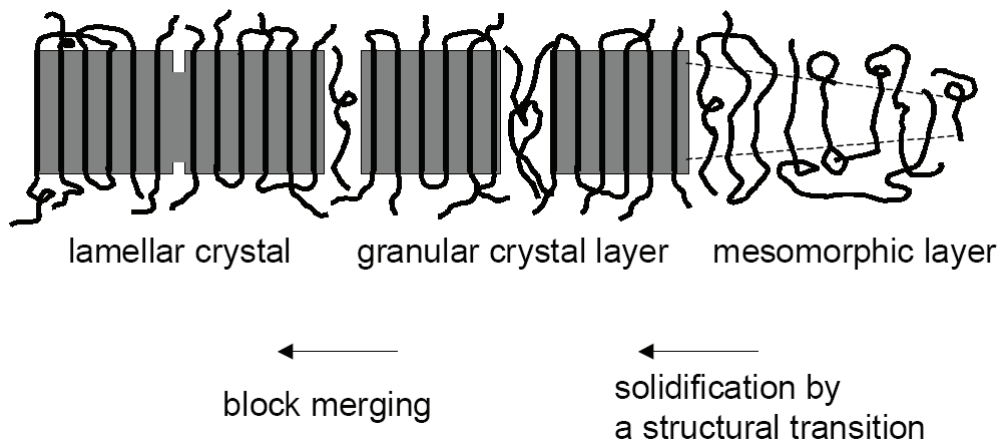
Figure 2.4. Sketch of the crystallization multistage model proposed by Strobl. Taken from reference 72.

Nucleation is assumed to occur from a small group of aligned segments, or nuclei, with the appropriate size. This local segmental alignment (embryo) is metastable, so it generates from random fluctuations and melts again. Only those which are big enough would act as nuclei. The way these nuclei are formed from the disordered state, i.e., their relation to the density fluctuations is still a matter of discussion. Of course, nucleation is commonly

originated by heterogeneous nuclei, i.e., any (low mass) particle with the correct size and surface.

Crystal growth is initially restricted to lamellae growing away from the nucleus, into the three-dimensional space. Each lamella grows linearly, creating the skeleton of the spherical semicrystalline entity, the *spherulite*. This growth is stopped by the –also growing– neighbor *spherulite*. In order to fill the three-dimensional space, the lamellae must twist, ramify, superpose or stack together. These processes are the only crystalline growing processes which occur after two neighbor *spherulites* contact each other, and they are known as secondary crystallization.

2.2.2. Crystallization Kinetics

Under standard conditions, polymer crystallization takes place during a given time period and over a certain temperature range. This results in a non-uniform crystalline structure in the polymer sample, where the formed lamellae present a distribution of lamellar thicknesses. A more uniform semicrystalline structure, where the lamellar thickness is constant (or has a very narrow distribution) is obtained when the crystallization occurs at a set temperature. The process is commonly referred to as isothermal crystallization, and can be followed for instance by differential scanning calorimetry (DSC), as shown in Figure 2.5. The kinetics of the crystallization of uniform crystals is then analyzed at different crystallization temperatures.

The kinetics of the overall crystallization process, considering both nucleation and growth, is described by the Avrami equation (Equation 2.2),[74-76] developed also simultaneously by Kolmorogov[77] and Johnson and Mehl.[78] The equation is also sometimes referred to as the Kolmorogov-Johnson-Mehl-Avrami (KJMA) model.[79]

$$1 - V_c(t) = \exp(-kt^n)$$ (Equation 2.2)
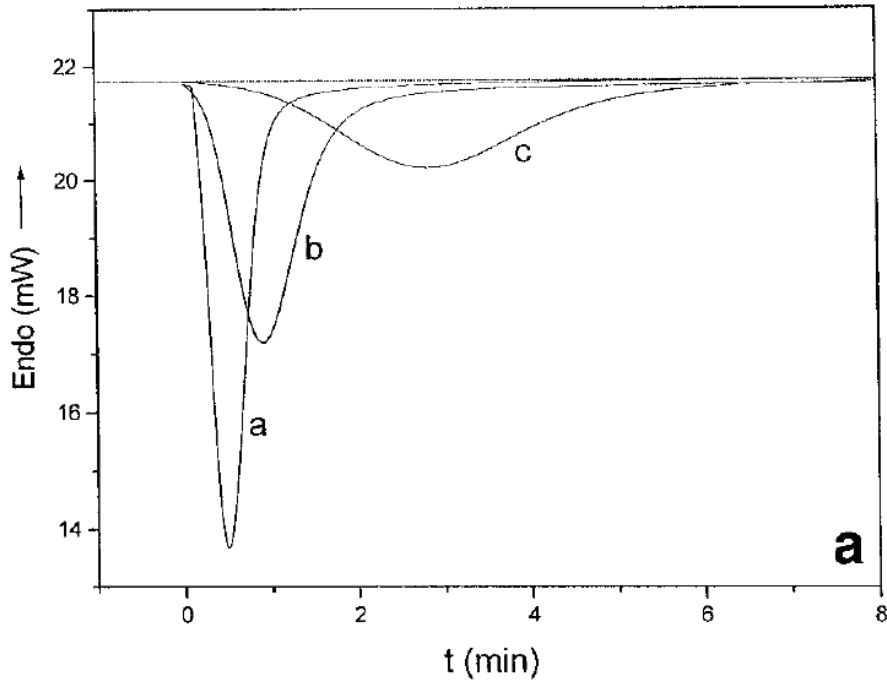
Figure 2.5. Isothermal crystallization for a poly(ethylene terephthalate) with disodium terephthalate at (a) 200 °C, (b) 210 °C, and (c) 220 °C. Taken from reference 73.

In Equation 2.2, V_c is the relative volumetric transformed fraction, k is an overall crystallization rate constant for nucleation and growth, and n is the constant known as Avrami index. In order to keep the non-dimensionality of the exponent, the units of the crystallization rate constant k are reciprocal time units to the power of n (i.e., min^{-n}). Therefore, this constant is not independent from the Avrami index and is rarely experimentally employed. Other variables, such as the inverse of the time at which the crystallization has achieved 50 % of the total crystallization ($1/\tau_{50\%}$), are commonly used for comparison among several samples since they are independent from the correspondent Avrami index values.

The Avrami index n in Equation 2.2 consists of two contributions, as described by Equation 2.3.[80, 81] The first contribution, n_n, is related to the nucleation process. The value of n_n is 0 when the nucleation is instantaneous and 1 when it occurs sporadic. The second

contribution, n_g, is defined by the number of dimensions in which growth takes place, and therefore is commonly expected to be 1, 2, or 3.

$$n = n_n + n_g$$ (Equation 2.3)

The Avrami index is in principle an integer number between 1 and 4, which describes the two stages of polymer crystallization. The summary of the Avrami index values theoretically expected is presented in Table 2.3. However, in practice the values encounter are rarely integer numbers, and even values lower than 1 have been calculated.[82, 83] These discrepancies are understandable, since the Avrami equation was developed for general crystallization, and therefore there are some considerations and limitations related to the polymer crystallization.

Table 2.3. Values of the Avrami index n for the different cases of nucleation and possible crystal dimensionalities.[64, 83, 84]

Dimension	Geometry	Instantaneous nucleation	Sporadic nucleation	Sporadic nucleation, diffusion controlled
1D	Line	1	2	1
2D	Circular	2	3	2
3D	Spherical	3	4	5/2
	Fibril	≤ 1	≤ 2	
	Circular lamellar	≤ 2	≤ 3	
	Solid sheaf	≥ 5	≥ 6	

The first particularity related to macromolecules is the imperfection of the crystals or semicrystallinity. The crystallinity behind the crystal front would never be 100 % due to the chain folds, and the Avrami equation has been redefined as:[83]

$$1 - \frac{V_c(t)}{V_\infty} = \exp(-kt^n)$$ (Equation 2.4)

which overcomes the mentioned limitation. Secondly, since the crystallization process goes on for some period of time, the decrease of system volume during the crystallization process becomes important, and can be considered by:[83]

$$1 - V_\text{c}(t) = \exp\left\{-k\left[1 - V_\text{c}\left(\frac{\rho_\text{c} - \rho_\text{a}}{\rho_\text{a}}\right)\right]t^n\right\}$$
(Equation 2.5)

where ρ_c is the density of the crystalline phase and ρ_a the correspondent to the amorphous phase. Another consideration to the Avrami equation applied to polymer crystallization is the occurrence of primary and secondary crystallization. The two processes have different crystal development rates, and that would affect the kinetic calculations. In order to avoid such associated errors, the Avrami equation is only applied to the early stages of crystallization, where only primary crystallization is present. The last limitation of the Avrami equation to be discussed here refers to the nucleation process. Nucleation is neither purely instantaneous nor sporadic, but a combination of both.[83] Therefore, the nucleation contribution to the Avrami index, n_n, is rarely an integer number.

The dependence of the Avrami index with the crystallization temperature is a compromise between the effects of the crystallization temperature on nucleation and crystal dimensionality.[64] When the crystallization temperature is increased, the probability of instantaneous nucleation decreases, and therefore the Avrami index increases. However, for the same case, the crystal dimensionality might decrease, which would cause a decrease in the Avrami index. The compromise between these two effects will determine the actual behavior of the Avrami index as a function of crystallization temperature.

From the aforementioned limitations of the Avrami equation, as well as based on the complex interpretation of the Avrami index, many discussions have taken place.[79] However, the fit still represents one fine way to analyze the overall crystallization kinetics, and the common miscalculations can be avoided.[85] The study of the overall crystallization

22

kinetics is employed as an approximation to the nucleation process kinetics. The crystallization growth kinetics can be calculated, for instance from optical microscopy, or it can be neglected, as is the case for confined crystallization.

2.3. References

1. Whitesides, G.; Mathias, J.; Seto, C. *Science* **1991,** 254, (5036), 1312-1319.

2. Bates, F. S. F., Glenn H. *Physics Today* **1999,** 52, (2), 32-38.

3. Whitmore, M. D., Theory of Block Copolymers. In *Supramolecular Polymers*, 2nd ed.; Ciferri, A., Ed. Taylor & Francis Group, LLC: New York, 2005; pp 301-350.

4. Whitmore, M. D.; Noolandi, J. *Macromolecules* **1988,** 21, 1482-1496.

5. Whitmore, M. D.; Vavasour, J. D. *Acta Polymerica* **1995,** 46, (5), 341-360.

6. Matsen, M. W. *Current Opinion in Colloid & Interface Science* **1996,** 1, 329-336.

7. Matsen, M. W. *Journal of Physics: Condensed Matter* **2002** 14, R21-R47.

8. Matsen, M. W.; Bates, F. S. *Macromolecules* **1996,** 29, (4), 1091-1098.

9. Matsen, M. W.; Schick, M. *Physical Review Letters* **1994,** 72, (16), 2660-2663.

10. Matsen, M. W.; Schick, M. *Macromolecules* **1994,** 27, 6761-6767.

11. Hajduk, D. A.; Harper, P. E.; Gruner, S. M.; Honeker, C. C.; Kim, G.; Thomas, E. L.; Fetters, L. J. *Macromolecules* **1994,** 27, 4063-4075.

12. Hajduk, D. A.; Harper, P. E.; Gruner, S. M.; Honeker, C. C.; Thomas, E. L.; Fetters, L. J. *Macromolecules* **1995,** 28, (7), 2570-2573.

13. Thomas, E. L.; Alward, D. B.; Kinning, D. J.; Martin, D. C.; Dale L. Handlin, J.; Fetters, L. J. *Macromolecules* **1986,** 19, 2197-2202.

14. Helfand, E.; Sapse, A. M. *The Journal of Chemical Physics* **1975,** 62, (4), 1327-1331.

15. Helfand, E.; Wasserman, Z. *Macromolecules* **1978,** 11, (5), 960-966.

16. Helfand, E.; Wasserman, Z. R. *Macromolecules* **1976,** 9, (6), 879-888.

17. Leibler, L. *Macromolecules* **1980,** 13, (6), 1602-1617.

18. Erukhimovich, I. Y. *Polymer Science U.S.S.R.* **1982,** 24, 2232-2241.

19. Matsen, M. W.; Bates, F. S. *Journal of Chemical Physics* **1997,** 106, (6), 2436-2448.

20. Matsen, M. W.; Bates, F. S. *Journal of Polymer Science Part B: Polymer Physics* **1997,** 35, (6), 945-952.

21. Arai, K.; Kotaka, T.; Kitano, Y.; Yoshimura, K. *Macromolecules* **1980,** 13, 1670-1678.

22. Kudose, I.; Kotaka, T. *Macromolecules* **1984,** 17, 2325-2332.

23. Breiner, U.; Krappe, U.; Thomas, E. L.; Stadler, R. *Macromolecules* **1998,** 31, (1), 135-141.

24. Jeong, U.; Lee, H. H.; Yang, H.; Kim, J. K.; Okamoto, S.; Aida, S.; Sakurai, S. *Macromolecules* **2003,** 36, (5), 1685-1693.

25. Ludwigs, S.; Boker, A.; Abetz, V.; Muller, A. H. E.; Krausch, G. *Polymer* **2003,** 44, (22), 6815-6823.

26. Mogi, Y.; Mori, K.; Matsushita, Y.; Noda, I. *Macromolecules* **1992,** 25, 5412-5415.

27. Jung, K.; Abetz, V.; Stadler, R. *Macromolecules* **1996,** 29, (3), 1076-1078.

28. Breiner, U.; Krappe, U.; Stadler, R. *Macromolecular Rapid Communications* **1996,** 17, (8), 567-575.

29. Breiner, U.; Krappe, U.; Jakob, T.; Abetz, V.; Stadler, R. *Polymer Bulletin* **1998,** 40, (2-3), 219-226.

30. Shefelbine, T. A.; Vigild, M. E.; Matsen, M. W.; Hajduk, D. A.; Hillmyer, M. A.; Cussler, E. L.; Bates, F. S. *J. Am. Chem. Soc.* **1999,** 121, (37), 8457-8465.

31. Mogi, Y.; Kotsuji, H.; Kaneko, Y.; Mori, K.; Matsushita, Y.; Noda, I. *Macromolecules* **1992,** 25, (20), 5408-5411.

32. Mogi, Y.; Nomura, M.; Kotsuji, H.; Ohnishi, K.; Matsushita, Y.; Noda, I. *Macromolecules* **1994,** 27, (23), 6755-6760.

33. Brinkmann, S.; Stadler, R.; Thomas, E. L. *Macromolecules* **1998,** 31, (19), 6566-6572.

34. Gido, S. P.; Schwark, D. W.; Thomas, E. L.; Goncalves, M. d. C. *Macromolecules* **1993,** 26, 2636-2640.

35. Breiner, U.; Krappe, U.; Abetz, V.; Stadler, R. *Macromolecular Chemistry and Physics* **1997,** 198, (4), 1051-1083.

36. Krappe, U.; Stadler, R.; Voigt-Martin, I. *Macromolecules* **1995,** 28, (13), 4558-4561.

37. Auschra, C.; Stadler, R. *Macromolecules* **1993,** 26, (9), 2171-2174.

38. Stadler, R.; Auschra, C.; Beckmann, J.; Krappe, U.; Voigt-Martin, I.; Leibler, L. *Macromolecules* **1995,** 28, (9), 3080-3097.

39. Matsushita, Y.; Choshi, H.; Fujimoto, T.; Nagasawa, M. *Macromolecules* **1980,** 13, 1053-1058.

40. Beckmann, J.; Auschra, C.; Stadler, R. *Macromol. Rapid Commun.* **1994,** 15, (1), 67-72.

41. Hamley, I. W., *The Physics of Block Copolymers*. Oxford University Press: Oxford, 1998.

42. Loo, Y.-L.; Register, R. A., Crystallization within block copolymer mesophases. In *Development in block copolymer science and technology*, Hamley, I. W., Ed. John Wiley & Sons, Ltd: 2004; pp 213-243.

43. Müller, A. J.; Balsamo, V.; Arnal, M. L. *Advances in Polymer Science* **2005,** 190, 1-63.

44. Müller, A. J.; Balsamo, V.; Arnal, M. L., In *Lecture Notes in Physics: Progress in Understanding of Polymer Crystallization*, Reiter, G.; Strobl, G., Eds. Springer: Berlin, 2007; pp 229-259.

45. Floudas, G.; Reiter, G.; Lambert, O.; Dumas, P. *Macromolecules* **1998,** 31, (21), 7279-7290.

46. Jiang, S.; He, C.; An, L.; Chen, X.; Jiang, B. *Macromolecular Chemistry and Physics* **2004,** 205, (16), 2229-2234.

47. Albuerne, J.; Márquez, L.; Müller, A. J.; Raquez, J. M.; Degée, P.; Dubois, P.; Castelletto, V.; Hamley, I. W. *Macromolecules* **2003,** 36, (5), 1633-1644.

48. Müller, A. J.; Albuerne, J.; Esteves, L. M.; Marquez, L.; Raquez, J.-M.; Degée, P.; Dubois, P.; Collins, S.; Hamley, I. W. *Macromolecular Symposia* **2004,** 215, (1), 369-382.

49. Müller, A. J.; Albuerne, J.; Márquez, L.; Raquez, J.-M.; Degée, P.; Dubois, P.; Hobbs, J.; Hamley, I. W. *Faraday Discussions* **2005,** 128, 231-252.

50. Sun, L.; Lui, Y.; Zhu, L.; Hsiao, B. S.; Avila-Orta, C. A. *Polymer* **2004,** 2004, 8181-8193.

51. Hamley, I. W.; Castelletto, V.; Castillo, R. V.; Müller, A. J.; Martin, C. M.; Pollet, E.; Dubois, P. *Macromolecules* **2005,** 38, (2), 463-472.

52. Hamley, I. W.; Parras, P.; Castelletto, V.; Castillo, R. V.; Müller, A. J.; Pollet, E.; Dubois, P.; Martin, C. M. *Macromolecular Chemistry and Physics* **2006,** 207, (11), 941-953.

53. Arnal, M. L.; Balsamo, V.; López-Carrasquero, F.; Contreras, J.; Carrillo, M.; Schmalz, H.; Abetz, V.; Laredo, E.; Müller, A. J. *Macromolecules* **2001,** 34, (23), 7973-7982.

54. Balsamo, V.; Von Gyldenfeldt, F.; Stadler, R. *Macromolecular Chemistry and Physics* **1996,** 197, 3317-3341.

55. Balsamo, V.; Müller, A. J.; Gyldenfeldt, F. v.; Stadler, R. *Macromolecular Chemistry and Physics* **1998,** 199, (6), 1063-1072.

56. Balsamo, V.; Müller, A. J.; Stadler, R. *Macromolecules* **1998,** 31, (22), 7756-7763.

57. Balsamo, V.; von Gyldenfeldt, F.; Stadler, R. *Macromolecules* **1999,** 32, (4), 1226-1232.

58. Schmalz, H.; Boker, A.; Lange, R.; Krausch, G.; Abetz, V. *Macromolecules* **2001,** 34, (25), 8720-8729.

59. Schmalz, H.; Knoll, A.; Müller, A. J.; Abetz, V. *Macromolecules* **2002,** 35, (27), 10004-10013.

60. Müller, A. J.; Balsamo, V.; Arnal, M. L.; Jakob, T.; Schmalz, H.; Abetz, V. *Macromolecules* **2002,** 35, (8), 3048-3058.

61. Reiter, G.; Castelein, G.; Sommer, J.-U., Crystallization of Polymers in Thin Films: Model Experiments. In *Lecture Notes in Physics: Polymer Crystallization: Observations, Concepts and Interpretations*, Reiter, G.; Sommer, J.-U., Eds. Springer: Berlin, 2003; Vol. 606, pp 131-152.

62. Strobl, G. *Progress in Polymer Science* **2006,** 31, (4), 398-442.

63. Strobl, G., *The Physics of Polymers*. 3rd ed.; Springer: Berlin, 2007; p 518.

64. Mandelkern, L., *Crystallization of Polymers*. 2nd ed.; Cambridge University Press: Cambridge, 2002; Vol. 1, p 550.

65. Imai, M.; Kaji, K.; Kanaya, T. *Macromolecules* **1994,** 27, (24), 7103-7108.

66. Olmsted, P. D.; Poon, W. C. K.; McLeish, T. C. B.; Terrill, N. J.; Ryan, A. J. *Physical Review Letters* **1998,** 81, (2), 373-376.

67. Muthukumar, M.; Welch, P. *Polymer* **2000,** 41, (25), 8833-8837.

68. Kaji, K.; Nishida, K.; Matsuba, G.; Kanaya, T.; Imai, M. *Journal of Macromolecular Science* **2003,** B42, (3 & 4), 709-715.

69. Zhang, J.; Duan, Y.; Sato, H.; Shen, D.; Yan, S.; Noda, I.; Ozaki, Y. *J. Phys. Chem. B* **2005,** 109, 5586-5591.

70. Gee, R. H.; Lacevic, N.; Fried, L. E. *Nature Materials* **2006,** 5, (1), 39-43.

71. Muthukumar, M. *The European Physical Journal E - Soft Matter* **2000,** 3, 199-202.

72. Strobl, G. *The European Physical Journal E - Soft Matter* **2000,** V3, (2), 165-183.

73. Bian, J.; Ye, S.-R.; Feng, L.-X. *Journal of Polymer Science, Part B: Polymer Physics* **2003,** 41, (18), 2135-2144.

74. Avrami, M. *Journal of Chemical Physics* **1939,** 7, 1103-1112.

75. Avrami, M. *Journal of Chemical Physics* **1940,** 8, 212-224.

76. Avrami, M. *Journal of Chemical Physics* **1941,** 9, 177-184.

77. Kolmogorov, A. N. *Bull. Acad. Sci. USSR. Ser. Math* **1937,** 1, 355-359.

78. Johnson, W. A.; Mehl, R. F. *Trans. AIME* **1939,** 135, 416-458.

79. Piorkowska, E.; Galeski, A.; Haudin, J.-M. *Progress in Polymer Science* **2006,** 31, (6), 549-575.

80. Balsamo, V.; Urdaneta, N.; Pérez, L.; Carrizales, P.; Abetz, V.; Müller, A. J. *European Polymer Journal* **2004,** 40, 1033-1049.

81. Suñol, J. J., Modeling Polymer Crystallization: DSC Approach. In *Lecture Notes in Physics: Polymer Crystallization: Observations, Concepts and Interpretations*, Reiter, G.; Sommer, J.-U., Eds. Springer: Berlin, 2003; Vol. 606, pp 297-311.

82. Lotz, B.; Kovacs, A. J. *Polym Prepr Am Chem Soc Div Polym Chem* **1969,** 10, 820-825.

83. Gedde, U. W., *Polymer Physics*. Chapman & Hall: London, 1995; p 298.

84. Hiemenz, P. C., *Polymer Chemistry: The Basic Concepts*. Dekker: New York, 1984; p 738.

85. Lorenzo, A. T.; Arnal, M. L.; Albuerne, J.; Müller, A. J. *Polymer Testing* **2007,** 26, 222-231.

Chapter 3. Experimental Part

3.1. Materials

Benzene (Acros) was purified by successive distillation over CaH_2 and potassium and stored under dry nitrogen atmosphere. Butadiene (Linde) was passed through columns with molecular sieve and activated alumina, and kept over Bu_2Mg under purified nitrogen before use. Styrene (Acros) was stirred over Bu_2Mg under nitrogen, and condensed into glass ampoules. Ethylene oxide (Linde) was condensed onto CaH_2 and stirred at -10 °C for 3 hours, followed by condensation into glass ampoules. sec-Butyl lithium (Acros, 1.3 M in cyclohexane/hexane: 92/8), phosphazene base t-BuP$_4$ (Fluka, 1 M in hexane), hydrochloric acid (p. a., Merck), toluene (p. a., Merck), Bu_2Mg (Aldrich, 1 M in heptane), and Wilkinson catalyst $(Ph_3P)_3Rh(I)Cl$ (Aldrich) were used without further purification.

3.2. Synthesis

3.2.1. Synthesis of PB-*b*-PS-*b*-PEO and PS-*b*-PB-*b*-PEO

Sequential anionic polymerization of butadiene, styrene, and ethylene oxide in benzene with *sec*-BuLi as initiator was employed in order to achieve the synthesis of poly(1,4-butadiene)-*block*-polystyrene-*block*-poly(ethylene oxide) (PB-*b*-PS-*b*-PEO) triblock terpolymers, as depicted in Figure 3.1. One day before polymerization, approximately 600 ml of purified and dried benzene were poured into the 1 L reactor. A couple of drops of styrene were added, together with enough *sec*-BuLi to detect a pale yellow color characteristic for styryl anions. These anions reacted overnight with the residuals impurities, and the color usually disappeared.
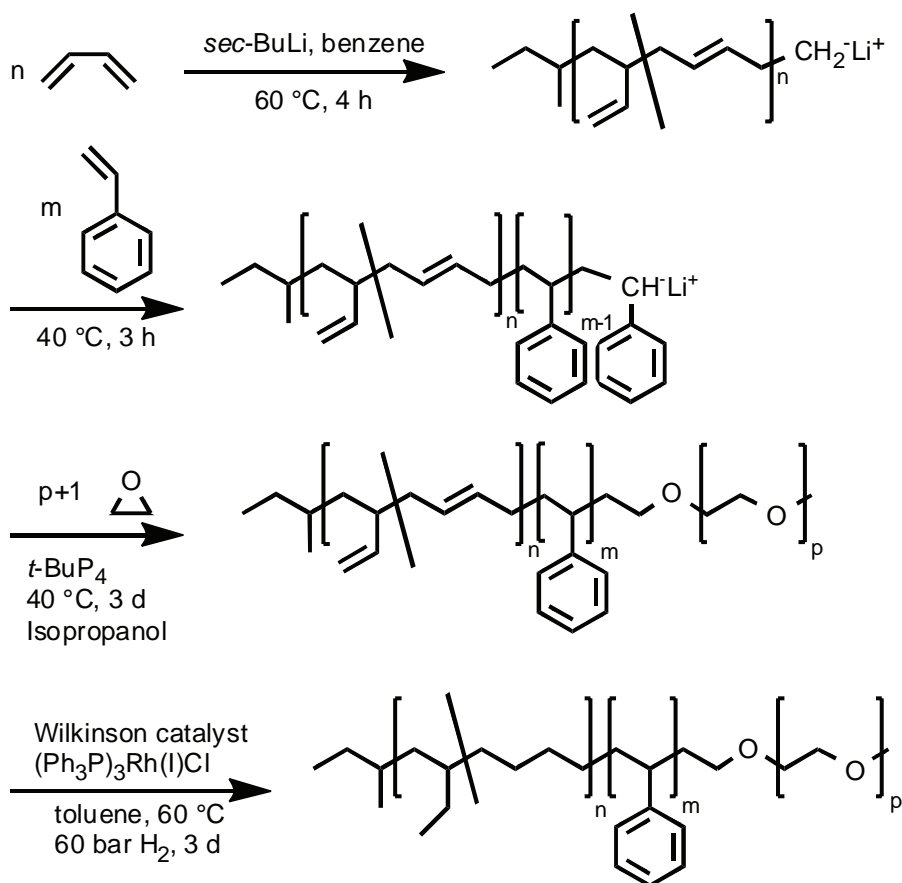
Figure 3.1. Scheme of the sequential anionic polymerization of PB-*b*-PS-*b*-PEO and further hydrogenation.

For the reaction, the solvent-filled reactor was set at 15 °C, and the necessary amount of *sec*-BuLi (calculated according to the desired terpolymer composition) was added. Previously purified 1,3 butadiene was condensed in a burette at -20 °C and poured into the reactor. The system temperature was increased to 60 °C and the polymerization reaction was completed after 2.5 hours. The reactor was then cooled down to 20 °C and a small sample was precipitated into degassed isopropanol in order to characterize the PB precursor. Purified styrene was then added to the reaction, the overall temperature was increased up to 40 °C and the monomer was allowed to polymerize for 2.5 hours at that temperature. Once the polymerization time was reached, the reactor was cooled down to 10°C, a second sample was taken for characterization and the purified ethylene oxide was added. During 1 hour, the addition of the first ethylene oxide molecule to the living chains

took place. No further addition is possible since the formed lithium alkoxides aggregate strongly. Afterwards, the temperature was increased to 40 °C, and the strong phosphazene base t-BuP$_4$ was added to give the ratio [Li$^+$]:[t-BuP$_4$] = 1:1. This allows the polymerization of ethylene oxide in the presence of a lithium counterion.[1-7] The polymerization of ethylene oxide was completed after 3 days and terminated with a degassed mixture of methanol:acetic acid (1:5 v:v). Finally, the polymer solution was cooled down to 25 °C, poured out of the reactor and precipitated in isopropanol. A small amount of stabilizer (2,6-di-t-butyl-4-methylphenol) was added to the polymer solution prior to precipitation in order to avoid crosslinking of the polybutadiene block.

The polymerization of 1,3-butadiene under the conditions of temperature and solvent polarity employed leads to a preferential 1,4-addition. This microstructure is essential in order to obtain the corresponding "high 1,4 hydrogenated PB" structure after hydrogenation, i.e., a random copolymer of ethylene and butylene, as depicted in Figure 3.1, with an ethylene content higher than 85 wt %.

3.2.2. Hydrogenation

Polyethylene-$block$-polystyrene-$block$-poly(ethylene oxide) (PE-b-PS-b-PEO) triblock terpolymers were obtained by hydrogenation of the PB-b-PS-b-PEO terpolymers (precursors). Typically, 10 g of non-hydrogenated triblock terpolymer were dissolved in 750 ml of degassed toluene (1.53 wt-% solution of the terpolymer) with a small amount of stabilizer (2,6-di-t-butyl-4-methylphenol), and stirred under nitrogen for 30 min. Wilkinson catalyst (Ph$_3$P)$_3$Rh(I)Cl was added in 1 mol-% with respect to the number of double bonds, under a slight nitrogen flow. The polymer solution was inserted into the previously hydrogen purged hydrogenation reactor. Then, the temperature was set at 60 °C and the H$_2$ pressure at 60 bar. The reaction was allowed to run for 3 days, after which time the pressure was realized, and the polymer solution was brought to room temperature,

poured out of the reactor and precipitated in isopropanol. ^{1}H NMR results of the hydrogenated terpolymers confirmed that the PB block was completely hydrogenated. Precipitation was not completely successful in removing the residual Wilkinson catalyst, since the highly polar PEO block tends to bind it. Further purification was achieved by dissolving the hydrogenated triblock terpolymer in 1.5 L of toluene (0.7 wt-% solution of the terpolymer) with a small amount of concentrated hydrochloric acid for 30 min at 40 °C, followed by refluxing for 2 min. Finally, the purified hydrogenated polymer was again precipitated into isopropanol.

The polymerization of polystyrene-*block*-poly(1,4-butadiene)-*block*-poly(ethylene oxide) (PS-*b*-PB-*b*-PEO) triblock terpolymers was achieved following the procedure previously explained adapted to the wished block sequence. The hydrogenation procedures were also as explained. A list of all triblock terpolymer synthesized is presented in Table 3.1 for the sake of completeness, although not all the PS-*b*-PB-*b*-PEO and their hydrogenated analogues were further analyzed. In the notation employed here ($A_xB_yC_z^m$), the subscripts denote the percentage mass fraction of each block component and the superscripts indicate the overall number-averaged molecular weight M_n in kg/mol of the block copolymer. B stands for polybutadiene, S for polystyrene, EO for poly(ethylene oxide) and E for polyethylene or poly(ethylene-*ran*-butylene).

3.3. Equipment

3.3.1. Size Exclusion Chromatography (SEC)

SEC experiments were performed on a Waters instrument. Four PSS-SDV columns (5 µm, Polymer Standards Service, Mainz) with a porosity range from 10^2 to 10^5 Å were used together with a differential refractometer and a UV-detector at 254 nm. Measurements on the non-hydrogenated triblock copolymers were performed in THF solutions (2 wt/v-%) at

30 °C with a flow rate of 1 ml/min using toluene as internal standard. The results were

calibrated with narrowly distributed polybutadiene standards.

Table 3.1. Molecular weight, molecular weight distributions and content of 1,2-units (wt-%) in the polybutadiene block of the triblock terpolymers.

	M_n (kg/mol)			M_w/M_n
	PB[a] (%1,2[b]) / PE[c]	PS[c]	PEO[c]	
$B_{29}S_{40}EO_{31}{}^{168}$ / $E_{29}S_{40}EO_{31}{}^{170}$	48 (12.9) / 50	67	53	1.03
$B_{19}S_{34}EO_{47}{}^{142}$ / $E_{19}S_{34}EO_{47}{}^{143}$	27 (12.8) / 28	48	67	1.03
$B_{19}S_{35}EO_{46}{}^{217}$ / $E_{19}S_{35}EO_{46}{}^{219}$	41 (10.8) / 43	76	100	1.01
$B_{16}S_{68}EO_{16}{}^{210}$ / $E_{17}S_{67}EO_{16}{}^{211}$	35 (11.5) / 36	142	33	1.01
$B_{16}S_{40}EO_{44}{}^{143}$ / $E_{16}S_{40}EO_{44}{}^{144}$	22 (14.0) / 23	58	63	1.05
$B_{37}S_{16}EO_{47}{}^{76}$ / $E_{38}S_{16}EO_{46}{}^{77}$	28 (11.8) / 29	13	36	1.03
$S_{14}B_{46}EO_{40}{}^{102}$ / $S_{14}E_{47}EO_{39}{}^{103}$	47 (10.9) / 49	14	40	1.01
$S_{18}B_{36}EO_{46}{}^{60}$ / $S_{18}E_{37}EO_{45}{}^{61}$	22 (17.6) / 23	11	27	1.02
$S_{30}B_{22}EO_{48}{}^{98}$ / $S_{30}E_{23}EO_{47}{}^{99}$	22 (11.1) / 23	29.5	47	1.01
$S_{15}B_{40}EO_{45}{}^{86}$ / $S_{15}E_{41}EO_{44}{}^{88}$	34 (11.5) / 35	13	39	1.01
$S_{43}B_{21}EO_{36}{}^{111}$ / $S_{43}B_{22}EO_{35}{}^{112}$	23 (11.7) / 24	48	39	1.05

[a] Determined by SEC in THF calibrated against PB standards. [b] Determined by ^1H NMR spectroscopy in $CDCl_3$. [c] Determined by ^1H NMR spectroscopy using the molecular weight of the PB precursor obtained by SEC in THF calibrated against PB standards.

3.3.2. Nuclear Magnetic Resonance Spectroscopy (^1H NMR)

^1H NMR spectra were recorded in a Bruker AC 250 spectrometer at 250 MHz. Triblock

terpolymer samples before hydrogenation were measured from solutions in $CDCl_3$ at room

temperature. Hydrogenated samples were dissolved in d_8-toluene at 70 °C for 3 hours and

measured at 40 °C. Solutions were prepared with 20 mg of the polymer in 0.8 ml of the

corresponding solvent. Tetramethylsilane (TMS) was used as internal standard in all cases.

3.3.3. Transmission Electron Microscopy (TEM)

The bulk morphology of the synthesized triblock terpolymers was studied by bright field

TEM. A Zeiss CEM 902 electron microscope operated at 80 kV and a FEI Tecnai 20

operated at 200 kV were used. Polymer films were cast from a 3 wt-% polymer solution in hot toluene. The solutions were allowed to evaporate inside an exsiccator provided with toluene atmosphere and a hot-plate at 70 °C. The high temperature was employed in order to avoid gelation upon solvent evaporation. After complete evaporation of the solvent (ca. 1 week), the films were slowly cooled to room temperature followed by drying under vacuum at room temperature for 1 day. A final film thickness around 0.5 mm was obtained. Thin sections of thickness between 50 and 100 nm were cut at ‑ 130 °C with a Reichert-Jung Ultracut E microtome equipped with a diamond knife. Contrast among the blocks was achieved by staining with either OsO_4 vapor for 60 sec or RuO_4 vapor for 30 min. The non-hydrogenated precursors were stained by exposure to OsO_4 vapor, which stains preferentially the PB block, and slightly the PS block. The amorphous PEO and PS segments in the hydrogenated terpolymers were stained by exposure to RuO_4 vapor, which leads to a preferential staining of the PEO/PS microdomain interphase.

3.3.4. Small Angle X-Ray Scattering (SAXS)

The bulk morphology was complementary studied by means of temperature dependant small angle X-ray scattering (SAXS). The experiments were carried out at the A2 beamline of DORIS III, HASYLAB at DESY, Germany. The temperature controlling system already available in the line was adapted to use liquid nitrogen as a cooling fluid. The control parameters of the controller were adjusted to optimize the operation under the experimental conditions. This allowed the equipment to cool down in a controlled manner using rates up to 40 K.min^{-1}. A 2D SAXS detector was used, with a sample – detector distance of 3250 mm and the wavelength was set to 1.5 Å.

Triblock terpolymer films prepared by casting from toluene solutions, as described in section 3.3.3., were used for the experiments. The samples were kept at 25 °C for 1 min, then heated up to 120 °C at 10 °C/min, kept 3 min at 120 °C in order to assure complete

melting, and cooled down to 25 °C at 10 °C/min. The SAXS diffraction patterns were recorded during the temperature program with proper time frames.

3.3.5. TappingMode^{TM} Atomic Force Microscopy

The AFM experiments were carried out on a "Digital Instruments" MultiMode^{TM} AFM (NanoScope IV controller) operating in tapping mode at ambient conditions. Commercial silicon TM AFM tips (model MPP 12100) with a free resonance frequency in the range from 123 to 151 kHz and spring constants in the range from 5 to 10 N/m were employed for the measurements.

Triblock terpolymer thin films were prepared by spin coating 10.0 wt/v-% polymer solutions in toluene. The solutions were spun on cleaned polished silicon wafers, at 2000 rpm during 20 sec. The silicon wafers were previously cleaned in a water-saturated UV-ozone atmosphere for at least 24 hours. The resultant films were immediately annealed at 200 °C under N_2 during 60 min on a Linkam THMS 600 hotstage equipped with a TMS 91 controller. Further thermal treatments could be applied on the thin films, either on the Linkam hotstage (temperatures above room temperature), in a fridge (0 °C) or in a freezer (-26 °C).

Swelling experiments. Terpolymer thin films prepared as described above were subjected to swelling with water. For this purpose, a drop of Millipore water was deposited on the film after spin-coating and annealing 60 min at 200 °C. This amount was enough to cover a significant area of the polymer film on the wafer, without covering it completely. In this way, control measurements could be carried out on the same sample after the treatment. After 30 min, the excess of water was removed with a pipette. The partially wet surface was measured immediately.

Temperature dependant experiments. The temperature dependant measurements were conducted employing a commercial thermal accessory supplied by the microscope

manufacturer. Heating of the sample, which was performed with a Pt-resistive element underneath the sample puck, was accompanied by heating of a probe. The employed dual heating has the advantage of proving a more controlled sample temperature and stable tapping mode imaging at elevated temperatures. The sample compartment was continuously purged with a light stream of He gas, in order to prevent block copolymer oxidation at high temperatures.

3.3.6. Differential Scanning Calorimetry (DSC)

The equipment employed for the DSC measurements was a Perkin-Elmer PYRIS 1 differential scanning calorimeter in dry nitrogen atmosphere with a CCA 7 liquid nitrogen cooling device. For all measurements, a two-point calibration with n-decane and indium was carried out, followed by two-point furnace calibration at 50 °C and 150 °C. Standard aluminum pans of 50 μL were used to encapsulate polymer samples of 8.0 ± 0.5 mg.

Standard scans. Heating and cooling scans were performed by initially heating the sample up to 120 °C and holding it at that temperature for 3 min in order to erase effects resulting from any previous thermal history. Then, the sample was cooled down to –100 °C and kept at that temperature for 1 min for the sake of equipment stabilization. Finally, a second heating scan up to 120 °C was applied. All the standard scan experiments were carried out at a scanning rate of 10 °C/min. As a general rule, the shown cooling traces correspond to the first cooling, while the shown heating traces correspond to the following (second) heating scan. In this way, the analyzed traces correspond to the applied thermal history and are independent of the previous treatments, i.e., conditions of precipitation from solution, storage, etc. The degree of crystallinity (α_c) for the PEO blocks was calculated from the measured heat of fusion normalized by the block content, while the degree of crystallinity for the PE blocks was determined from the normalized heat of

crystallization, since the estimation of the heat of fusion resulted uncertain due to the vicinity of the melting endotherms of both blocks.

Isothermal scans. The determination of the isothermal crystallization of PE in the hydrogenated samples or of PEO block either in the non-hydrogenated or in the hydrogenated terpolymers was achieved by two different thermal protocols. As a preparation step for the isothermal experiments, the minimum crystallization temperature $T_{c, min}$ was determined in all cases. This temperature is the lowest value of T_c such that crystallization does not occur during the fast cooling scan. In order to determine whether crystallization has occurred, the endotherm of the immediate heating after the quenching to T_c was recorded. $T_{c, min}$ is the lowest temperature where no heat of fusion was seen in the endotherm.

PE block and PEO block in non-hydrogenated terpolymers: samples were initially heated up to 120 °C and held during 3 min at that temperature in order to erase thermal history. Later, they were quenched down to T_c at 80 °C/min, and the isothermal crystallization at the selected temperature was followed for a time long enough to warranty the crystallization occurs until saturation.

PEO block in hydrogenated terpolymers: the previous thermal history of the samples was also erased by heating them up to 120 °C and holding at the temperature for 3 min. This was followed by a cooling scan down to –100 °C at 10 °C/min, in order to induce crystallization in both PE and PEO blocks. A heating scan was performed at 10 °C/min up to 70 °C, and the sample was kept at that temperature for 75 min. This procedure produces the complete melting of the PEO block, while the PE block reaches saturation in crystallization degree. The conditions were carefully chosen so no further PE crystallization took place during the following step. The sample then was cooled down to

T_c at 80 °C/min, and the isothermal crystallization of the PEO block was recorded during the appropriate crystallization time.

Step crystallization: when the crystallization enthalpy is very low, the signal to noise ratio might be too low and the calculated degree of crystallization as a function of time have high associated errors. In order to overcome this difficulty, the isothermal crystallization was followed by the so-called "step crystallization" method. The initial step was, as explained before, to heat the sample up to 120 °C and hold it for 3 min at that temperature in order to erase thermal history. Then, the sample was quenched down to T_c at 80 °C/min, and kept at that temperature for a given time t_c. Later, the sample was heated up to 120 °C at 10 °C/min and the melting enthalpy of the crystals formed at T_c during t_c was determined. This procedure was carried out several times, employing crystallization times that vary from 0.1 min to 300 min, or until a saturation in the melting enthalpy was reached. The obtained saturation enthalpy was assigned to a degree of crystallinity of 100 % ($\Delta H_{100\%}$), and it therefore was possible to calculate the degree of crystallinity for each crystallization time.

Self-nucleation (SN) experiments. The procedure employed in the self-nucleation experiments is based on the one described by Fillon et al.[8] A representation of the thermal protocol is depicted in Figure 3.2. The self-nucleation domains are identified analyzing the steps (e) and (f) for a wide range of self-nucleation temperatures, as will be described later. The domain delimitation is then carried out on top of a standard heating scan, as shown in Figure 3.3.

The steps identified in Figure 3.2 correspond to the following: (a) melting of the sample in order to erase any previous thermal history, which was achieved at 120 °C during 5 min; (b) creation of a new ''standard'' thermal history by subsequent cooling to -100 °C at a controlled rate of 10 °C/min, and keeping the sample for 1 min at that temperature for the

sake of equipment stability; (c) partial or complete melting of the sample by heating up to the "self-nucleation temperature", T_s, at 10 °C/min (d) thermal conditioning achieved by keeping the sample at T_s for 5 min.
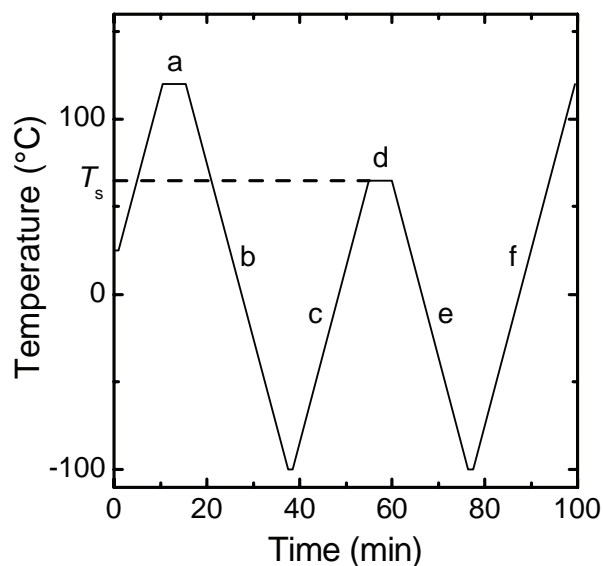
Figure 3.2. Representation of the thermal protocol employed in the self-nucleation experiments.

Depending on the chosen T_s, the crystalline domains could completely melt, only self-nucleate, or self-nucleate and anneal during this step. When T_s is sufficiently high, any self-nuclei or crystal fragments remain unmolten. In the range of temperatures with that characteristic, the sample is said to be under "Domain I", also known as the complete melting domain. At lower T_s values, some small crystal fragments can remain unmolten in the sample. They will act as self-nuclei during any immediate subsequent cooling, and the sample is said to be under "Domain II", the self-nucleation domain. At last, when the chosen T_s is too low, the crystals are only partially molten. The remaining crystals experience annealing during the 5 min at T_s and the molten crystals self-nucleate during the posterior cooling. In that case, the sample is under the self-nucleation and annealing domain, or "Domain III".
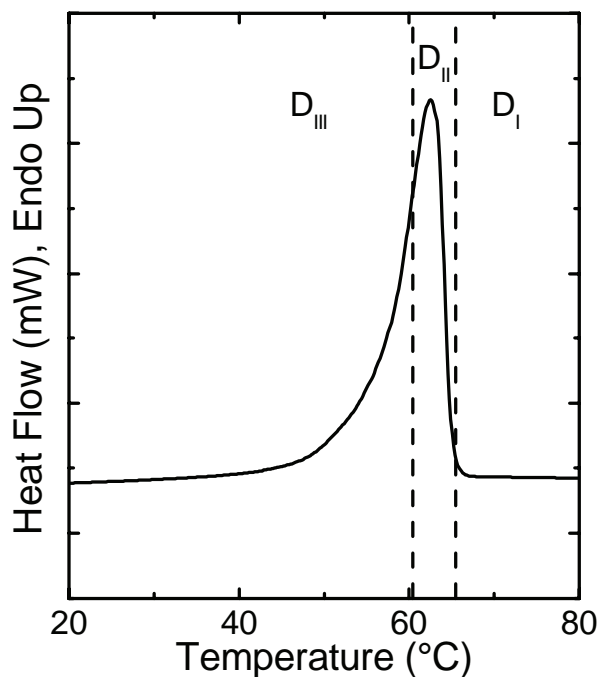
Figure 3.3. Representation of self-nucleation domain identification on a DSC heating scan.

The last steps in Figure 3.2 are (e) a cooling scan from T_s to -100 °C at 10 °C/min will reveal the effects of the applied thermal treatment on the crystallization signals; and (f) and the following heating scan at 10 °C/min up to 120 °C will make evident the effects of the thermal history on the melting signal. The analysis of the results of these steps provides the domain identification, as shown in Figure 3.3.

3.4. References

1. Esswein, B.; Molenberg, A.; Möller, M. Macromol. Symp. 1996, 107, (331-340).
2. Esswein, B.; Möller, M. Angew. Chem. 1996, 108, 703-705.
3. Esswein, B.; Steidl, N. M.; Möller, M. Macromol. Rapid Commun. 1996, 17, 143-148.
4. Förster, S.; Krämer, E. Macromolecules 1999, 32, 2783-2785.
5. Zhu, L.; Chen, H.-L.; Calhoun, B. H.; Ge, Q.; Quirk, R. P.; Thomas, E. L.; Hsiao, B. S.; Yeh, F.; Lotz, B. Polymer 2001, 42, 5829-5839.
6. Floudas, G.; Vazaiou, B.; Schipper, F.; Ulrich, R.; Wiesner, U.; Iatrou, H.; Hadjichristidis, N. Macromolecules 2001, 34, 2947-2957.

7. Schmalz, H.; Knoll, A.; Müller, A. J.; Abetz, V. Macromolecules 2002, 35, (27), 10004-10013.

8. Fillon, B.; Wittmann, J. C.; Lotz, B.; Thierry, A. Journal of Polymer Science Part B: Polymer Physics 1993, 31, 1383-1393.

Chapter 4. Synthesis and characterization of novel linear PB-*b*-PS-*b*-PEO and PE-*b*-PS-*b*-PEO triblock terpolymers

Novel polybutadiene-*block*-polystyrene-*block*-poly(ethylene oxide) (PB-*b*-PS-*b*-PEO) linear triblock terpolymers have been synthesized by sequential living anionic polymerization. Further catalytic hydrogenation lead to polyethylene-*block*-polystyrene-*block*-poly(ethylene oxide) (PE-*b*-PS-*b*-PEO), a triblock terpolymer with two crystallizable blocks and a glassy middle block. Bulk morphologies have been studied by transmission electron microscopy (TEM) and small angle X-ray scattering (SAXS) for different compositions. Thermal properties of the PEO block, as determined by differential scanning calorimetry (DSC), showed dependence with the block volume fraction (ϕ_{PEO}) and its polymerization degree (N_{PEO}). The corresponding properties for the PE block are also functions of the polymerization degree (N_{PE}) and the volume fraction of the PEO block (ϕ_{PEO}). Since the PEO block is the first to segregate from solution in toluene, its volume fraction determines the overall morphology and consequently the thermal properties of the studied terpolymers.

4.1. Introduction

Block copolymers constitute an intensively studied field due to their ability of self-assembly into ordered microphases in case the blocks are incompatible.[1] The polymer-polymer interaction will generally drive the separation into microphases according to the volume fractions of the different blocks. If other processes come into play, such as crystallization, then the microphase separation from the homogeneous melt will compete

with the development of crystals. Therefore, crystallization can occur within the microdomains and be confined into a given geometry (spheres, cylinders, lamellae), or it can overcome the previously generated microphases and undergo the so-called *break-out crystallization*.[2,3]

The morphology of diblock copolymers with one crystallizable block has already been studied for polybutadiene-*block*-poly(ethylene oxide),[4,5] polystyrene-*block*-poly(ethylene oxide)[6-9] and polystyrene-*block*-polyethylene[10-12] among many others,[2,13] where confined crystallization was observed and the melt morphology was preserved.

An even more complicated situation is given by increasing the number of crystallizable blocks within diblock copolymers or triblock terpolymers with two crystalline blocks. In those cases the morphology generation is now in competition with two crystallization processes, and the crystallization of the block crystallizing at lower temperature can be either enhanced or disturbed by the already crystallized block. Some examples are the studies of poly(ε-caprolactone)-*block*-poly(ethylene oxide),[14,15] poly(*p*-dioxanone)-*block*-poly(ε-caprolactone),[16-18] polyethylene-*block*-poly(ethylene oxide),[19] poly(L-lactide)-block-poly(ε-caprolactone),[20,21] polystyrene-*block*-poly(ethylene oxide)-*block*-poly(ε-caprolactone)[22] and polystyrene-*block*-polyethylene-*block*-poly(ε-caprolactone).[23-25] The crystallization of diblock copolymers and terpolymers with more than one crystallizable block has been the subject of a recent review.[26]

In this chapter the synthesis of novel polybutadiene-*block*-polystyrene-*block*-poly(ethylene oxide)s with different compositions and their hydrogenation into polyethylene-*block*-polystyrene-*block*-poly(ethylene oxide)s by sequential anionic polymerization is presented. The morphology of the triblock terpolymers was studied by means of transmission electron microscopy (TEM) and small angle X-ray scattering (SAXS). The thermal properties were determined by standard differential scanning calorimetry (DSC) measurements. The

values corresponding to the PEO block are here reported as a function of the volume fraction of the block in the terpolymer and the corresponding molecular weight. In this way we are able to account the effect of the morphology in terms of the volume fraction, but also in terms of the molecular weight, which is of particular importance on the crystallization. Meanwhile, the properties calculated for the PE block are presented as a function of the polymerization degree and the volume fraction of either the PE or the PEO block. The last variable was employed because the PEO block is driving the microphase separation during the sample preparation.

4.2. Experimental Part

4.2.1. Synthesis

Anionic polymerization was carried out using solvents and monomers purified according to procedures described elsewhere.[27,28] The synthesis of poly(1,4-butadiene)-*block*-polystyrene-*block*-poly(ethylene oxide) (PB-*b*-PS-*b*-PEO) triblock terpolymers was realized by sequential anionic polymerization of butadiene, styrene, and ethylene oxide in benzene at 60 °C for butadiene and 40 °C for styrene and ethylene oxide using *sec*-BuLi as initiator. Polymerization of ethylene oxide in the presence of a lithium counterion was accomplished by using the strong phosphazene base *t*-BuP$_4$ (Fluka, 1 M in hexane, Li$^+$:*t*-BuP$_4$ 1:1).[8,29-33] The polymerization of ethylene oxide was completed after 3 days and terminated with a mixture of methanol/acetic acid (1/5: v/v) followed by precipitation in isopropanol. In the notation employed here ($A_xB_yC_z^m$), subscripts denote the percentage mass fraction of each block component and superscripts indicate the overall number-averaged molecular weight M_n in kg/mol of the block copolymer.

4.2.2. Hydrogenation

The hydrogenation of the PB-*b*-PS-*b*-PEO terpolymers (precursors) leads to PE-*b*-PS-*b*-PEO terpolymers. Homogeneous catalytic hydrogenation was carried out with Wilkinson catalyst $(Ph_3P)_3Rh(I)Cl$ (Aldrich, 1 mol-% with respect to the number of double bonds) in degassed toluene (1.53 wt-% solution of the terpolymer) at 60 °C and 60 bar H_2 pressure for 3 days. ^{1}H NMR results of the hydrogenated terpolymers were used to confirm whether the PB block is completely hydrogenated. Further purification in order to eliminate residual Wilkinson catalyst was achieved by precipitation into isopropanol followed by refluxing a toluene solution (0.7 wt-% solution of the terpolymer) with a small amount of concentrated hydrochloric acid, again followed by precipitation into isopropanol.

4.2.3. Size Exclusion Chromatography (SEC)

SEC experiments of the polymer solutions in THF (2 wt/v-%) were performed on a Waters instrument calibrated with narrowly distributed polybutadiene standards at 30 °C. Four PSS-SDV columns (5 µm, Polymer Standards Service, Mainz) with a porosity range from 10^2 to 10^5 Å were used together with a differential refractometer and a UV-detector at 254 nm. Measurements on the non-hydrogenated triblock copolymers were performed in THF with a flow rate of 1 ml/min using toluene as internal standard.

4.2.4. Nuclear Magnetic Resonance Spectroscopy (^{1}H NMR)

^{1}H NMR spectra were recorded using a Bruker AC 250 spectrometer at 250 MHz. Non-hydrogenated samples were measured as solutions in $CDCl_3$ at room temperature, while hydrogenated samples were dissolved in d_8-toluene and measured at 40 °C. Solutions were prepared with 20 mg of the polymer in 0.8 ml of the corresponding solvent. Spectra were referenced to tetramethylsilane (TMS) as internal standard.

4.2.5. Transmission Electron Microscopy (TEM)

The bulk morphology of PE-*b*-PS-*b*-PEO terpolymers and their corresponding precursors was studied by bright field TEM using a Zeiss CEM 902 electron microscope operated at 80 kV and a FEI Tecnai 20 operated at 200 kV. Films (around 0.5 mm thick) were prepared by casting from a 3 wt-% solution of the terpolymer in toluene at 70 °C in order to avoid gelation upon solvent evaporation. After complete evaporation of the solvent (ca. 1 week), the films were slowly cooled to room temperature followed by drying under vacuum at room temperature for 1 day. Thin sections (thickness 50 – 100 nm) were cut at - 130 °C using a Reichert-Jung Ultracut E microtome equipped with a diamond knife. In the hydrogenated terpolymers, staining of amorphous PEO and PS segments was accomplished by exposure of the thin sections to RuO_4 vapor for 30-40 min, which leads to a preferential staining of the PEO/PS microdomain interphase. The non-hydrogenated precursors were stained by exposure to OsO_4 vapor for 60 sec, staining preferentially the PB block, and the PS block to a smaller extend.

4.2.6. Small Angle X-Ray Scattering (SAXS)

The material morphology was studied by means of temperature dependant small angle X-ray scattering (SAXS) at the A2 beamline of DORIS III, HASYLAB at DESY, Germany, using a temperature controlling system with liquid nitrogen as cooling fluid and 2D SAXS detector. The sample – detector distance was 3250 mm and the wavelength was 1.5 Å. During the experiment, the sample was kept at 25 °C for 1 min to stabilize it, then heated up to 120 °C at 10 °C/min, kept 3 min at 120 °C in order to assure complete melting, and cooled down to 25 °C at 10 °C/min. The SAXS diffraction patterns were recorded during the temperature program with 20 s frames starting every 30 s. Films cast as described in the previous section were used for the experiments.

4.2.7. Differential Scanning Calorimetry (DSC)

A Perkin-Elmer PYRIS 1 differential scanning calorimeter in a dry nitrogen atmosphere with a CCA 7 liquid nitrogen cooling device was utilized. For all measurements a two-point calibration with n-decane and indium was carried out. Samples of 8 ± 0.5 mg were placed in the DSC pans. Standard heating and cooling scans were performed. The samples were heated up to 120°C in order to exclude effects resulting from any previous thermal history, held at that temperature for 3 min and then cooled down to –100 °C followed by the heating scan up to 120 °C. All experiments were carried out at a scanning rate of 10 °C/min. The shown cooling traces correspond to the first cooling, and the shown heating traces correspond to the following (second) heating scan. The degree of crystallinity for the PEO blocks was established from the normalized heat of fusion, while the degree of crystallinity for the PE blocks was calculated from the normalized heat of crystallization due to the vicinity of the melting endotherms of both blocks.

4.3. Results and Discussion

4.3.1. Synthesis

The PE-*b*-PS-*b*-PEO linear triblock terpolymers were prepared by homogeneous catalytic hydrogenation of the corresponding PB-*b*-PS-*b*-PEO linear triblock terpolymers. The synthesis of PB-*b*-PS-*b*-PEO terpolymers was accomplished by sequential anionic polymerization of butadiene, styrene, and ethylene oxide in benzene, as illustrated in Scheme 4.1. The polymerization of butadiene under the conditions employed leads to a preferential 1,4-addition (Table 4.1), which is essential in order to obtain the corresponding "high 1,4 hydrogenated PB" structure after hydrogenation, i.e., a random copolymer of ethylene and butene with a high ethylene content. Polymerization in a one-step procedure

was achieved using the strong phosphazene base t-BuP$_4$,[8,29-33] allowing polymerization of ethylene oxide despite the presence of a Li$^+$ counterion.
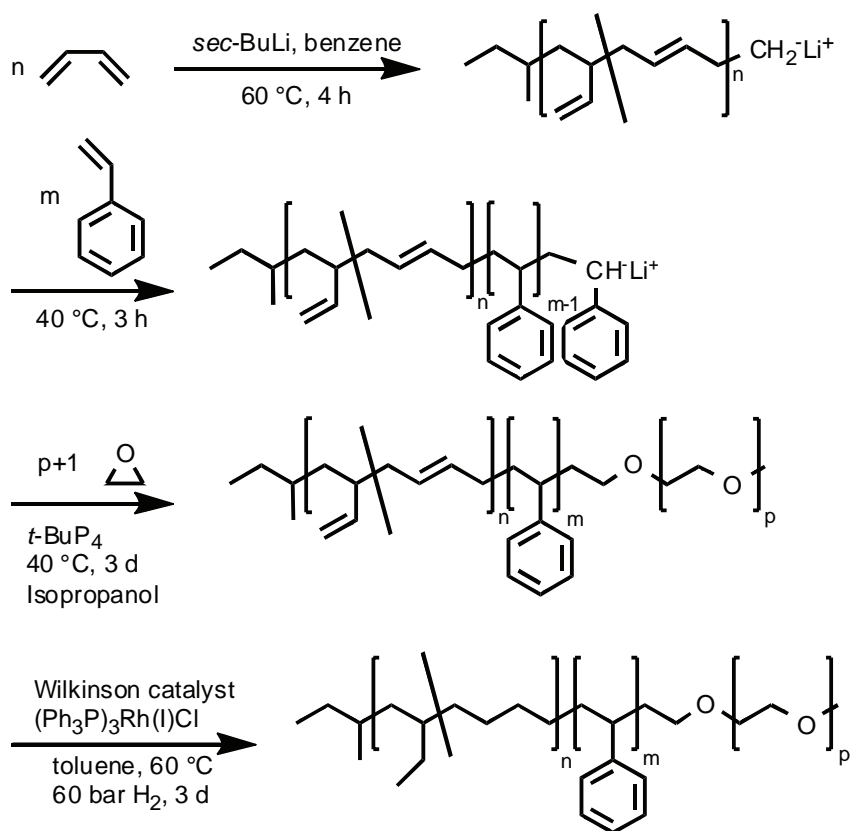
Scheme 4.1. Scheme of the sequential anionic polymerization of PB-b-PS-b-PEO.

Table 4.1. Molecular weight, molecular weight distributions and content of 1,2-units (wt-%) in the polybutadiene block of the PB-b-PS-b-PEO triblock terpolymers, and their hydrogenated PE-b-PS-b-PEO triblock terpolymers.

	M_n (kg/mol)			M_w/M_n
	PB[a] (% 1,2[b]) / PE[c]	PS[c]	PEO[c]	
B$_{29}$S$_{40}$EO$_{31}$[168] / E$_{29}$S$_{40}$EO$_{31}$[170]	48 (12.9) / 50	67	53	1.03
B$_{19}$S$_{34}$EO$_{47}$[142] / E$_{19}$S$_{34}$EO$_{47}$[143]	27 (12.8) / 28	48	67	1.03
B$_{19}$S$_{35}$EO$_{46}$[217] / E$_{19}$S$_{35}$EO$_{46}$[219]	41 (10.8) / 43	76	100	1.01
B$_{16}$S$_{68}$EO$_{16}$[210] / E$_{17}$S$_{67}$EO$_{16}$[211]	35 (11.5) / 36	142	33	1.01
B$_{16}$S$_{40}$EO$_{44}$[143] / E$_{16}$S$_{40}$EO$_{44}$[144]	22 (14.0) / 23	58	63	1.05
B$_{37}$S$_{16}$EO$_{47}$[76] / E$_{38}$S$_{16}$EO$_{46}$[77]	28 (11.8) / 29	13	36	1.03

[a] Determined by SEC in THF calibrated against PB standards. [b] Determined by ^{1}H NMR spectroscopy in CDCl$_3$. [c] Determined by ^{1}H NMR spectroscopy using the molecular weight of the PB precursor obtained by SEC in THF calibrated against PB standards.

SEC experiments (Figure 4.1) show that the reaction occurs without any significant termination, resulting in narrowly distributed PB-*b*-PS-*b*-PEO terpolymers (Table 4.1). Homogeneous catalytic hydrogenation was performed with a solution of the precursor triblock terpolymer in toluene using Wilkinson catalyst $(Ph_3P)_3Rh(I)Cl$ (Scheme 1). The hydrogenation efficiency under the experimental conditions was verified by ^1H NMR spectroscopy, showing a complete hydrogenation of the PB block (Figure 4.2).
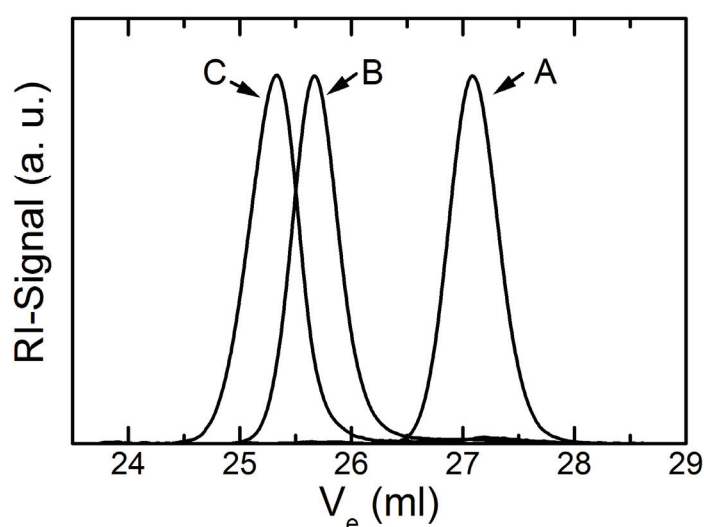
Figure 4.1. SEC traces of a synthesized PB-*b*-PS-*b*-PEO (C) linear triblock terpolymer including the PB (A) and PB-*b*-PS (B) precursors using THF as eluent, toluene as internal standard and a Bischoff RI detector.

4.3.2. Morphological characterization

PB-*b*-PS-*b*-PEO and PE-*b*-PS-*b*-PEO terpolymers were analyzed by transmission electron microscopy (TEM) and small angle X-ray scattering (SAXS) with the purpose of determining their morphology in bulk. In order to generate the contrast required for microscopy the non-hydrogenated triblock terpolymers were stained with OsO_4 vapor, leading to a preferential staining of the PB block, while the hydrogenated triblock

terpolymers were exposed to RuO_4 vapor, which favors the staining of the PEO/PS microdomain interphase. Figure 4.3 shows the TEM micrographs and Figure 4.4 the SAXS patterns for the PB-*b*-PS-*b*-PEO and their corresponding PE-*b*-PS-*b*-PEO triblock terpolymers (described in Table 4.1).
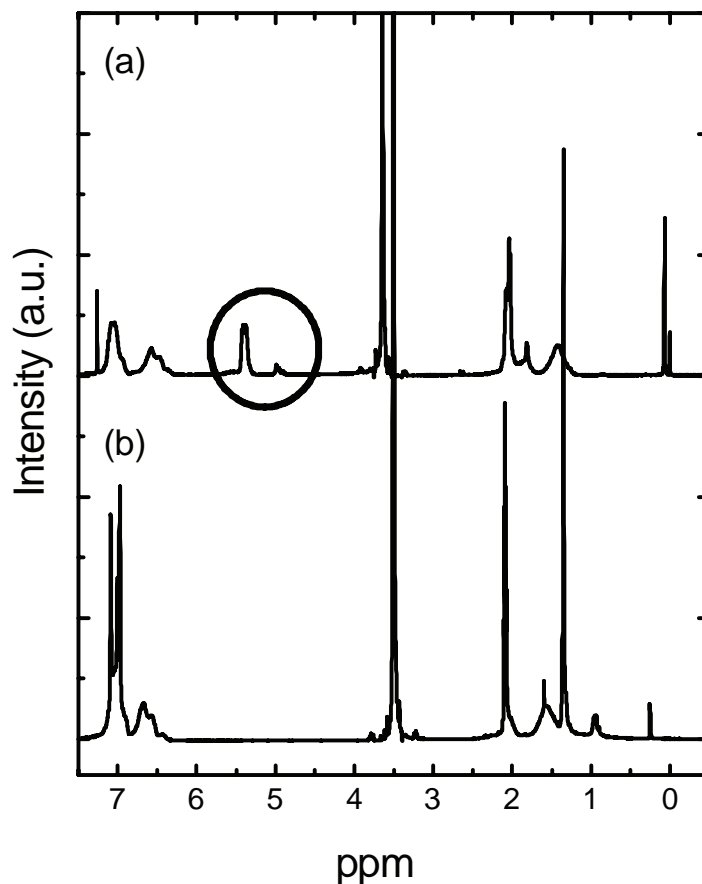
Figure 4.2. ^{1}H NMR spectra of a synthesized PB-*b*-PS-*b*-PEO (a) terpolymer and the corresponding PE-*b*-PS-*b*-PEO (b) terpolymer after hydrogenation with Wilkinson catalyst. Signals at δ = 5.8-5.4 ppm corresponding to -CH$_2$= bonds are presented in (a) (circled) but not in (b). Solvents employed were (a) CDCl$_3$, δ = 7.26 ppm; and (b) d$_8$-toluene, δ = 2.09 ppm.

Figure 4.3. TEM micrograph for PB-*b*-PS-*b*-PEO (OsO$_4$ stained) and PE-*b*-PS-*b*-PEO (RuO$_4$ stained) triblock terpolymers. Ultrathin sections were obtained from films cast from toluene solutions at 70 °C. *a*) B$_{16}$S$_{68}$EO$_{16}$[210], *b*) E$_{17}$S$_{67}$EO$_{16}$[211], *c*) B$_{29}$S$_{40}$EO$_{31}$[168], *d*) E$_{29}$S$_{40}$EO$_{31}$[170], *e*) B$_{16}$S$_{40}$EO$_{44}$[143], *f*) E$_{16}$S$_{40}$EO$_{44}$[144], *g*) B$_{19}$S$_{34}$EO$_{47}$[142], *h*) E$_{19}$S$_{34}$EO$_{47}$[143], *i*) B$_{19}$S$_{35}$EO$_{46}$[217], *j*) E$_{19}$S$_{35}$EO$_{46}$[219], *k*) B$_{37}$S$_{16}$EO$_{47}$[76], *l*) E$_{38}$S$_{16}$EO$_{46}$[77].

Figure 4.3. TEM micrograph for PB-*b*-PS-*b*-PEO (OsO$_4$ stained) and PE-*b*-PS-*b*-PEO (RuO$_4$ stained) triblock terpolymers. Ultrathin sections were obtained from films cast from toluene solutions at 70 °C. *a*) B$_{16}$S$_{68}$EO$_{16}$[210], *b*) E$_{17}$S$_{67}$EO$_{16}$[211], *c*) B$_{29}$S$_{40}$EO$_{31}$[168], *d*) E$_{29}$S$_{40}$EO$_{31}$[170], *e*) B$_{16}$S$_{40}$EO$_{44}$[143], *f*) E$_{16}$S$_{40}$EO$_{44}$[144], *g*) B$_{19}$S$_{34}$EO$_{47}$[142], *h*) E$_{19}$S$_{34}$EO$_{47}$[143], *i*) B$_{19}$S$_{35}$EO$_{46}$[217], *j*) E$_{19}$S$_{35}$EO$_{46}$[219], *k*) B$_{37}$S$_{16}$EO$_{47}$[76], *l*) E$_{38}$S$_{16}$EO$_{46}$[77].

Figure 4.4. SAXS patterns for PB-*b*-PS-*b*-PEO and PE-*b*-PS-*b*-PEO triblock terpolymers at the molten state (120 °C) and after cooling down at 10 °C/min to 0 °C. Films cast from toluene solutions at 70 °C. *a*) $B_{16}S_{68}EO_{16}$[210], *b*) $E_{17}S_{67}EO_{16}$[211], *c*) $B_{29}S_{40}EO_{31}$[168], *d*) $E_{29}S_{40}EO_{31}$[170], *e*) $B_{16}S_{40}EO_{44}$[143], *f*) $E_{16}S_{40}EO_{44}$[144], *g*) $B_{19}S_{34}EO_{47}$[142], *h*) $E_{19}S_{34}EO_{47}$[143], *i*) $B_{37}S_{16}EO_{47}$[76], *j*) $E_{38}S_{16}EO_{46}$[77].

The micrographs presented in Figure 4.3 and the scattering patterns in Figure 4.4 evidence different morphologies for the synthesized triblock terpolymers according to their compositions. For the non-hydrogenated triblock terpolymers, *fcc*–packed spheres ($B_{16}S_{68}EO_{16}{}^{210}$, Figure 4.3a and 4.4a), connected hexagonally packed cylinders ($B_{29}S_{40}EO_{31}{}^{168}$, Figure 4.3c and 4.4c) and lamellar morphologies ($B_{16}S_{40}EO_{44}{}^{143}$, Figure 4.3e and 4.4e, $B_{19}S_{34}EO_{47}{}^{142}$, Figure 4.3g and 4.4g, $B_{19}S_{35}EO_{46}{}^{217}$, Figure 4.3i and no SAXS pattern, and $B_{37}S_{16}EO_{47}{}^{76}$, Figure 4.3k and 4.4i are observed. The morphologies are formed by a compromise between PEO block crystallization and the interaction among the blocks (the segmental interaction parameters χ are listed in Table 4.2). With PEO being the less soluble block in the common solvent (i.e., toluene) and the only crystallizable block, it is expected to separate from the solution a lot earlier than PB or PS blocks, considering also that the PB/PS interaction parameter is the lowest among the three blocks. Therefore, the generated morphology will correspond to the one expected from a diblock, with a PEO block composition as in these triblocks. This may explain why four triblock terpolymers with different compositions but similar PEO block content (between 44 and 47 wt-%) show all a lamellar morphology. It should be noted that the behavior depends on the solvent quality. Further annealing of the samples for times longer than 6 hours or temperatures higher than 120 °C lead to more perfect structures, but did not change the morphology. It was not possible to determine whether those were equilibrium states, what was partially due to the high molecular weight of the terpolymers.

The SAXS patterns displayed in Figure 4.4 show better defined reflections in the molten state, meaning that the crystallization does affect the ordering of the microphases. However, most of the differences are in intensity and only slight shifts in q values were observed in some of the cases. Mostly no real order-disorder neither order-order phase

transitions were observed upon cooling the molten structure. Further insight will be given

in Chapter 5.

Table 4.2. Flory-Huggins-Staverman enthalpic segmental interaction parameters, calculated at different temperatures[a].

	T (°C)		
	25	60	120
$\chi_{PB/PS}$	0.047	0.042	0.036
$\chi_{PE/PS}$	0.096	0.086	0.073
$\chi_{PB/PEO}$	0.14	0.12	0.10
$\chi_{PE/PEO}$	0.17	0.16	0.13
$\chi_{PS/PEO}$	0.052	0.046	0.039

[a] According to Equation 4.1:

$$\chi = \frac{v}{RT}\left(\delta_i - \delta_j\right)^2 \qquad \text{(Equation 4.1)}$$

where v is the geometric average of the molar segmental volume calculated from the densities at room temperature (Density of the semicrystalline polymer were employed, using the correspondent crystallinity degrees calculated by DSC, and crystalline and amorphous values taken from the literature (ρ_{PB} = 0.9 kg/m^3, ρ_{PS} = 1.05 kg/m^3; $\rho_{am\text{-}PE}$ = 0.887 kg/m^3; $\rho_{cr\text{-}PE}$ = 0.999 kg/m^3; $\rho_{am\text{-}PEO}$ = 1.123 kg/m^3; $\rho_{cr\text{-}PEO}$ = 1.227 kg/m^3),[34] density corrections for the real temperature are neglected), RT is the molar thermal energy at the given temperature.[35,36] The solubility parameters δ were taken from the literature.[34,36]

From the results shown in Figure 4.3 and 4.4 it is evident that the overall morphology of

the non-hydrogenated triblock terpolymer is preserved in the corresponding hydrogenated

triblock terpolymer after the hydrogenation procedures. The dimensions calculated from

the patterns are presented in Table 4.3. Since in some cases the reflections are not well

distinguished at 0 °C, the dimensions corresponding to the molten state are presented. It is

worth noticing that the listed dimensions (i.e., lamellar spacing, sphere diameter) display

differences mainly due to the presence of a second crystallizable block (hydrogenated PB

or PE) which introduces restrictions and stresses to the microphase formation. Initially,

two effects were expected. If crystallization occurs within the microphase, this will

generate volume constrictions inside the given microphase due to increase in density. On

56

the other hand, if crystallization breaks-out or disrupt the microphase separation, then the crystals could dictate the morphology. The results here presented point towards the first situation. An example is given by the fact that the lamellar spacing of the lamellae-forming triblock terpolymers is always smaller after hydrogenation.

Table 4.3. Periodic distances (l) and diameters (D) of the microphases formed by the triblock terpolymers, determined from the SAXS patterns at 120 °C.

Non-hydrogenated terpolymers	Hydrogenated terpolymers	{hkl}	l (nm)	D (nm)
$B_{16}S_{68}EO_{16}{}^{210}$		111	75	25
	$E_{17}S_{67}EO_{16}{}^{211}$	111	97	36
$B_{29}S_{40}EO_{31}{}^{168}$		100	59	
	$E_{29}S_{40}EO_{31}{}^{170}$	100	54	
$B_{16}S_{40}EO_{44}{}^{143}$		100	82	
	$E_{16}S_{40}EO_{44}{}^{144}$	100	87	
$B_{19}S_{34}EO_{47}{}^{142}$		100	94	
	$E_{19}S_{34}EO_{47}{}^{143}$	100	87	
$B_{37}S_{16}EO_{47}{}^{76}$		100	75	
	$E_{38}S_{16}EO_{46}{}^{77}$	100	66	

Very interesting exceptions of the above mentioned tendency are the morphologies of $B_{16}S_{68}EO_{16}{}^{210}$ and $E_{17}S_{67}EO_{16}{}^{211}$ triblock terpolymers, as well as those corresponding to the pair of $B_{16}S_{40}EO_{44}{}^{143}$ and $E_{16}S_{40}EO_{44}{}^{144}$. In the case of $B_{16}S_{68}EO_{16}{}^{210}$ and $E_{17}S_{67}EO_{16}{}^{211}$, due to the low content of both end blocks, in the non-hydrogenated triblock the resulting morphology is a typical cubic *fcc* array of PB (black) and PEO (white) spheres (reflections at q^*, 1.6 q^*, 2 q^*). However, in the hydrogenated $E_{17}S_{67}EO_{16}{}^{211}$ we observed only one kind of PEO or PE containing spheres without a long-range order. Detailed work involving atomic force microscopy (AFM) measurements in order to investigate this particular case is the topic of Chapter 6.

The difference in morphology after hydrogenation of $B_{16}S_{40}EO_{44}$[143] is given by the slight increase in interaction parameter of the PE block with the other two blocks and its crystallization ability. We assume that the PEO is the first block separating from the solution, since it is the block with the lowest solublity in toluene in the non-hydrogenated terpolymer and the resultant morphologies do not vary significantly by hydrogenating the triblock terpolymer. After the PEO phase separation takes place, the PE is the first block to crystallize due to the set temperature for the film formation (none of the PEO blocks crystallizes above 70 °C, as will be presented later in Figure 4.7 and 4.8a). For this particular case, the crystallized PE cannot keep the lamellar morphology generated by the PEO block and causes a transformation of the PEO domains to cylinders. The PE domains could be distributed along the PS matrix forming a continuous phase, according to the TEM micrograph (Figure 4.3f). This fact points towards the possibility of disrupting the microphase separation by the PE crystallization under given conditions. Here we have only analyzed the morphologies after crystallization at 10 °C/min. The behavior could be affected when faster crystallization kinetics occurs, i.e., under quenching from the molten state.

4.3.3. Differential Scanning Calorimetry (DSC)

In order to analyze and properly compare the thermal behavior of the triblock terpolymers, the projection of a 3D plot using the volume fraction ϕ and the polymerization degree N as the x and y axes will be used for the sake of comparison. In this way, it is possible to appreciate the influence of the volume fraction independently of the molecular weight and vice versa. The corresponding values of volume fraction ϕ and the polymerization degree N are presented in Table 4.4.

All the standard scans (shown in Figure 4.5 and 4.6) were performed at 10 °C/min, after melting the sample at 120 °C in order to erase any previous thermal history. Figure 4.7

shows the crystallization temperatures T_c, the melting temperatures T_m and crystallinity α_c of the PEO block in the non-hydrogenated triblock terpolymers (PB-*b*-PS-*b*-PEO), as a function of the volume fraction ϕ and the polymerization degree N.

Table 4.4. Volume fraction ϕ^{a} of the PEO and PE blocks within the triblock terpolymers, as well as the polymerization degree, N, of the corresponding block.

Non-hydrogenated terpolymers	Hydrogenated terpolymers	ϕ_{PEO}	N_{PEO}	ϕ_{PE}	N_{PE}
$B_{16}S_{68}EO_{16}{}^{210}$		0.14	743		
	$E_{17}S_{67}EO_{16}{}^{211}$	0.14	743	0.19	643
$B_{29}S_{40}EO_{31}{}^{168}$		0.27	1196		
	$E_{29}S_{40}EO_{31}{}^{170}$	0.27	1196	0.34	887
$B_{37}S_{16}EO_{47}{}^{76}$		0.41	808		
	$E_{38}S_{16}EO_{46}{}^{77}$	0.40	808	0.43	523
$B_{16}S_{40}EO_{44}{}^{143}$		0.40	1440		
	$E_{16}S_{40}EO_{44}{}^{144}$	0.40	1440	0.19	413
$B_{19}S_{34}EO_{47}{}^{142}$		0.43	1521		
	$E_{19}S_{34}EO_{47}{}^{143}$	0.42	1521	0.23	503
$B_{19}S_{35}EO_{46}{}^{217}$		0.41	2268		
	$E_{19}S_{35}EO_{46}{}^{219}$	0.41	2268	0.23	765

[a] Determined assuming additive volumes. Density of the semicrystalline polymer were employed, using the correspondent crystallinity degrees calculated by DSC, and crystalline and amorphous values taken from the literature (ρ_{PB} = 0.9 kg/m^3, ρ_{PS} = 1.05 kg/m^3; $\rho_{\text{am-PE}}$ = 0.887 kg/m^3; $\rho_{\text{cr-PE}}$ = 0.999 kg/m^3; $\rho_{\text{am-PEO}}$ = 1.123 kg/m^3; $\rho_{\text{cr-PEO}}$ = 1.227 kg/m^3).[34]

Most of the triblock terpolymers presented two crystallization peaks corresponding to the PEO block. The low temperature exotherm was usually small and in several cases cannot be seen in Figure 4.5 in view of the scale employed to show all traces but was clearly visible upon scale magnification. These values are plotted in Figure 4.7 with the subscripts 1 and 2, corresponding to the low and high crystallization temperature, respectively. The subscripts are maintained even when one of the two peaks is not evident. This behavior is characteristic for fractionated crystallization and its origin is related to the difficulties that
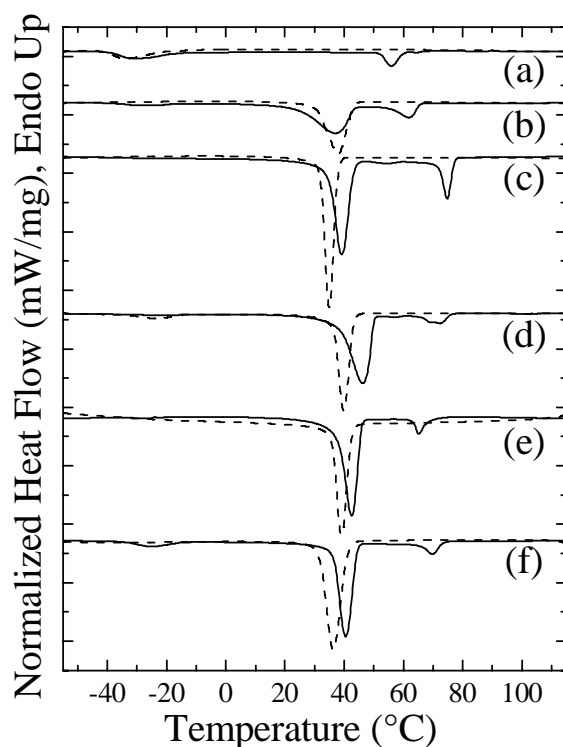
Figure 4.5. Standard DSC cooling traces recorded at 10 °C/min for the triblock terpolymers. The dashed traces correspond to the non-hydrogenated triblock terpolymers and the continuous traces correspond to the hydrogenated ones. *a*) $B_{16}S_{68}EO_{16}{}^{210}$ and $E_{17}S_{67}EO_{16}{}^{211}$, *b*) $B_{29}S_{40}EO_{31}{}^{168}$ and $E_{29}S_{40}EO_{31}{}^{170}$, *c*) $B_{37}S_{16}EO_{47}{}^{76}$ and $E_{38}S_{16}EO_{46}{}^{77}$, *d*)$B_{16}S_{40}EO_{44}{}^{143}$ and $E_{16}S_{40}EO_{44}{}^{144}$, *e*) $B_{19}S_{34}EO_{47}{}^{142}$ and $E_{19}S_{34}EO_{47}{}^{143}$, *f*) $B_{19}S_{35}EO_{46}{}^{217}$ and $E_{19}S_{35}EO_{46}{}^{219}$.

dispersed isolated phases encounter when the number of potentially crystallizing microdomains is orders of magnitude larger than the number of highly active heterogeneities in the system (more details of this well known behavior can be found in references).[13,37] In this case, the high temperature exotherm of the PEO block is due to the crystallization of microdomains that contain highly active heterogeneities and are probably connected with one another. The low temperature exotherm corresponds to the crystallization of strictly isolated microdomains that either nucleate homogeneously (because they do not have any nucleating heterogeneity) or superficially and therefore need extreme supercoolings to crystallize (i.e., close to the T_g of the PEO block). The

homogeneous nucleation of PEO nanospheres within block copolymers leads to peak crystallization temperatures (when cooled from the melt at 10 °C/min) of approximately -45 °C to -35 °C, while that of superficially nucleated droplets is speculated to occur at around -25 °C to -20 °C.[13,37]
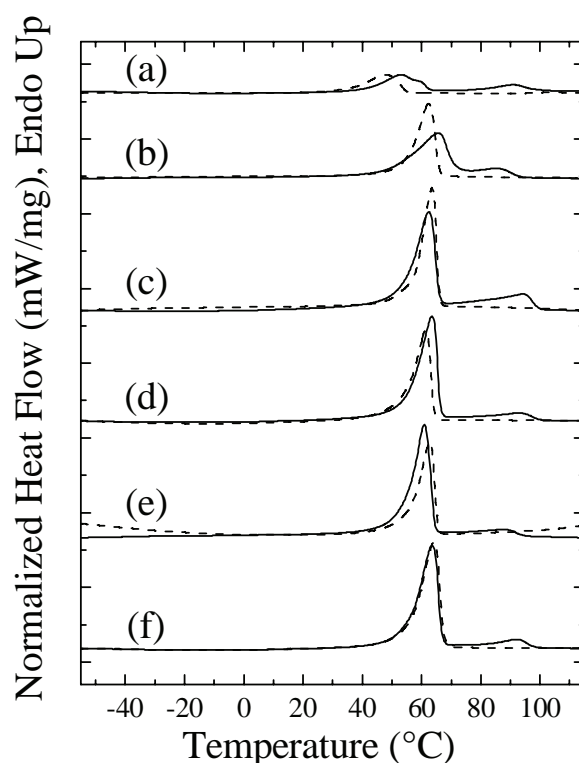
Figure 4.6. Standard DSC heating traces recorded at 10 °C/min for the triblock terpolymers. The dash traces correspond to the non-hydrogenated triblock terpolymers and the continuous traces correspond to the hydrogenated ones. *a*) $B_{16}S_{68}EO_{16}^{210}$ and $E_{17}S_{67}EO_{16}^{211}$, *b*) $B_{29}S_{40}EO_{31}^{168}$ and $E_{29}S_{40}EO_{31}^{170}$, *c*) $B_{37}S_{16}EO_{47}^{76}$ and $E_{38}S_{16}EO_{46}^{77}$, *d*)$B_{16}S_{40}EO_{44}^{143}$ and $E_{16}S_{40}EO_{44}^{144}$, *e*) $B_{19}S_{34}EO_{47}^{142}$ and $E_{19}S_{34}EO_{47}^{143}$, *f*) $B_{19}S_{35}EO_{46}^{217}$ and $E_{19}S_{35}EO_{46}^{219}$.

In Figure 4.7 the values of T_{c1}, T_{c2}, T_m and α_c for the PEO block within PB-b-PS-b-PEO are presented as a function of the block volume fraction, ϕ_{PEO}, and its polymerization degree, N_{PEO}. The plot of a projection of the thermal properties against these two values will allow the interpretation of the influence of block content independently from molecular weight. The effect of molecular weight on thermal transitions is well known,

but the effect of the volume fraction is more complicated since it indicates the influence of the microphase geometry on crystallization. Usually, it is expected that the thermal properties, i.e., T_c, T_m and α_c, increase with the polymerization degree.[38] Additionally, it has been observed that the properties also increase with the volume fraction in block copolymers when the molecular weight of the block is constant.[11] These tendencies are mostly shown by the presented results, as can be appreciated in Figure 4.7.

The values of crystallization temperature at low temperatures are presented in Figure 4.7a. Not all terpolymers presented a significant signal, since it will only occur when the PEO domain is isolated. It is peculiar that $B_{16}S_{40}EO_{44}^{143}$ ($\phi = 0.40$; $N = 1440$) shows the low temperature crystallization and corresponds to a lamellar morphology. This fact reflects that connectivity among the lamellae is not high enough and some of the material is therefore isolated, showing the effects of a homogeneous or superficial nucleation. Additionally, it could seem curious that $B_{19}S_{35}EO_{46}^{217}$ (0.41; 2268) showed a signal corresponding to T_{c1}, being the block with the higher volume fraction and molecular weight among the studied terpolymers. This could be related to the high molecular weight that implies a high segregation strength among the blocks. If this high segregation results in a low connectivity between the microphases, then the crystallization temperature could decrease significantly and even fractionate, as observed in this case. Note that the T_{c1} is lower for $B_{19}S_{35}EO_{46}^{217}$ than the one for $B_{16}S_{40}EO_{44}^{143}$ despite the molecular weight difference, indicating a higher amount of isolated lamellae in the former triblock terpolymer. Additionally, it was already mentioned that the structures were not everywhere in the sample in the equilibrium state, and therefore a small fraction could form a structure other than lamellae. Due to its high molecular weight, it would be more difficult for $B_{19}S_{35}EO_{46}^{217}$ to achieve the equilibrium.
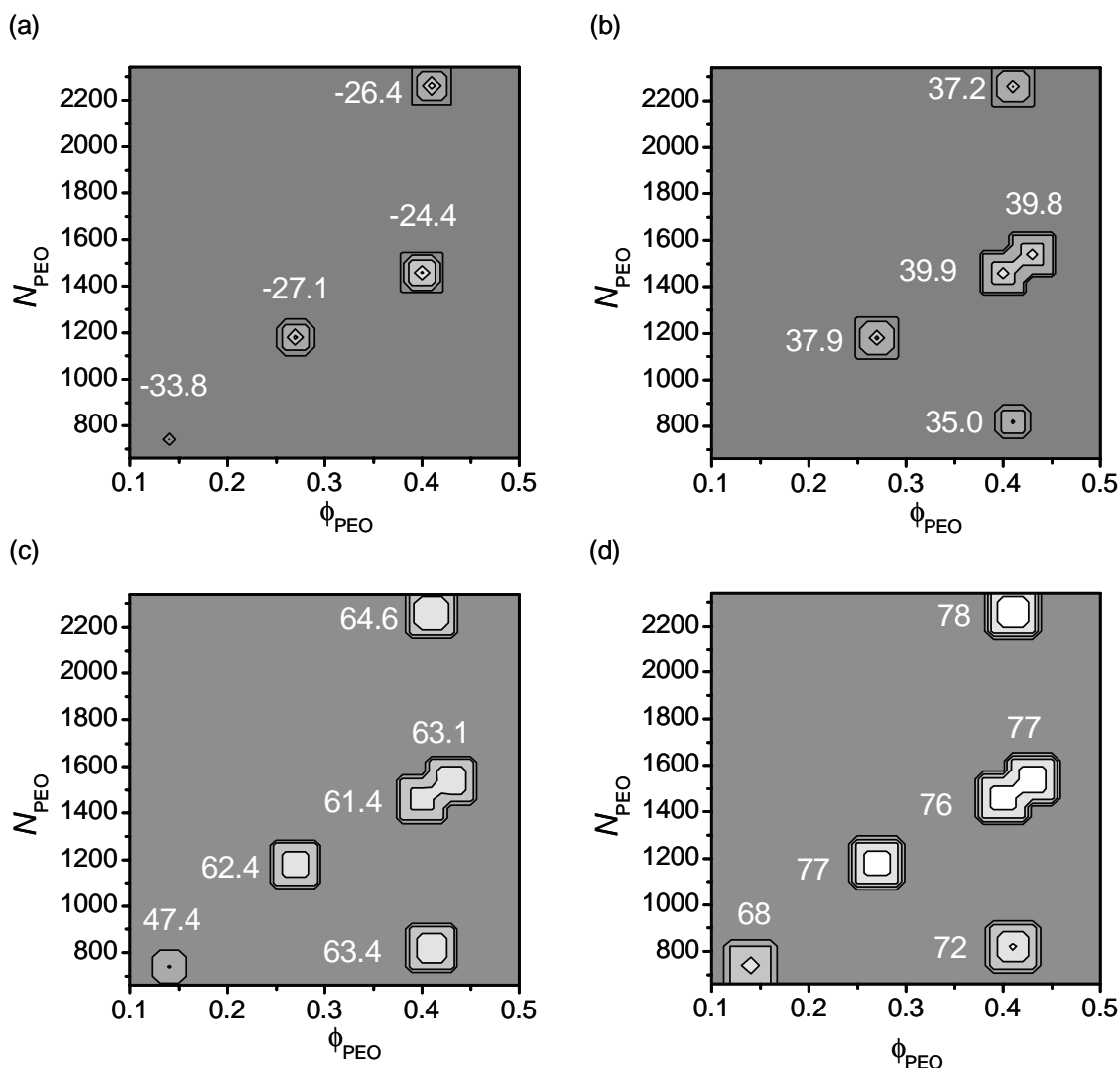
Figure 4.7. (a) T_{c1}, (b) T_{c2}, (c) T_m and (d) α_c for the poly(ethylene oxide) block within the PB-*b*-PS-*b*-PEO triblock terpolymers as a function of ϕ_{PEO} and N_{PEO}. The color scale is lighter for higher values, and the numbers indicate the peak values. The crystallinity degree was calculated considering $\Delta H_{100\%} = 8.7$ kJ/mol,[34] and normalizing the ΔH with the block weight.

Figure 4.7b shows the crystallization temperature values at high temperatures, T_{c2}, corresponding to heterogeneous nucleation. The effect of the polymerization degree is stronger than the one of the volume fraction, as shown by $B_{29}S_{40}EO_{31}{}^{168}$ (0.27; 1196) having a higher T_{c2} than $B_{37}S_{16}EO_{47}{}^{76}$ (0.40; 808). The low T_{c2} value presented by $B_{19}S_{35}EO_{46}{}^{217}$ is due to the lack of connectivity discussed previously. There is no signal corresponding to $B_{16}S_{68}EO_{16}{}^{210}$ (0.14; 743). This, together with its low value of peak

crystallization temperature T_{c1} indicate that most of the blocks are crystallizing from homogeneous nuclei generated within the isolated microdomains.[3,4,5,13,37,39,40]

The behavior corresponding to T_m is presented in Figure 4.7c. There is a marked difference between $B_{16}S_{68}EO_{16}{}^{210}$ and all the other terpolymers. The melting point is significantly lower when the material has crystallized in isolated domains exclusively. The corresponding values for the other terpolymers do not differ much, which is expected due to the crystal rearrangements that take place during heating. Finally, Figure 4.7d shows the variations in the crystallinity degree with N and ϕ for the PEO block. It is important to highlight that the percentage crystallinities derived from integrating enthalpies of DSC data have a large error, because of base line fluctuations and uncertainties in establishing the limits of integration. Therefore, the variations here observed should not be taken too rigorously within the associated error. However, one could say that α_c is observed to increase with both polymerization degree and volume fraction.

A representation of the thermal properties for the PEO block in the hydrogenated triblock terpolymers is presented in Figure 4.8. The crystallization temperature is presented for low temperatures, T_{c1} (Figure 4.8a) and high temperatures, T_{c2} (Figure 4.8b). The behavior of $E_{17}S_{67}EO_{16}{}^{211}$, $E_{29}S_{40}EO_{31}{}^{170}$, $E_{16}S_{40}EO_{44}{}^{144}$ and $E_{19}S_{35}EO_{46}{}^{219}$ for T_{c1} remains the same as it was before the hydrogenation (Figure 4.7a), mainly increasing with ϕ and N, with the particular case of $E_{19}S_{35}EO_{46}{}^{219}$ (0.41; 2268) being lower than $E_{16}S_{40}EO_{44}{}^{144}$ (0.40; 1440) due to a better segregation based on a higher molecular weight. However, new signals with low enthalpy changes appear for low temperature crystallization of $E_{19}S_{34}EO_{47}{}^{143}$ (0.42; 1521) and $E_{38}S_{16}EO_{46}{}^{77}$ (0.40; 808), at very low T_{c1} values. This indicates that a very small population of PEO chains is crystallizing in isolated domains. Those domains have to be generated by the presence of either the PE block ($\chi_{PB/PEO}$ is slightly lower than

χ PE/PEO, as reported in Table 4.2) or the PE crystals (physical constrains), since they were not evident on the non-hydrogenated terpolymers.
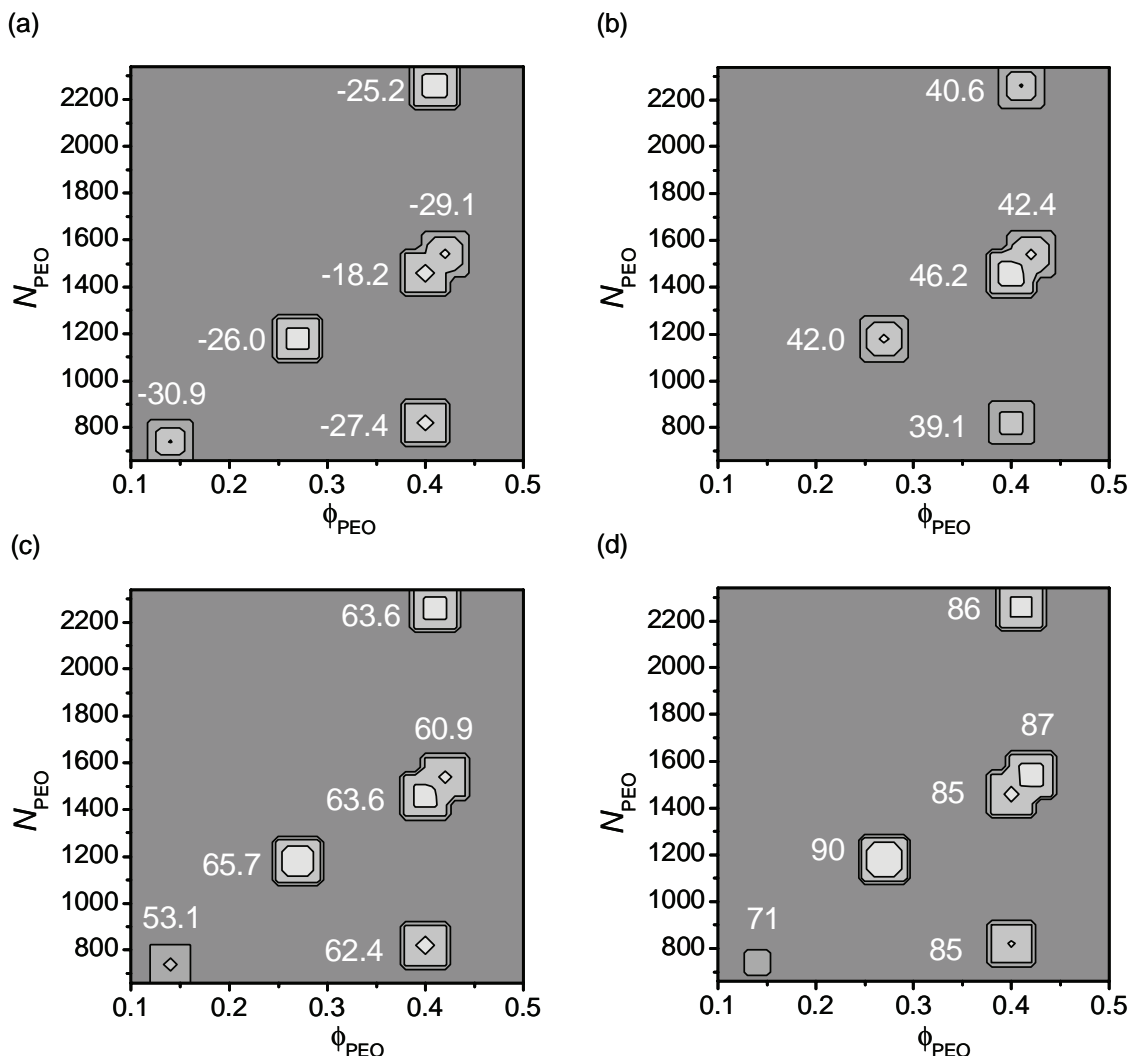
Figure 4.8. (a) T_{c1}, (b) T_{c2}, (c) T_m and (d) α_c for the poly(ethylene oxide) block within the PE-*b*-PS-*b*-PEO triblock terpolymers as a function of ϕ_{PEO} and N_{PEO}. The color scale is lighter for higher values, and the numbers indicate the peak values. The crystallinity degree was calculated considering $\Delta H_{100\%} = 8.7$ kJ/mol,[34] and normalizing the ΔH with the block weight.

The high crystallization temperature T_{c2} shown in Figure 4.8b shows the same tendency as the corresponding non-hydrogenated terpolymers presented in Figure 4.7b and discussed previously. The polymerization degree has a greater influence than the volume fraction,

the high molecular weight reflects high segregation strength and therefore isolated domains, and a very low volume fraction of PEO can lead to completely isolated domains that crystallize exclusively at low temperatures. Also a similar behavior is shown by the melting temperature T_m (Figure 4.8c) and crystallinity degree α_c (Figure 4.8d), when compared to the corresponding results for PB-*b*-PS-*b*-PEO (Figure 4.7c and 4.7d, respectively).

Based on the evaluation of Figure 4.7 and 4.8, some comparison can be made in order to check the influence of the higher temperature crystallizable PE block on the thermal properties of the PEO block. In all cases it can be seen that the crystallization temperature T_{c2} of PEO increases after hydrogenation. A similar effect has been previously reported for PE-*b*-PEP-*b*-PEO and it was attributed to the nucleating effect of some remaining Wilkinson catalyst,[3,13,37] and a consistent increase in T_m and in the crystallinity degree can also be observed. This could also be a plausible explanation in the present case since it is known that it is very difficult to completely remove the impurities produced by adding this catalyst.[3]

The thermal properties of the PE block were plotted in Figure 4.9 as a function of the corresponding volume fraction (ϕ_{PE}), but also as a function of the volume fraction of the PEO block (ϕ_{PEO}). The later parameter turns out to be important since the PEO block is generally the first one that separates from the toluene solution, and therefore templates the resulting morphology, as already discussed. Consequently, the PEO volume fraction is usually a better parameter for describing the overall morphology than the PE volume fraction itself.
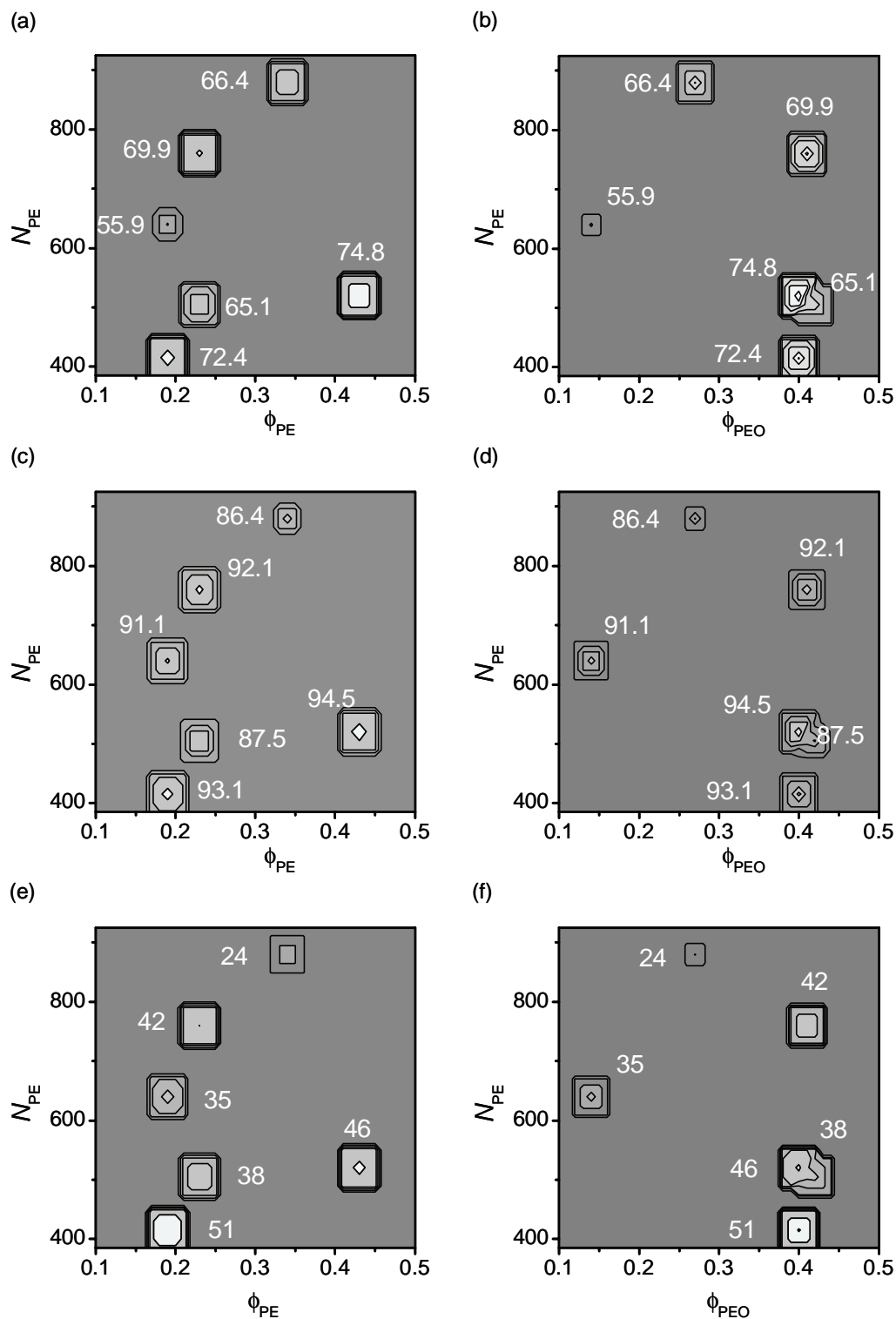
Figure 4.9. (a-b) T_c, (c-d) T_m and (e-f) α_c for the polyethylene block within the PE-*b*-PS-*b*-PEO triblock terpolymers as a function of N_{PE} and (a,c,e) ϕ_{PE} or (b,d,f) ϕ_{PEO}. The color scale is lighter for higher values, and the numbers indicate the peak values. The crystallinity degree was calculated considering $\Delta H_{100\%} = 8.12$ kJ/mol,[34] and normalizing the ΔH with the block weight.

The values of crystallization temperature T_c are presented in Figure 4.9a and 4.9b against ϕ_{PE} and ϕ_{PEO}, respectively. There is no recognizable tendency as a function of ϕ_{PE} (Figure 4.9a). However, T_c is observed to increase with the polymerization degree and the ϕ_{PEO} in Figure 4.9b. The effect of the PEO volume fraction on T_c is stronger than the one of the molecular weight, as described by the low T_c value of $E_{29}S_{40}EO_{31}{}^{170}$ (ϕ_{PEO} = 0.27; N_{PE} = 887) despite the high molecular weight. There are two exceptions of the mentioned explanation. The first one is given by $E_{38}S_{16}EO_{46}{}^{77}$ (ϕ_{PE} = 0.43; ϕ_{PEO} = 0.40; N_{PE}= 523), which showed the highest T_c value despite its comparatively low polymerization degree. The reason could be related to the high PE content, which is the highest among the studied group. This could imply that there is a threshold in ϕ_{PE}, above which the crystallization temperature is much higher than the one for polymers with a similar ϕ_{PEO} but lower ϕ_{PE}. The second exception is $E_{16}S_{40}EO_{44}{}^{144}$ (ϕ_{PE} = 0.19; ϕ_{PEO} = 0.40; N_{PE}= 413) that has a high value of T_c for its low molecular weight and a low PE volume fraction. This is the only terpolymer where the PEO is not completely governing the microphase formation, and a contribution of the PE block distorts the original lamellae to generate PEO cylinders and a distributed PE phase in a PS matrix, as discussed before. The continuity of the PE phase is not described by any of the parameters employed in order to reflect the morphology, i.e., ϕ_{PEO} nor ϕ_{PE}, and continuous phases tend to have thermal properties similar to those corresponding to homopolymers, overcoming the restrictions imposed by the defined microphases.

The former situation is mostly repeated in Figure 4.9c and 4.9d for the melting temperature T_m. As for T_c, there is no obvious tendency when the variable is plotted as a function of ϕ_{PE}. The melting temperature increases with ϕ_{PE} and, more evidently, with ϕ_{PEO}. The case of $E_{38}S_{16}EO_{46}{}^{77}$ is an exception probably due to the high ϕ_{PE}, while the high value for $E_{16}S_{40}EO_{44}{}^{144}$ is due to the continuity of its PE phase. The melting temperature is also

relatively high for $E_{17}S_{67}EO_{16}{}^{211}$ ($\phi_{PEO} = 0.14$; $N_{PE} = 643$), given the low crystallization temperature and low volume fractions of both PE and PEO blocks. In this case, the PE block probably undergoes massive reorganization during the heating scan since the originally generated lamellae should be very small (as expected from the fact that the PE block here exhibits the lowest crystallization temperature as compared to other samples, this may be associated with homogeneous or superficial nucleation).[11,13] This is in good agreement with the broad melting peak observed in the DSC traces (Figure 4.6a). Even though the PEO block within this terpolymer crystallizes under similar conditions, the recrystallization and annealing of the PEO crystals take place to a lower extend than in the PE crystals. The high chain mobility and crystallization ability of the PE has been well studied.[41]

Finally, Figure 4.9e and 4.9f show the tendency of the crystallinity degree with the volume fractions and the molecular weight. The results agree with the previously observed trend of increasing with N and ϕ_{PEO}, showing a higher value than the expected for $E_{38}S_{16}EO_{46}{}^{77}$ attributed to the high ϕ_{PE}, and for $E_{16}S_{40}EO_{44}{}^{144}$ because the PE phase is distributed along the matrix instead of being confined in a domain. Also, a higher than expected value of α_c for $E_{17}S_{67}EO_{16}{}^{211}$ was observed, probably caused by recrystallization upon heating.

4.4. Conclusions

The synthesis of novel poly(1,4-butadiene)-*block*-polystyrene-*block*-poly(ethylene oxide) (PB-*b*-PS-*b*-PEO) triblock terpolymers was successfully achieved by sequential anionic polymerization. Further hydrogenation of the high 1,4-PB block was also accomplished, obtaining triblock terpolymers with two crystallizable blocks. The morphology of the triblock terpolymers is determined by a compromise between crystallization of the polyethylene block and the segregation of the poly(ethylene oxide) block from the residual

system. The observed morphologies from non-hydrogenated and hydrogenated triblock terpolymers indicate a sequential microphase separation where a template influence of the poly(ethylene oxide) domain prevailed. The effect was observed although the polyethylene block was the only one able to crystallize at the given film preparation conditions. However, due to the lower solubility of PEO it microphase separates first and thus controls the overall formed morphology. The projection of a 3D plot of the thermal properties such as T_c, T_m and α_c of the PE and PEO blocks against volume fraction and polymerization degree was successfully used to describe the dependence on domain geometry and molecular weight. A marked tendency of the PE block thermal properties with the PEO volume fraction was found, confirming that the PEO block templates the morphology and that the thermal properties are highly influenced by the morphology when the crystallization occurs inside the microphases. Some very interesting results were found, such as low crystallization temperature values for blocks with high molecular weights due to high segregation strength.

4.5. References

1. Hamley, I. W. The Physics of Block Copolymers, 1st ed.; Oxford: New York, 1998.

2. Loo, Y. L.; Register, R. A. In Developments in block copolymer science and technology; Hamley, I. W.; Eds.; Wiley: New York, 2004; p 213.

3. Schmalz, H.; Knoll, A.; Müller, A. J.; Abetz, V. *Macromolecules* **2002**, 35, 10004-10013.

4. Chen, H. -L.; Li, H. -C.; Huang, Y. -Y.; Chiu, F. -C. *Macromolecules* **2002**, 35, 2417-2422.

5. Huang, Y. -Y.; Yang, C. H.; Chen, H. -L.; Chiu, F. -C.; Lin, T. -L.; Liou, W. *Macromolecules* **2004**, 37, 486-493.

6. Reiter, G.; Castelein, G.; Sommer, J. -U. In Polymer crystallization: observations, concepts and interpretations ; Reiter, G.; Sommer, J. -U. ; Eds. ; Springer : Berlin, 2003 ; p. 196.

7. Zhu, L.; Huang, P.; Chen, W. Y. ; Ge, Q.; Quirk, R. P.; Cheng, S. Z. D.; Thomas, E. L.; Lotz, B.; Hsiao, B. S.; Yeh, F.; Liu, L. *Macromolecules* **2002**, 35, 3553-3562.

8. Zhu, L.; Cheng, S. Z. D.; Calhoun, B. H.; Ge, Q.; Quirk, R. P.; Thomas, E. L.; Hsiao, B. S.; Yeh, F.; Lotz, B. *Polymer* **2001**, 42, 5829-5839.

9. Zhu, L.; Chen, Y.; Zhang, A.; Calhoun, B. H.; Chun, M.; Quirk, R. P.; Cheng, S. Z. D.; Hsiao, B. S.; Yeh, F.; Hashimoto, T. *Phys. Rev. B* **1999**, 60, 10022-10031.

10. Cohen, R. E.; Cheng, P. -L.; Douzinas, K.; Kofinas, P.; Berney, C. V. *Macromolecules* **1990**, 23, 324-327.

11. Lorenzo, A. T.; Arnal, M. L.; Müller, A. J.; Boschetti-de-Fierro, A.; Abetz, V. *Eur. Polym. J.* **2006**, 42, 516-533.

12. Takeshita, H.; Ishii, N.; Araki, C.; Miya, M.; Takenaka, K.; Shiomi, T. *J. Polym. Sci. Pt. B-Polym. Phys.* **2004**, 42, 4199-4206.

13. Müller, A. J.; Balsamo, V.; Arnal, M. L. *Adv. Polym. Sci.* **2005**, 190, 1-63.

14. Fluodas, G.; Reiter, G.; Lambert, O.; Dumas, P. *Macromolecules* **1998**, 31, 7279-7290.

15. Jiang, S.; Chaoliang, H.; An, L.; Chen, X.; Jiang, B. *Macrom. Chem. Phys.* **2004**, 205, 2229-2234.

16. Albuerne, J.; Márquez, L.; Müller, A. J.; Raquez, J. M.; Degée, P.; Dubois, P.; Castelleto, V.; Hamley, I. W. *Macromolecules* **2003**, 36, 1633-1644.

17. Müller, A. J.; Albuerne, J.; Esteves, L. M.; Márquez, L.; Raquez, J. M.; Degée, P.; Dubois, P.; Collins, S.; Hamley, I. W. *Macromol. Symp.* **2004**, 215, 369-382.

18. Müller, A. J.; Albuerne, J.; Márquez, L.; Raquez, J.-M.; Degée, P.; Dubois, P.; Hobbs, J.; Hamley I. W. *Faraday Discussions* **2005**, 128, 231-252.

19. Sun, L.; Liu, Y.; Zhu, L.; Hsiao, B. S.; Avila-Orta, C. A. *Polymer* **2004**, 45, 8181-8193.

20. Hamley, I. W. Castelletto, V. Castillo, R. V. Müller, A. J. Martin, C. M. Pollet, E. Dubois, P. *Macromolecules* **2005**, 38, 463-472.

21. Hamley, I. W.; Parras, P.; Castelletto, V.; Castillo, R. V.; Müller, A. J.; Pollet, E.; Dubois, P.; Martin, C. M. *Macrom. Chem. Phys.* **2006**, 207, 941-953.

22. Arnal, M. L.; Balsamo, V.; López-Carrasquero, F.; Contreras, J.; Carrillo, M.; Schmalz, H.; Abetz, V.; Laredo, E.; Müller, A. J. *Macromolecules* **2001**, 34, 7973-7982.

23. Balsamo, V.; Von Gyldenfeldt, F.; Stadler, R. *Macrom. Chem. Phys.* **1996**, 197, 3317-3341.

24. Balsamo, V.; Müller, A.J.; von Gyldenfeldt, F.; Stadler R. *Macrom. Chem. Phys.* **1998**, 199, 1063-1072.

25. Balsamo, V.; Müller, A.J.; Stadler, R. *Macromolecules* **1998**, 31, 7756-7763.

26. Müller, A. J.; Balsamo, V.; Arnal, M. L. in Lecture Notes in Physics: Progress in Understanding of Polymer Crystallization; Reiter, G.; Strobl, G.; Eds.; Springer: Berlin, Lect. Notes Phys. 2007, 714, 229–259.

27. Schmalz, H.; Abetz, V.; Lange, R.; Soliman, M. *Macromolecules* **2001**, 34, 795-800.

28. Schmalz, H.; Böker, A.; Lange, R.; Krausch, G.; Abetz, V. *Macromolecules* **2001**, 34, 8720-8729.

29. Esswein, B.; Molenberg, A.; Möller, M. *Macromol. Symp.* **1996**, 107, 331-340.

30. Esswein, B.; Möller, M. *Angew. Chem.* **1996**, 108, 703-705.

31. Esswein, B.; Steidl, N. M.; Möller, M. *Macromol. Rapid Commun.* 1996, 17, 143-148.

32. Förster, S.; Krämer, E. *Macromolecules* **1999**, 32, 2783-2785.

33. Floudas, G.; Vazaiou, B.; Schipper, F.; Ulrich, R.; Wiesner, U.; Iatrou, H.; Hadjichristidis, N. *Macromolecules* **2001**, 34, 2947-2957.

34. Grulke, E. A. In Polymer Handbook, 4th ed.; Brandrup, J.; Immergut, E. H.; Grulke, E. A.; Eds.; J. Wiley & Sons: New York, 1999; p. VII/675.

35. Stadler, R.; Auschra, C.; Beckmann, J.; Krapper, U.; Voigt-Martin, I.; Leibler, L. *Macromolecules* **1995**, 28, 3080-3097.

36. Barton, A. F. CRC Handbook of Polymer Liquid Interaction Parameters and Solubility Parameters; CRC Press: Boca Raton, 1990; p. 245.

37. Müller, A. J.; Balsamo, V.; Arnal, M. L.; Jakob, T.; Schmalz, H.; Abetz, V. *Macromolecules* **2002**, 35, 3048-3058.

38. Evans, R. D. M.; Harold R.; Flory, P. J. *J. Chem. Phys.* **1947**, 15, 685.

39. Massa, M. V.; Dalnoki-Veress, K. *Phys. Rev. Lett.* **2004**, 92, 255509.

40. Reiter, G.; Castelein, G.; Sommer, J. –U.; Röttele, A.; Thurn-Albrecht, T. *Phys. Rev. Lett.* **2001**, 87, 226101.

41. Organ, S. J.; Keller, A. *J. Polym. Sci. Pt. C-Polym. Lett.* **1987**, 25, 67-72.

Chapter 5. Thermal Monitoring of Morphology in Triblock Terpolymers with Crystallizable Blocks

The bulk morphology of poly(1,4-butadiene)–*block*–polystyrene–*block*–poly(ethylene oxide) (PB-*b*-PS-*b*-PEO) and polyethylene–*block*–polystyrene–*block*–poly(ethylene oxide) (PE-*b*-PS-*b*-PEO) triblock terpolymers is analyzed under a thermal protocol. This allows the investigation of the morphology during the occurrence of thermal transitions, such as crystallization and melting, which is a neat way of studying the competition between microphase separation and crystallization for the morphology formation. Only one of the studied systems presented a morphological transition upon melting of the PEO and the PE blocks, attributed to the compromise between mobility and thermodynamically favored structures instead of a disruption of the morphology caused by crystallization. All the other systems presented no morphological transitions during the thermal scan. The results prove that the crystallization does not disrupt significantly the microphases generated in the molten state for these block copolymers.

5.1. Introduction

Block copolymers are widely studied materials, basically due to their self-assembling ability in microphases. The segregation strength between two blocks is the driving force for the self-assembly of the blocks into microphases and the consequent generation of a defined morphology.[1-6] Because of the nanometric scale dimensions inherent to their microphases, every molecular process or transition occurring inside them is interesting. The morphology generated by the self-assembling of block copolymers depends on the chain architecture and the polymer composition.[6] Additionally, if at least one of the two blocks is able to crystallize, then the morphology development will be a competition

between the microphase separation and the crystallization process. It is generally assumed that in strongly segregated systems the crystallization will occur within the microphases. On the other hand, when the blocks are only weakly segregated the crystallization process will take over the microphase separation.[7-10]

The morphology of self-assembled block copolymers in bulk can be mainly determined by two techniques: transmission electron microscopy (TEM) and small angle X-ray or neutron scattering (SAXS or SANS).[3] With TEM it is possible to observe the morphology directly, usually after selective staining of the given blocks in order to increase the electron density contrast between the microphases.[11] However, the technique allows only the observation of limited areas of the ultrathin cut slices of the sample. On the contrary, with the scattering techniques a larger part of sample is measured (depending on the diameter of the beam and sample thickness) and the results are therefore considered to be representative and an average for the sample. Another important advantage of the scattering methods is the possibility of studying the sample under different conditions, such as mechanical loads, thermal treatments or controlled environments, obtaining on-line information during the occurrence of a given process.

The following chapter deals with a complex system, namely a triblock terpolymer with one or two crystallizable blocks, i.e., polybutadiene–*block*–polystyrene–*block*–poly(ethylene oxide) and polyethylene–*block*–polystyrene–*block*–poly(ethylene oxide). In the latter case there are two different blocks undergoing a crystallization process, and also the interaction between three pairs of different blocks influences the very complex process of morphology formation. The synthesis, bulk morphology and thermal properties of this material with different compositions has been studied and presented in Chapter 4. It is the aim of this chapter, to analyze the morphology as a function of temperature. The samples are investigated as each of the blocks melts upon heating up to the microphase separated

molten state, by means of temperature dependant small angle X-ray scattering. The reverse process is also observed during the cooling step. The results are intended to give insight into the influence of the crystallization on the morphology formation, as of its competition with the self-assembly driven by the segregation between the blocks.

5.2. Experimental Part

Poly(1,4-butadiene)–*block*–polystyrene–*block*–poly(ethylene oxide) triblock terpolymers (PB-*b*-PS-*b*-PEO) were synthesized by sequential anionic polymerization, Further, catalytic hydrogenation using Wilkinson catalyst was employed in order to obtain poly(ethylene)–*block*–polystyrene–*block*–poly(ethylene oxide) (PE-*b*-PS-*b*-PEO) triblock terpolymers, as presented in the previous chapter. In the notation here employed, i.e., $A_x B_y C_z^m$, the subscripts denote the percentage weight fraction of the block and the superscript denotes the number averaged molecular weight M_n of the terpolymer in kg/mol. The samples were prepared by casting a film from a polymer solution in toluene at 70 °C for one week. The polymer films were then dried under vacuum over night and further annealed at 120 °C for 6 h under inert conditions (nitrogen flow).

Triblock terpolymers with one or two crystallizable blocks were studied by means of time dependant small angle X-ray scattering (SAXS). The experiments were carried out at the A2 beamline of DORIS, HASYLAB, DESY, using a sample-SAXS detector distance of 3250 mm and a wavelength of 1.5 Å. The temperature chamber already available in the line was adapted to use liquid nitrogen as cooling fluid. The control parameters of the controller were adjusted and the equipment is able to cool down in a controlled manner using rates up to 40 °C/min. The samples were held for 1 min at the initial temperature of 25 °C, then heated up to 120 °C at 10 °C/min, held there for 3 min, and then cooled down to 0 °C at 10 °C/min. The SAXS diffraction patterns were obtained with frames taken during 15 sec every 20 sec. The results will be related to the thermal properties of the

materials presented in Table 5.1, determined by differential scanning calorimetry (DSC), as reported in Chapter 4.

Table 5.1. Thermal properties of the studied triblock terpolymers, determined by standard differential scanning calorimetry (DSC) scans at 10 °C/min. Melting points correspond to the second heating scan.

Triblock terpolymer	PEO block		PE block	
	T_m (°C)	T_c (°C)	T_m (°C)	T_c (°C)
$B_{37}S_{16}EO_{47}$[76]	63.4	35.0		
$E_{38}S_{16}EO_{46}$[77]	62.4	39.1	94.5	74.8
$B_{16}S_{40}EO_{44}$[143]	61.4	39.9		
$E_{16}S_{40}EO_{44}$[144]	63.9	46.2	93.1	72.4

Ultrathin cuts (thickness 50 – 100 nm) were obtained from the polymer films using a Reichert-Jung Ultracut E microtome equipped with a diamond knife at ‑ 130 °C. The non-hydrogenated triblock terpolymers were stained by exposure to OsO_4 vapor for 60 sec. This procedure stains preferentially the PB block, and the PS block to a smaller extend. In the hydrogenated terpolymers, amorphous PEO and PS segments were stained by exposure to RuO_4 vapor for 15‑30 min, which stains the PEO/PS microdomain interphase preferentially. Morphology observations with bright field transmission electron microscopy (TEM) were achieved using a Zeiss CEM 902 electron microscope operated at 80 kV and a FEI Tecnai 20 operated at 200 kV.

5.3. Results and Discussion

The morphologies of the non-hydrogenated and hydrogenated triblock terpolymers were studied by TEM at room temperature (Figure 5.1) and under a thermal protocol by small angle X-ray scattering. SAXS patterns for the triblock terpolymers are presented in Figures 5.2 to 5.5, where the upper part shows a top view of the SAXS patterns as a function of the temperature during the thermal protocol ((a) for heating and (b) for

subsequent cooling). In this representation, it is possible to follow the shifts in q value as well as the intensity changes upon heating and cooling, with limitations arising from discretizing the intensity values. The lower part of the figures includes SAXS patterns at different selected temperatures, which are useful for morphology identification. The morphology assignment at room temperature is finally compared to the correspondent TEM results of Figure 5.1.
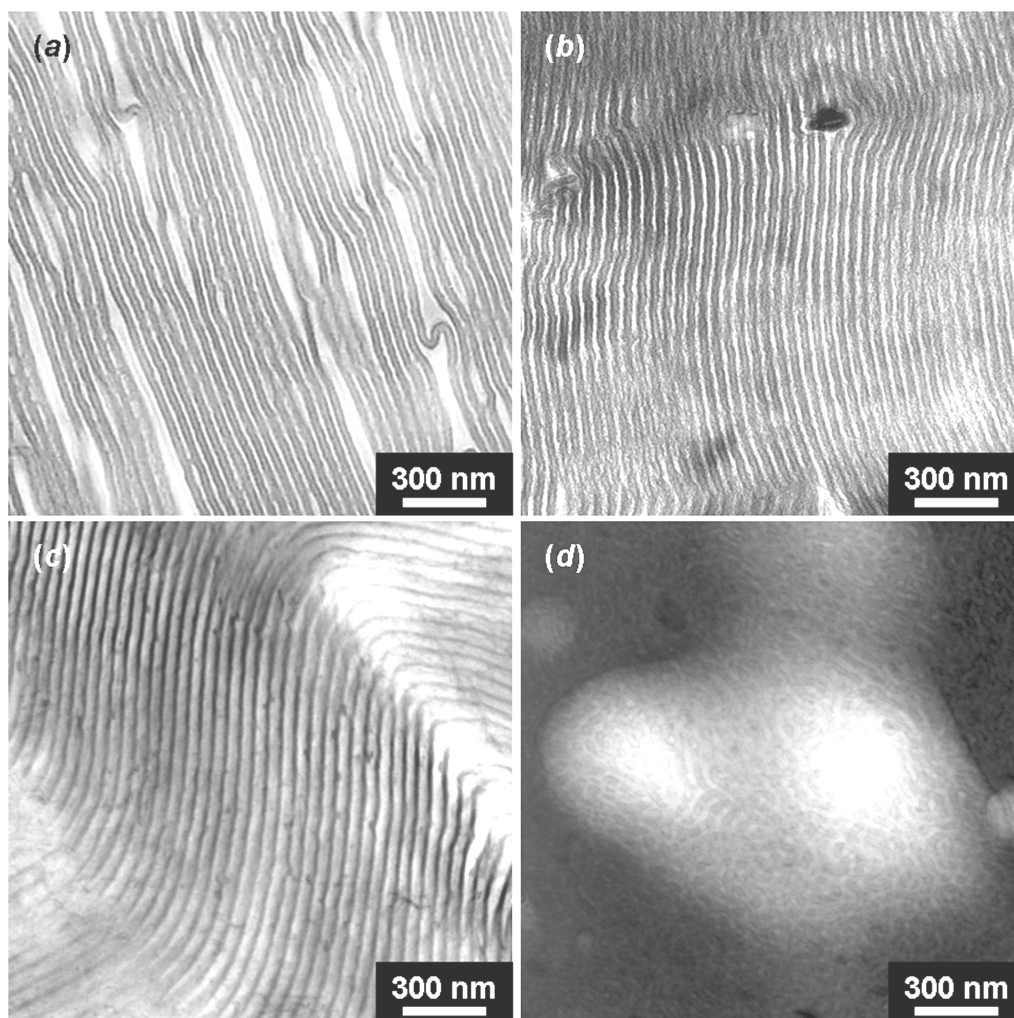
Figure 5.1. TEM micrographs of non-hydrogenated (OsO$_4$ stained; black = PB, gray = PS, white = PEO) and hydrogenated (RuO$_4$ stained; white = PE, gray = PS, white = PEO) triblock terpolymers. Ultra thin sections were obtained from films cast from toluene solutions. *a*) B$_{37}$S$_{16}$EO$_{47}$[76], *b*) E$_{38}$S$_{16}$EO$_{46}$[77], *c*) B$_{16}$S$_{40}$EO$_{44}$[143], *d*) E$_{16}$S$_{40}$EO$_{44}$[144].

In Figure 5.2 the diffraction results for $B_{37}S_{16}EO_{47}^{76}$ are presented. In the initial state presented in Figure 5.2a, two reflections at q^* and $2 \cdot q^*$ are observed, coinciding with the lamellar morphology observed by TEM (Figure 5.1a). The periodicity of the lamellae at 25 °C was calculated as 81.9 nm and 87 ± 2 nm by scattering and microscopy methods, respectively. As the periodicity of the TEM micrographs, the thickness of four domains (gray = PS, black = PB, gray = PS and white = PEO) were measured. Periodic distances by TEM measurements lead usually to higher l values than the actual ones, since the lamellae are not necessarily cut perpendicular. The cutting angle can be estimated from the two periodicity values, and in this case it is close to 20°.

The effect of the heating scan on $B_{37}S_{16}EO_{47}^{76}$ is observed in Figure 5.2a. The main peak position shifts to slightly higher q values by increasing the temperature, resulting in a lower periodicity in the molten state. This effect has been observed in other block copolymer systems,[12] and it is usual that increasing the temperature contracts the chains due to the reduction of repulsive interactions and thus decreases the domain spacing. The shift of the main peak position causes the shift of all the higher order reflection peaks, too, as can be observed in the top view in Figure 5.2a. The relative q_i/q^* values, however, remain constant through the whole applied thermal protocol. The intensity of the second order reflection decreases until the peak almost disappears, and a new reflection at $3 \cdot q^*$ is observed over 68 °C. This situation is kept at the molten state, and it is reversed upon the cooling scan, as shown in Figure 5.2b. In that case, the transition takes place around 40 °C. The transition temperatures correspond nicely to the PEO block melting and crystallization transitions observed by calorimetry presented in Table 5.1. Upon cooling, the reverse shift of the reflection peaks (to lower q values) is also observed, and the relative ratios q_i/q^* remain constant.

Figure 5.2. SAXS patterns for the triblock terpolymer $B_{37}S_{16}EO_{47}$[76]. Upper part: Top view of the SAXS scans as a function of the temperature during the thermal protocol. The horizontal lines indicate selected temperatures of representative morphological stages. Lower part: SAXS patterns at different selected temperatures indicated in the temperature dependant representation. (a) Heating scan and (b) subsequent cooling scan.

The diffraction pattern of the sample in the molten state, presented both in Figure 5.2a and 5.2b, corresponds to a lamellar morphology. Above the melting temperature of the PEO block, the reflections are sharper. In particular, the third order reflection becomes evident. This indicates that the long-range order of the lamellar morphology is improved. The decrease of intensity, mainly observed for the second order reflection, upon melting of the PEO block can be attributed to the reduction of the electron density contrast (the density of

the PEO block decreases from 1.195 to 1.123 kg/m^3). The density of the semicrystalline

blocks for all the terpolymers studied were calculated using the correspondent crystallinity

degrees determined by DSC, and crystalline and amorphous values were taken from the

literature (ρ_{PB} = 0.9 kg/m^3, ρ_{PS} = 1.05 kg/m^3; ρ_{am-PE} = 0.887 kg/m^3; ρ_{cr-PE} = 0.999 kg/m^3;

ρ_{am-PEO} = 1.123 kg/m^3; ρ_{cr-PEO} = 1.227 kg/m^3),[13] neglecting density corrections for the real

temperature. The results are presented in Table 5.2, along with the volume fractions of

each block.

Table 5.2.   Composition and semicrytalline densities of the triblock terpolymers studied
under thermal monitoring of their morphology.

Triblock terpolymer	Volume fractions				Semicrystalline densities	
	ϕ_{PB}	ϕ_{PE}	ϕ_{PS}	ϕ_{PEO}	ρ_{PE}	ρ_{PEO}
$B_{37}S_{16}EO_{47}$[76]	0.43		0.16	0.41		1.195
$E_{38}S_{16}EO_{46}$[77]		0.433	0.163	0.404	0.920	1.195
$B_{16}S_{40}EO_{44}$[143]	0.19		0.41	0.40		1.196
$E_{16}S_{40}EO_{44}$[144]		0.19	0.41	0.40	0.920	1.200

The next morphology to be studied corresponds to $E_{38}S_{16}EO_{46}$[77] in Figure 5.3. As for the

non-hydrogenated counterpart, the pattern of the sample at the initial state (Figure 5.3a)

shows two reflections indicating lamellae, with a periodicity at 25 °C of 63.8 nm. The

morphology is also confirmed by the TEM micrograph shown in Figure 5.1b, where a

periodicity of 89 ± 4 nm can be measured. In this case, the sample was stained with RuO$_4$,

and the periodicity is again then calculated by measuring four domains as white = PE, gray

= PS, white = PEO and gray = PS. Again, the periodicity observed by microscopy is

higher than the one calculated from the scattering data, and the calculated tilt angle is 45°in

this case. Since the angle is big, there could also be an influence of the cut on the actual

microphase dimensions. Therefore, the TEM micrographs are referred to as a qualitative

indication of the morphological array in the sample. The quantitative evaluation is carried out based on the scattering results.

Figure 5.3. SAXS patterns for the triblock terpolymer $E_{38}S_{16}EO_{46}$[77]. Upper part: Top view of the SAXS scans as a function of the temperature during the thermal protocol. The horizontal lines indicate selected temperatures of representative morphological stages. Lower part: SAXS patterns at different selected temperatures indicated in the temperature dependant representation. (a) Heating scan and (b) subsequent cooling scan.

The morphology of $E_{38}S_{16}EO_{46}$[77] the triblock terpolymer as a function of the thermal scan is also consistent with the results presented for $B_{37}S_{16}EO_{47}$[76]. In the heating scan presented in Fig. 3(a), the second reflection is suppressed after the PEO melts at 60 °C. Meanwhile, the second reflection reappears during the subsequent cooling (Figure 5.3b) at 42 °C, close

to the PEO crystallization. The suppression of the second order reflection in lamellar morphologies is typical for symmetric diblock copolymers.[2] Here this could be caused by the decrease in electron density contrast between PS and PEO after melting. If this contrast is low enough, the two blocks would behave like one block in terms of small angle X-ray scattering. Therefore, the actual triblock terpolymer behaves like a diblock terpolymer for the X-ray scattering, which according to the data presented in Table 5.2, would have a composition of $\phi_{PE} = 0.433$ and $\phi_{PS+PEO} = 0.567$. These values can be interpreted as close to a symmetric composition, and turns the studied triblock terpolymer into a symmetric diblock copolymer for the SAXS measurement.

It is appropriate to dedicate some thoughts to the comparison between $B_{37}S_{16}EO_{47}$[76] and $E_{38}S_{16}EO_{46}$[77], that is namely before and after hydrogenation of the PB block. The structure formed remains the same in both cases, as was previously observed by TEM results. The periodic distance of the lamellar morphology decreases from 75 nm before hydrogenation to 66 nm after hydrogenation. A slight decrease in periodicity is expected due to the increase in density caused by the substitution of a rubbery block (PB) for a semicrystalline one (PE). Also, the tendency of the semicrystalline sample to increase the interfacial area cooperates with the reduction in periodicity. A simultaneous analysis of the thermal monitoring of the morphology leads to the observation of the second order reflection peak. This decreases in intensity when the PEO block is molten, both in $B_{37}S_{16}EO_{47}$[76] and $E_{38}S_{16}EO_{46}$[77]. For the latter case, the reflection is difficult to detect above the melting point of the PEO, and we argue that a *quasi*-symmetric diblock behavior could be the cause of such suppression. Since the conditions for assuming the diblock copolymer behavior are also valid for the non-hydrogenated triblock terpolymer, such argument should also be applied. The question remaining is now that the second reflection peak in Figure 5.2 does

not completely disappear, but substantially decreases above $T_{m, PEO}$. We assume that this situation is given due to the deviations from the ideal symmetric case.

Moving the analysis to a terpolymer with different composition, Figure 5.4 shows the results obtained for $B_{16}S_{40}EO_{44}$[143]. From the temperature dependant measurements presented in the upper part one can see that there is no significant shift of the main peak position (q^*) through the thermal scan. The initial diffraction pattern in Figure 5.4a only shows a main peak at $q^* = 0.077$ nm^{-1}. As can be seen in the top view of the SAXS patterns, the reflections at $2 \cdot q^*$ and $3 \cdot q^*$ arise at around 68 °C. Simultaneously, the first reflection peak becomes narrow. This reflects a morphological modification to a well defined lamellae order, driven by melting of the PEO block (at 62 °C, according to the DSC results presented in Table 5.1). The patterns of the molten sample, i.e., the state where all the crystals are molten, indicate that the microphases are arranged in lamellae with a periodicity of $l = 82$ nm. The periodicity of the main reflection at 25 °C is virtually identical, i.e., $l = 80$ nm. The morphology is in good agreement whit the one observed by TEM (Figure 5.1c), and the periodicity measured in the micrographs is higher, $l = 110 \pm 4$ nm. This value indicates again a high tilt angle, i.e., 44°, very similar to the results obtained for $E_{38}S_{16}EO_{46}$[77].

When the sample $B_{16}S_{40}EO_{44}$[143] is cooled down, the second and third order reflection decrease in intensity until they are completely absent at temperatures less than 40 °C (Figure 5.4b). The morphology transformation observed upon heating can, therefore, be described as reversible. There is a particular temperature window where only the first and the third reflections are seen. On the heating scan this takes place between 44 and 68 °C, while it starts at 38 °C and ends at 26 °C during the cooling process.
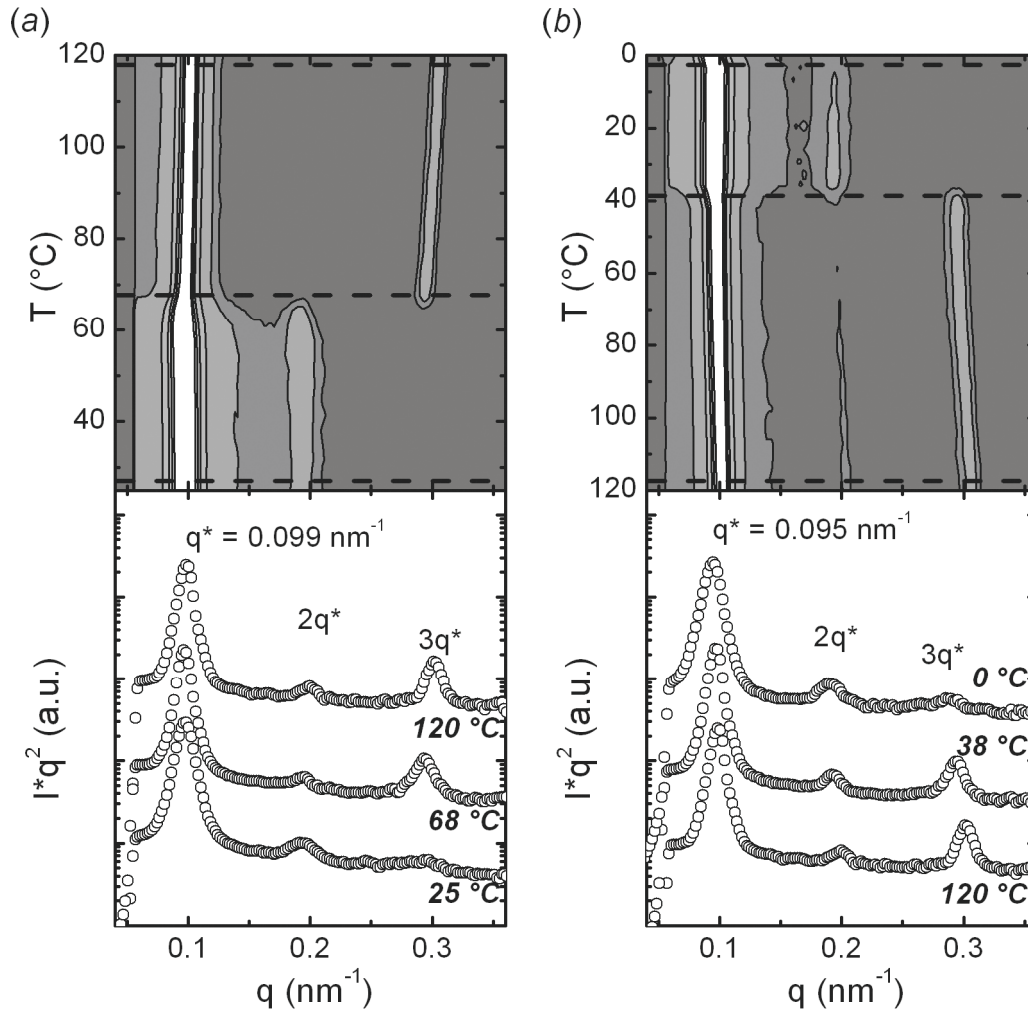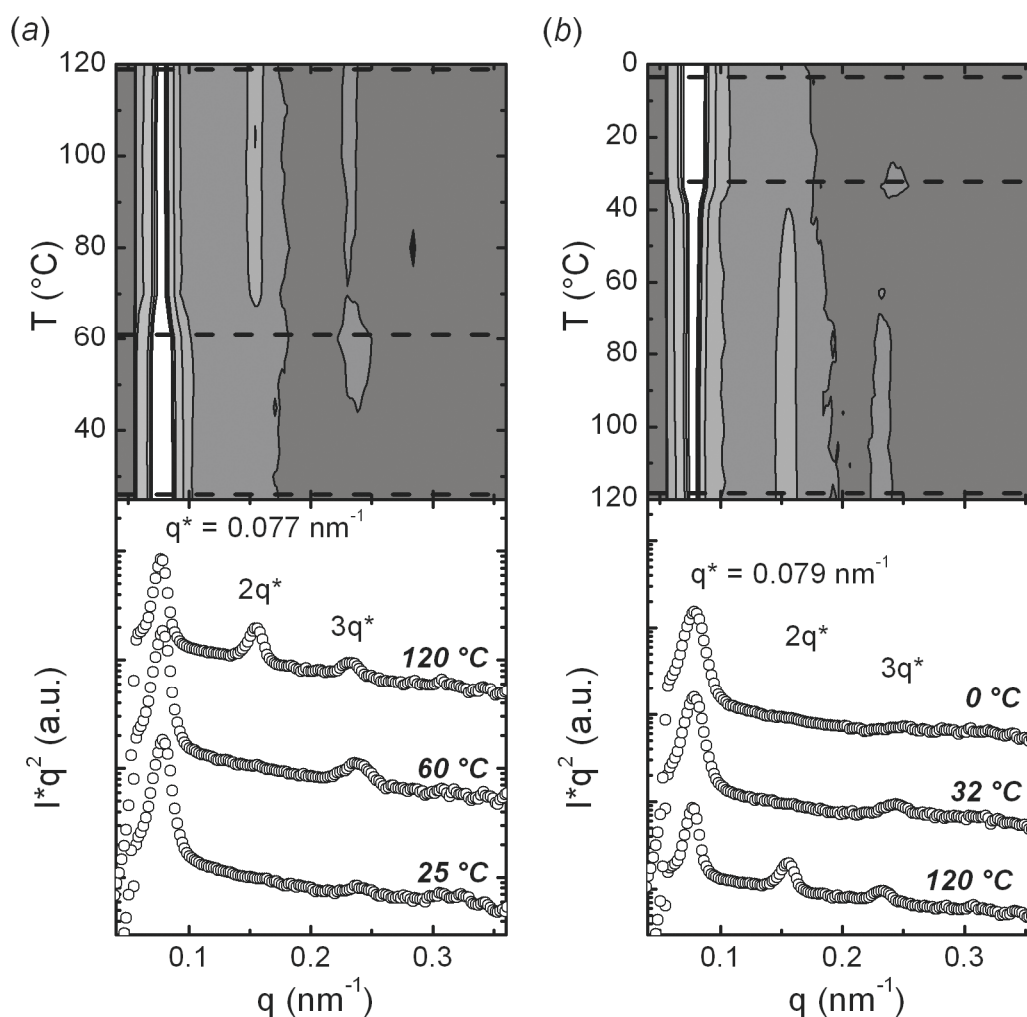
Figure 5.4. SAXS patterns for the triblock terpolymer $B_{16}S_{40}EO_{44}$[143]. Upper part: Top view of the SAXS scans as a function of the temperature during the thermal protocol. The horizontal lines indicate selected temperatures of representative morphological stages. Lower part: SAXS patterns at different selected temperatures indicated in the temperature dependant representation. (a) Heating scan and (b) subsequent cooling scan.

The SAXS results from $E_{16}S_{40}EO_{44}$[144] are presented in Figure 5.5. The initially annealed film shows two diffraction peaks. The second peak is rather weak, and could be assigned to a lamellar morphology. However, the weakness of the reflection and the TEM micrographs do not correspond to lamellae. From the TEM result shown in Figure 5.1d, either cocontinuous morphology or not ordered microphases could be assumed. Upon heating (see Figure 5.5a), the intensity of the weak peak decreases until it is no longer

noticeable at rather low temperatures (40-50 °C). A shoulder appears in the main reflection, at $q_1 = 1.65 \cdot q^*$, after the system reaches 92 °C. The complete process reverses during the subsequent cooling: the shoulder disappears at 70 °C and the peak at $2 \cdot q^*$ appears at 10 °C, as can be seen in Figure 5.5b.

The structure at room temperature corresponds to cocontinuous or disordered phases, while the one at the molten state described hexagonally packed cylinders. The transition occurs in two stages: the initial state is lost close before the melting of the PEO crystals (64 °C), and the cylinders are formed when the PE crystals melt (93 °C). After melting, the polymer chains gain mobility and can therefore self-assemble into a more energetically favorable morphology. On the other hand, crystallization introduces restrictions into the system and it is the driving force for the quasi phase transition.

A morphological comparison between $B_{16}S_{40}EO_{44}$[143] and $E_{16}S_{40}EO_{44}$[144] can be done based on the SAXS patterns presented in Figure 5.4 and 5.5. The terpolymer presents a different morphology after hydrogenation, which is a particularity of this system. Besides the slight increase in interaction parameters of the PE compared to the PB with the other two blocks (calculated at 60 °C as:[14-16] $\chi_{PB/PS} = 0.042$ *vs.* $\chi_{PE/PS} = 0.086$, and $\chi_{PB/PEO} = 0.12$ *vs.* $\chi_{PE/PEO} = 0.16$) also the composition (close to a morphological transition between spheres and cylinders) is a reason for this behavior. The smaller interaction parameters with PB allow the formation of dispersed spherical domains of the short PB blocks within the PS-lamellae. This morphology is unstable after hydrogenation, when the interaction parameter has increased and the PE blocks forms most likely cylinders in the PS-microdomain.
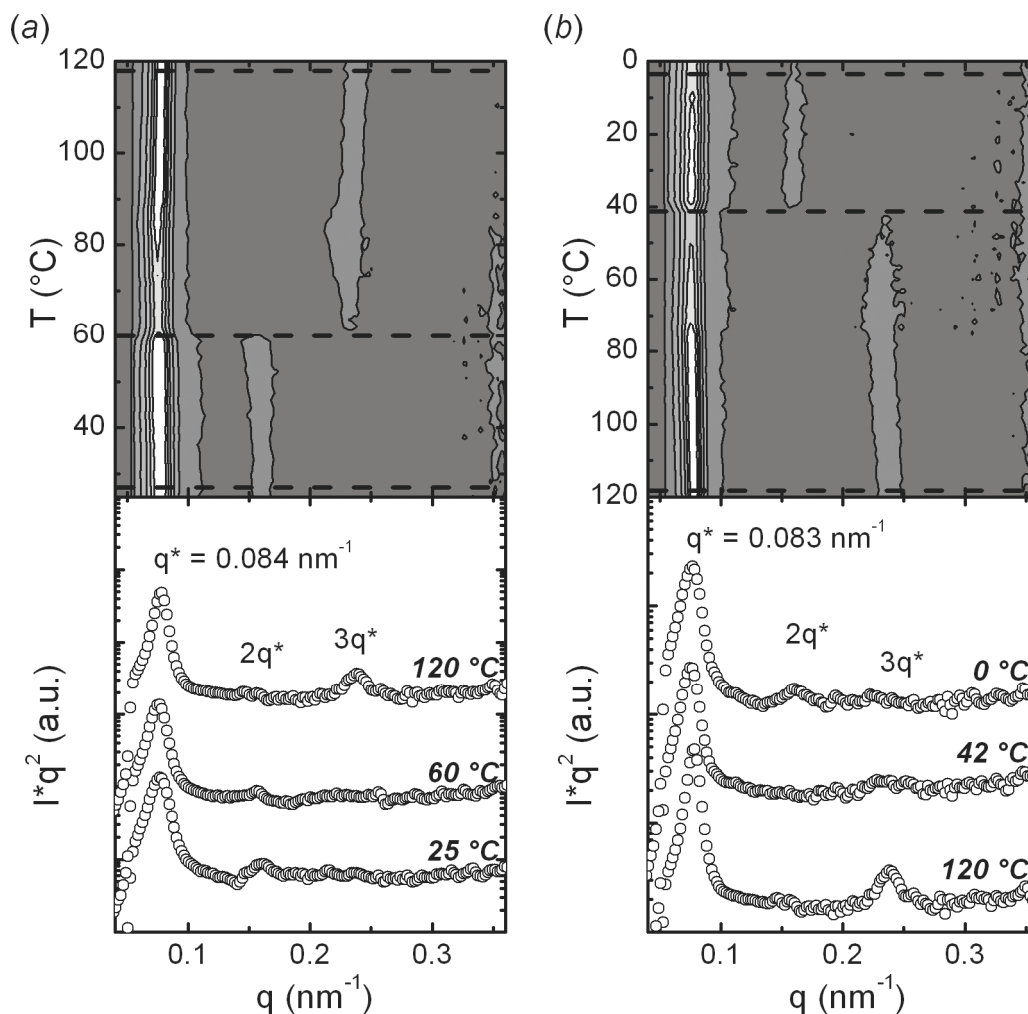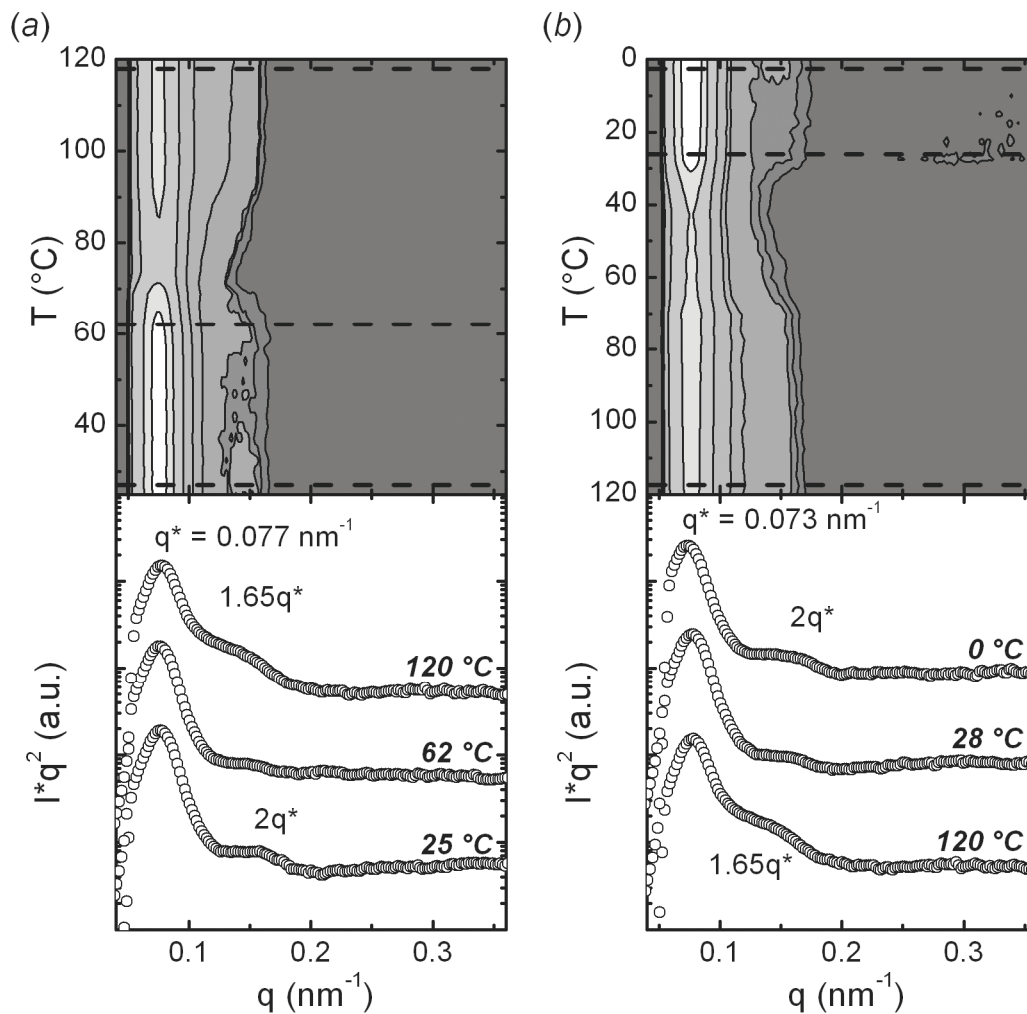
Figure 5.5. SAXS patterns for the triblock terpolymer $E_{16}S_{40}EO_{44}$[144]. Upper part: Top view of the SAXS scans as a function of the temperature during the thermal protocol. The horizontal lines indicate selected temperatures of representative morphological stages. Lower part: SAXS patterns at different selected temperatures indicated in the temperature dependant representation. (a) Heating scan and (b) subsequent cooling scan.

5.4. Conclusions

The thermal monitoring of the morphology of non-hydrogenated and hydrogenated triblock terpolymers with two different compositions has been successfully carried out upon heating and cooling scans. The technique allowed the detection of the effects of

crystallization on the morphology formation. For the triblock terpolymer with high content of both end blocks only lamellae are observed. A change in the diffraction pattern was found above the melting temperature of PEO, attributed to a decrease in the electron density contrast between the PEO and PS blocks, which sum up to a volume fraction around 50% of the whole macromolecule. This leads to a suppression of the second order reflection. It was found that the terpolymer with low content of PB formed lamellae, while the hydrogenated counterpart showed poor lamellar order at room temperature, but self-assembled nicely into cylinders above the melting temperature of PEO. This particular morphological change was not detected by any other method employed. The fact that the morphologies before and after hydrogenation were different was attributed to the slight increase of the interaction parameter of the PE with the other two blocks, in combination with the composition of the terpolymer.

5.5.   References

1.   Neumann, C.; Loveday, D. R.; Abetz, V.; Stadler, R. *Macromolecules* **1998,** 31, (8), 2493-2500.

2.   Hamley, I. W.; Castelletto, V. *Progress in Polymer Science* **2004,** 29, (9), 909-948.

3.   Castelletto, V.; Hamley, I. W. *Current Opinion in Solid State and Materials Science* **2004,** 8, (6), 426-438.

4.   Floudas, G.; Vazaiou, B.; Schipper, F.; Ulrich, R.; Wiesner, U.; Iatrou, H.; Hadjichristidis, N. *Macromolecules* **2001,** 34, (9), 2947-2957.

5.   Huckstadt, H.; Gopfert, A.; Abetz, V. *Polymer* **2000,** 41, (26), 9089-9094.

6.   Hamley, I. W., *The Physics of Block Copolymers*. Oxford University Press: Oxford, 1998.

7.   Schmalz, H.; Abetz, V.; Lange, R.; Soliman, M. *Macromolecules* **2001,** 34, (4), 795-800.

8.   Schmalz, H.; Boker, A.; Lange, R.; Krausch, G.; Abetz, V. *Macromolecules* **2001,** 34, (25), 8720-8729.

9. Müller, A. J.; Balsamo, V.; Arnal, M. L. *Advances in Polymer Science* **2005,** 190, 1-63.

10. De Jeu, W. H., Lamellar Ethylene Oxide-Butadiene Block Copolymers Films as Model Systems for Confined Crystallization. In *Lecture Notes in Physics: Polymer Crystallization: Observations, Concepts and Interpretations*, Sommer, J.-U.; Reiter, G., Eds. Springer: Berlin, 2003; Vol. 606, pp 196-207.

11. Kato, K. *J Electron Microsc (Jpn)* **1965,** 14, 220.

12. Zhu, L.; Chen, H.-L.; Calhoun, B. H.; Ge, Q.; Quirk, R. P.; Thomas, E. L.; Hsiao, B. S.; Yeh, F.; Lotz, B. *Polymer* **2001,** 42, 5829-5839.

13. Grulke, E. A., In *Polymer Handbook*, 4th ed.; Brandrup, J.; Immergut, E. H.; Grulke, E. A., Eds. J. Wiley & Sons: New York, 1999; p VII/675.

14. Stadler, R.; Auschra, C.; Beckmann, J.; Krappe, U.; Voight-Martin, I.; Leibler, L. *Macromolecules* **1995,** 28, (9), 3080-3097.

15. Barton, A. F. M., *CRC Handbook of Polymer Liquid Interaction Parameters and Solubility Parameters*. CRC Press: Boca Raton, 1990; p 768.

16. $\chi = \frac{v}{RT}\left(\delta_i - \delta_j\right)^2$, where v is the geometric average of the molar segmental volume calculated from the densities at room temperature (density corrections for the real temperature are neglected), RT is the molar thermal energy at 60 °C.

Chapter 6. Thin Film Morphology in Triblock Terpolymers with One and Two Crystallizable Blocks

The thin film morphology of novel polybutadiene-*block*-polystyrene-*block*-poly(ethylene oxide) (PB-*b*-PS-*b*-PEO) and polyethylene-*block*-polystyrene-*block*-poly(ethylene oxide) (PE-*b*-PS-*b*-PEO) triblock terpolymers was determined by atomic force microscopy (AFM). The experiments were carried out on dry, wet and heated samples, in order to vary the contrast among the blocks. The different measurements allowed the discrimination between the PE and the PEO blocks, which was otherwise not possible. The effect of different thermal treatments (related to the crystallization temperatures) on the generated morphology was studied for a confined spherical morphology. The domain size, i.e., disk diameter, was found to increase as the crystallization temperature was increased.

6.1. Introduction

Block copolymers are widely studied materials. One of the reasons is that their properties depend on the properties of the constituent blocks, and can therefore be tailored.[1-3] The second reason is their ability to self-assemble into microphases with dimensions in the nanometer range when the blocks are incompatible.[1-18] This allows the use of block copolymers in bulk as compatibilizers, dispersion agents, impact modifiers, and carriers.[8, 19-22] Taking advantage of the surface properties, as in the case of thin films, they find applications as selective surfaces, patterning surfaces, and templates for nanotopography.[8, 23-27] The complete characterization of a given block copolymer is not only based on its molecular properties, but also comprises the determination of its morphology.

The process of self-assembly is thermodynamically based on the segmental interaction parameters between the constituent blocks, but it is also affected by the presence of any

given surface, usually in the form of a substrate, a nanoparticle or a crystal. Although there are a wide number of publications reporting morphological studies of diblock copolymers with one crystallizable block,[18, 28-38] the analysis of more complex cases has been the topic of only few contributions.[39-50] For the simplest case, i.e., an amorphous diblock copolymer, the generated morphologies vary generally from disordered state to spheres, cylinders, cocontinuous gyroid and lamella when the volume fraction of one block increases from 0 to 0.5.[1]

A variety of different fascinating morphologies arises when more than two blocks are included in the system. In the most simple case these are amorphous triblock terpolymers, where morphologies such as core-shell cylinders or core-shell gyroid are found.[51] Also tetrablock quarterpolymers and higher systems have been reported.[52] Including a crystallizable block in the system will imply that the crystallization could occur within the microphase, or it could take over the microphase separation process and completely disrupt the self-assembly, which is known as break-out.[53] Furthermore, one can imagine the additional contribution of a second crystallizable block with lower T_c, which might interact with the already created crystal.

In order to address this interesting subject, polybutadiene-*block*-polystyrene-*block*-poly(ethylene oxide) (PB-*b*-PS-*b*-PEO) and polyethylene-*block*-polystyrene-*block*-poly(ethylene oxide) (PE-*b*-PS-*b*-PEO) triblock terpolymers have been synthesized by sequential anionic polymerization in different compositions. The corresponding morphological characterization in the bulk state was carried out by small angle X-ray scattering and transmission electron microscopy, as described in Chapter 4. Since none of the mentioned methods allows the discrimination between the two crystalline blocks, i.e., PE and PEO, the designation of the observed morphologies was not achieved. In this chapter, atomic force microscopy (AFM) is used in order to overcome this handicap and to

achieve a complete morphological characterization, attaining the differentiation between the two crystalline blocks both by imaging wet surfaces (where the PEO blocks gets swollen) and by temperature-dependant imaging (where the thermal transitions of each block can be identified). Since the AFM technique is used on thin films, in this contribution we also compare the bulk and thin film morphology. Finally, different thermal treatments are applied to the samples in order to modify the restrictions imposed by the surface and control the crystallization. In this simple way, the generated morphology is influenced.

6.2. Experimental Part

6.2.1. Materials

Polybutadiene-*block*-polystyrene-*block*-poly(ethylene oxide) (PB-*b*-PS-*b*-PEO) linear triblock terpolymers have been synthesized by sequential anionic polymerization, as described in Chapter 4. Further catalytical hydrogenation produced polyethylene-*block*-polystyrene-*block*-poly(ethylene oxide) (PE-*b*-PS-*b*-PEO), a linear triblock terpolymer with two crystallizable blocks separated by a glassy middle block. Molecular characteristics of the triblock terpolymers used in the present study are presented in Table 6.1. In the notation here employed, $A_xB_yC_z^m$, the subscripts stand for the mass fraction in percent and the superscript indicates the overall number-averaged molecular weight M_n of the block copolymer in kg/mol.

6.2.2. Transmission Electron Microscopy (TEM)

The bulk morphology of PB-*b*-PS-*b*-PEO and PE-*b*-PS-*b*-PEO triblock terpolymers was studied by bright field TEM using a Zeiss CEM 902 electron microscope operated at 80 kV and a Tecnai G2 F20 electron microscope operated at 200 kV. Films were prepared by casting from a 3 wt-% hot (70°C) toluene polymer solution. After one week the solvent

was completely evaporated, the films were slowly cooled to room temperature and dried under vacuum at room temperature for 24 h. Further annealing treatment was carried out under nitrogen flow, holding the samples at 120 °C for 6 h. Thin sections were cut at - 130 °C with a Reichert-Jung Ultracut E microtome equipped with a diamond knife. The non-hydrogenated precursors were stained by exposure to OsO_4 vapor for 60 sec, and the hydrogenated terpolymers were stained by exposure of the thin sections to RuO_4 vapor for 30-40 min.

Table 6.1. Molecular weight (M_n) of each block and molecular weight distributions (M_w/M_n) of the triblock terpolymers employed in the thin film morphology studies. The content of 1,2-units in the PB block is given in brackets.

	M_n (Kg/mol)			M_w/M_n
	PB[a] (%1,2[b]) / PE[c]	PS[c]	PEO[c]	
$B_{16}S_{68}EO_{16}^{210}$ / $E_{17}S_{67}EO_{16}^{211}$	35 (11.5) / 36	142	33	1.01
$B_{29}S_{40}EO_{31}^{168}$ / $E_{29}S_{40}EO_{31}^{170}$	48 (12.9) / 50	67	53	1.03
$B_{37}S_{16}EO_{47}^{76}$ / $E_{38}S_{16}EO_{46}^{77}$	28 (11.8) / 29	13	36	1.03

[a] Determined by size exclusion chromatography experiments in THF calibrated against PB standards.
[b] Determined by ^{1}H NMR spectroscopy in $CDCl_3$.
[c] Determined by ^{1}H NMR spectroscopy using the molecular weight of the PB precursor obtained by SEC in THF calibrated against PB standards.

6.2.3. TappingMode^{TM} atomic force microscopy

The images were taken on a "Digital Instruments" MultiMode^{TM} AFM (NanoScope IV controller) operating in tapping mode at ambient conditions, using commercial silicon TM AFM tips (model MPP 12100) with a free resonance frequency in the range from 123 to 151 kHz and spring constants in the range from 5 to 10 N/m.

Thin films of PB-*b*-PS-*b*-PEO and PE-*b*-PS-*b*-PEO triblock terpolymers were prepared by spin coating (2000 rpm, 20 sec) from 10.0 mg/ml toluene solutions, on cleaned polished silicon wafers. The silicon wafers were cleaned in a water-saturated UV-ozone atmosphere for at least 24 hours. The spin coated films were annealed at 200 °C under N_2 during 60

min, using a Linkam THMS 600 hotstage with TMS 91 controller. The annealing step was followed by different isothermal crystallization treatments. The resultant film under these conditions have thicknesses around 60 – 70 nm.

6.2.4. Swelling experiments

Swelling experiments were performed on annealed thin films. A drop of Millipore water was deposited on the film after spin-coating and annealing 60 min at 200 ℃. The excess of water was removed with a pipette after 30 min, and the sample was measured immediately.

6.2.5. Heating experiments

The measurements at elevated temperatures were conducted with a commercial thermal accessory supplied by the microscope manufacturer. Heating of the sample, which was performed with a Pt-resistive element underneath the sample puck, was accompanied by heating of a probe. Such dual heating provides a more controlled sample temperature and stable tapping mode imaging at elevated temperatures up to 250ºC. Purging of a sample compartment with a light stream of He gas was arranged to prevent block copolymer oxidation at high temperatures.

6.3. Results and Discussion

6.3.1. Morphology Determination for $E_{17}S_{67}EO_{16}$[211]

In images obtained by AFM measurements, the height image reflects the sample topography. Since the samples were prepared by spin-coating and later annealing, this image will give information related to the smoothness of the film and to the film morphology. However, the possibility of sample preparation effects and artifacts should be always considered. In case of block copolymers with rubbery and glassy blocks, low-force

conditions are those at which a tip properly tracks the sample surface. Otherwise an assignment of height images features to surface topography might be misleading.[54]

In crystallizable block copolymers, the AFM phase mode gives very rich information due to the large difference in viscoelastic properties between crystalline and amorphous phases. Based on the nature of the blocks, the corresponding phase images will feature bright or white domains corresponding to a polyethylene or a poly(ethylene oxide) crystal. The dark domains correspond to the polybutadiene block or the amorphous part of either crystallizable block. The intermediate or gray domain will represent the polystyrene block, which stiffness is relatively high (when the block is below its glass transition temperature), although it is lower than the stiffness of any crystal.

The results of AFM imaging for the pair $B_{16}S_{68}EO_{16}^{210}$ / $E_{17}S_{67}EO_{16}^{211}$ are presented in Figure 6.1. As it can be seen from the data scale ($z_{max} = 20$ nm), the films are very smooth after the spin-coating and further thermal treatment. In the phase image presented in Figure 6.1c some crystalline lamellae can be identified inside the circular domains. However, from the AFM image alone it would not be possible to differentiate between the two crystallizable blocks, since the viscoelastic difference between two crystals does not give sufficient contrast. Analogously, one is also not able to differentiate between the two amorphous phases, which show up as low AFM-phase materials (i.e., dark in the color scale).

In the phase image presented in Figure 6.1a, it is possible to distinguish some bright domains corresponding to crystalline spheres of poly(ethylene oxide), which despite its low crystallization temperature (presented in Chapter 4 , $T_c = -33.8$ °C) has crystallized after long storage time, i.e., 20 months, at room temperature (the freshly prepared film did not present any phase contrast, results not shown). Within the crystalline domains it is not possible to identify crystalline lamellae (only a solid bright sphere is visible and the
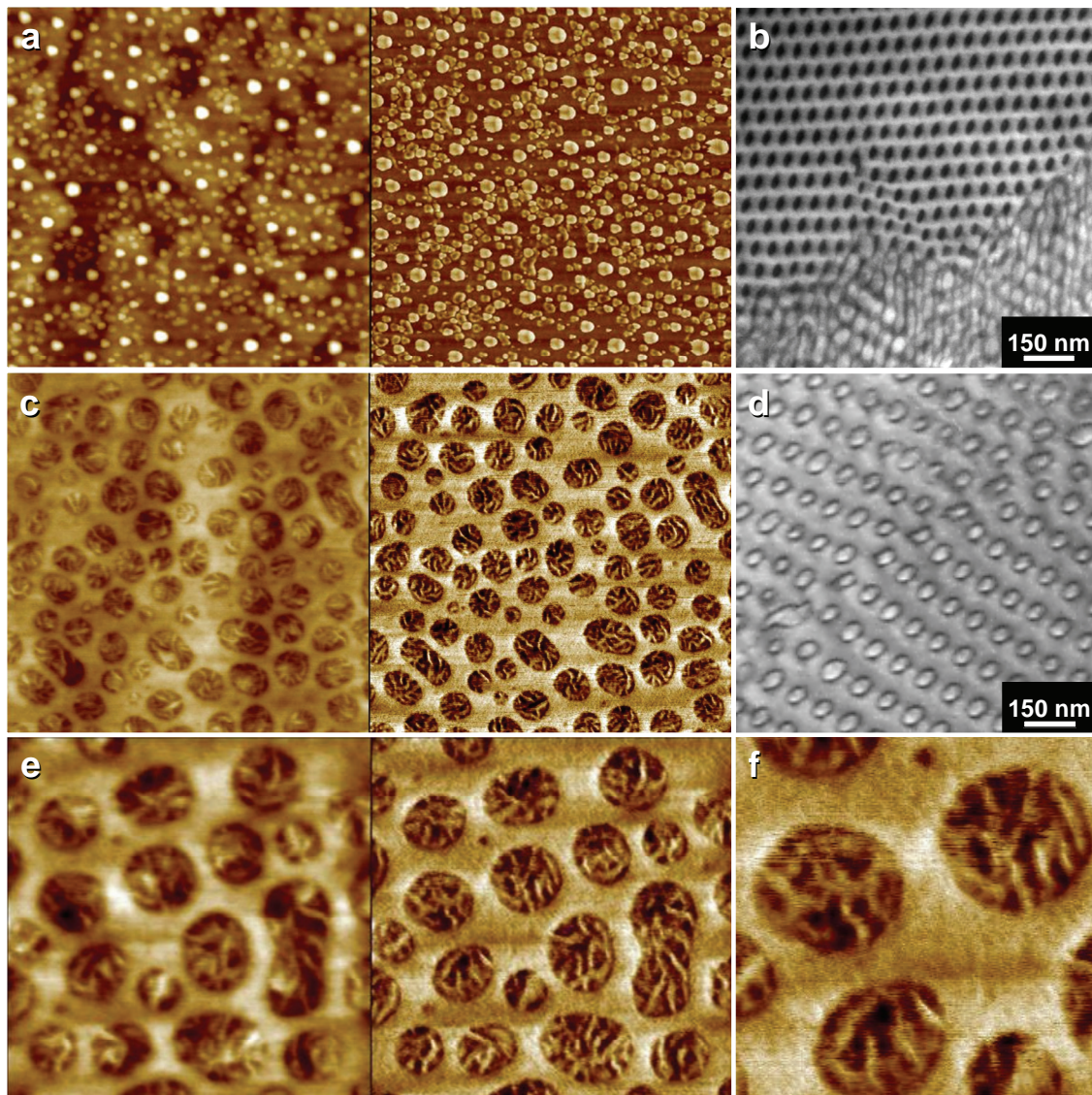
Figure 6.1. AFM height (left) and phase (right) images, 1 μm · 1 μm, with $z_{max,\ height}$ = 20 nm, and TEM micrographs of ultrathin sections. (a) AFM image and (b) TEM micrograph of $B_{17}S_{68}EO_{16}^{210}$. (c) AFM image and (d) TEM micrograph of $E_{17}S_{67}EO_{16}^{211}$. (e) AFM image of $E_{17}S_{67}EO_{16}^{211}$, 500 nm · 500 nm, and (f) Zoom-in of the phase image in (e).

amorphous part is not resolved). The polybutadiene block remains unidentified in both height and phase images, which might indicate that it forms a layer most probably towards the air surface. The morphology of the hydrogenated $E_{17}S_{67}EO_{16}^{211}$ terpolymer is different (see Figure 6.1c). It is possible to see spherical domains filled with crystalline lamellae and amorphous phase. The polystyrene block forms the matrix for the spherical or disk-

like domains of the polyethylene and/or poly(ethylene oxide), which are the two blocks being able to undergo crystallization. However, in this system large supercoolings are required to initiate crystallization, as was presented elsewhere.[55] At this point, as has already been mentioned, it is not possible to differentiate between the two crystallizable phases (or the two amorphous phases) based only on the presented AFM images.

Closer looks into the morphology are provided by imaging at a 500 nm window (Figure 6.1e) and a zoom-in into its phase image (Figure 6.1f). There, the inner domain structure is nicely observed. The supposed lamellae are observed as filling the domains by linking two points of the surface or being linked to the interface at one end and linked at another lamella at the other end. Actually, crystal nucleation from the surface is expected in this system, as observed by crystallization kinetic studies. This topic will be discussed in Chapter 6.

It is evident from the results presented in Fig. 1 that the thin film morphology is similar to the bulk morphology (TEM micrographs are shown in Figure 6.1b and 6.1d, SAXS scattering patterns have shown an *fcc*-packed spheres structure, as discussed in Chapter 4, Figure 4.4). However, the long range order obtained in the spin coated film is not as good as the one observed in the cast film used for studies of the behavior in the bulk. This relates to the lower mobility of the polymer chain in the thin film, caused by the interaction forces with the substrate.

To completely define the morphology in the hydrogenated triblock terpolymer, it is necessary to be able to distinguish the polyethylene crystals from the poly(ethylene oxide) crystals. For this purpose, the thin film sample was subjected to swelling in water for 30 min. Water is a solvent only for the poly(ethylene oxide) block, but a non-solvent for polyethylene and polystyrene blocks. Therefore, it is expected that only the poly(ethylene oxide) domains swell. The result of such experiment is presented in Figure 6.2.
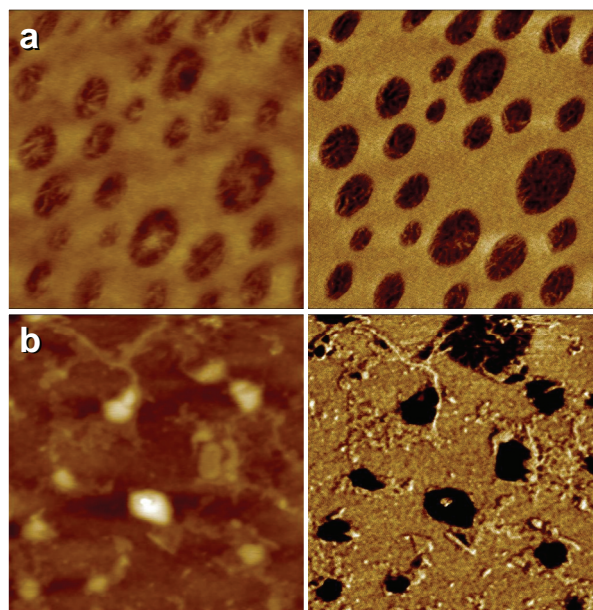
Figure 6.2. AFM height (left) and phase (right) images of $E_{17}S_{67}EO_{16}{}^{211}$ (1 µm $\cdot$ 1 µm, with $z_{max,\ height}$ = 20 nm) (a) before and (b) after swelling 30 min with water.

The height and phase images presented in Figure 6.2 give insight into the morphology of the triblock terpolymer. It is possible to locate the poly(ethylene oxide) domains as the swollen circular domains in Figure 6.2b, since they are bumps in the height image and are soft areas in the phase image (the non-swollen film is presented in Figure 6.2a for the sake of comparison). The swollen (or partially dissolved) PEO block can only expand towards the top of the polymer film, and covers therefore the PE lamellae observed previously. Only one of the circular domains does not seem to contain a significant amount of poly(ethylene oxide) in the 1 µm^2 area shown. This could indicate that both polyethylene and poly(ethylene oxide) blocks share the circular domains in most of the cases. Also, this method allowed the identification of a few PEO chains dispersed in the PS matrix, given the mobility restrictions associated to such high molecular weight and substrate interactions that evidence that the obtained morphologies could not be completely in equilibrium.

Now that the poly(ethylene oxide) block has been located in the observed thin film morphology thanks to the water swelling experiments, heating experiments have been conducted on $E_{17}S_{67}EO_{16}{}^{211}$, in order to identify also the polyethylene block. The initial concentration of the polymer solution was 9 mg/ml, so the thin films here presented are slightly thinner than the ones presented before. Phase images of a heating sequence are shown in Figure 6.3, and the subsequent cooling is presented in Figure 6.4.
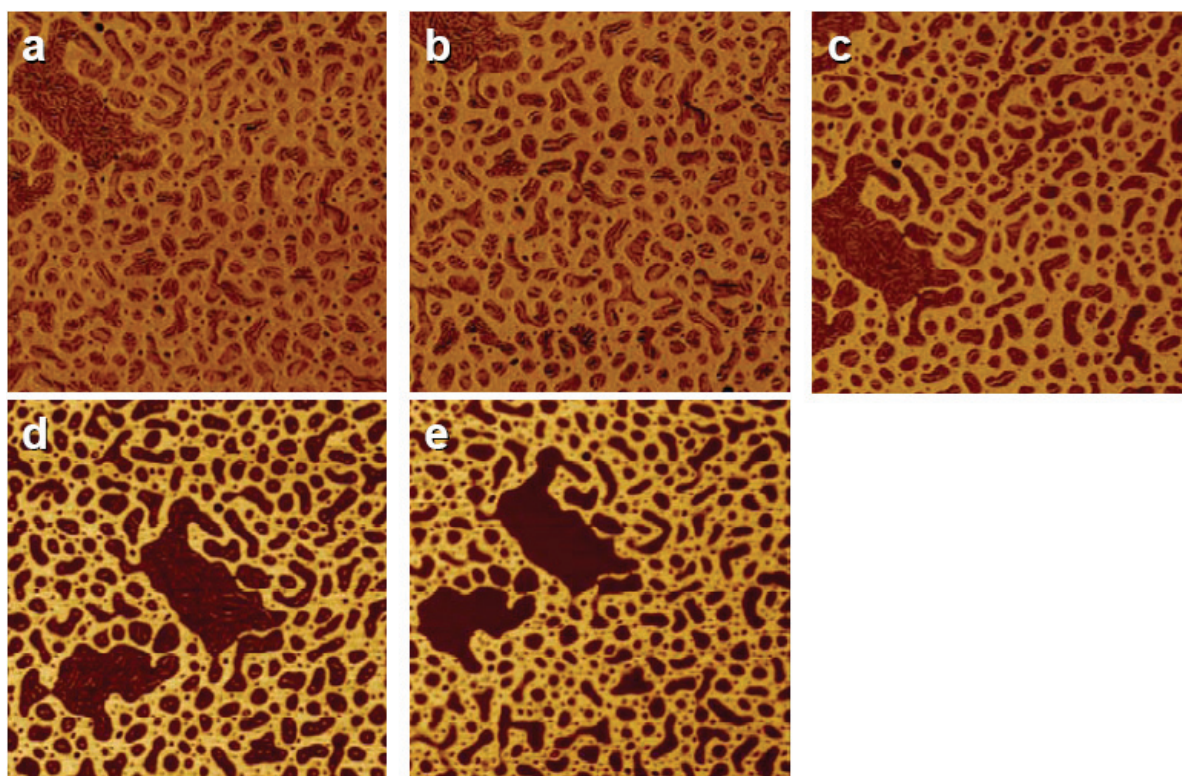
Figure 6.3. AFM phase images for $E_{17}S_{67}EO_{16}{}^{211}$ (2 µm · 2 µm, with $z_{max,\ phase}$ = 100 °) during a heating protocol. (a) T = 25 °C, (b) T = 50 °C, (c) T = 75 °C, (d) T = 100 °C, (e) T = 110 °C.

The initial morphology shown in Figure 6.3a is very similar to the one presented before (see Figure 6.1c) although in this case some domains are evidently bigger than others. It is possible to follow the beginning of the melting at 75 °C (Figure 6.3c) while most of the polyethylene crystals remain. It is worth noting that this temperature is above the maximum possible melting point of the PEO block, as derived from differential scanning

calorimetry (DSC) experiments presented in Chapter 4, Figure 4.8. At 100 °C (Figure 6.3d) some polyethylene crystals melt, but the complete melting is seen only at 110 °C (Figure 6.3e). The polyethylene crystals remaining above 75 °C can be observed in all the circular domains. Since the PEO block was identified in virtually every domain during the water-swelling experiments and the PE lamellae were found in every domain above 75 °C during the heating experiments, it is therefore confirmed that the two blocks PE and PEO share the confined domains in this morphology within the studied temperature range.
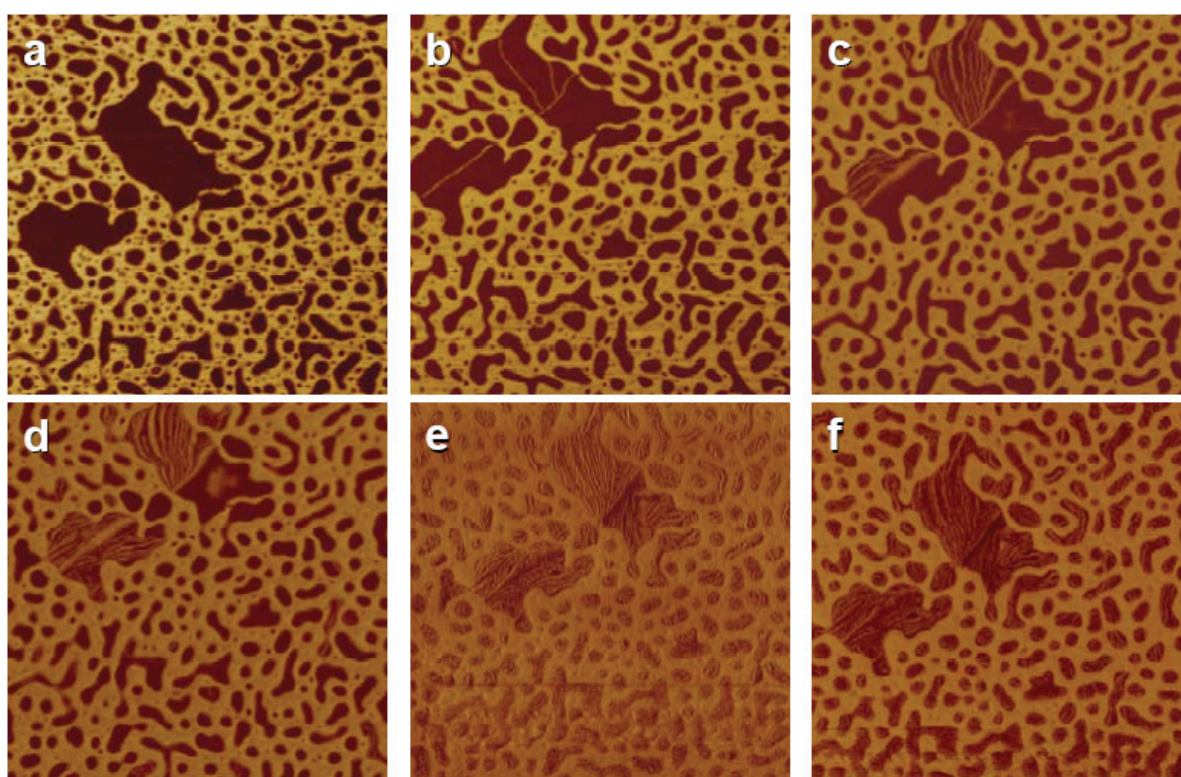
Figure 6.4. AFM phase images for $E_{17}S_{67}EO_{16}{}^{211}$ (2 μm · 2 μm, with $z_{max, phase}$ = 100 °) during a cooling protocol. (a) T = 110 °C, (b) T = 100 °C, (c) T = 90 °C, (d) T = 75 °C, (e) T = 50 °C, (f) T = 25 °C.

The crystallization from the melt can be analyzed from the results shown in Figure 6.4. A small amount of crystallization is already observed at 100 °C (Figure 6.4b) in the bigger domains, where the crystals are observed to grow at the domain interface, as was already seen in Figure 6.1f. From thermal studies carried out in bulk samples, the crystallization

temperatures of the two blocks were determined by DSC as $T_{c, PE} = 55.9$ °C and $T_{c, PEO} = -30.9$ °C (Chapter 4, Figure 4.8 and 4.9). Those are average values, and it comes as no surprise that the onset of PE crystallization is observed at 100 °C. The sample at 50 °C (Figure 6.4e) looks as it has reached (or it is close to) the highest crystallization degree possible under the given conditions. Due to the low crystallization temperature of the PEO block, it is only expected to undergo crystallization under very large supercoolings, which were not achieved during the presented experiment. Only temperatures well below room temperature or long storage times will allow the crystallization. Therefore, the observed lamellae are exclusively PE crystals, and the PEO block forms an amorphous phase inside the domains, depicted as the darker areas since it appears as a low AFM-phase material.

As was already mentioned, the experiments presented in Figure 6.3 and 6.4 indicate that the PE block is located in every domain. The swelling experiments (Figure 6.2) indicate that the PEO block is also present in all the spherical domains. In this way it is demonstrated that the PE and the PEO block are sharing the confined domains in the temperature range studied, i.e., from room temperature to the melting point of the PE block (further experiments and analysis regarding the molten state were not carried out and they are beyond the scope of the present contribution). The tendency of the two blocks to segregate is expected, since the segmental interaction parameter has a value of 0.16 at 60°C,[51, 56, 57] and it is the largest among all the possible pairs (see Chapter 4, Table 4.2). However, it seems that certain particularities of the system, such as the low content of crystalline blocks, low molecular weight of the crystallizable blocks compared to the PS block, surface interaction and restriction arising from the solvent employed (toluene is a very good solvent for PS, a non-ideal solvent for PEO and a poor solvent for PE) and from crystallization, allow the formation of such shared domains in a case of otherwise immiscible blocks. It has been observed that polymer crystallization is able to overcome

miscibility driven phase behavior, as it can produce fractionation of chemically identical polymer chains as a function of their molecular weight, caused by molecular weight-dependent crystallization kinetics and melting temperatures.[36, 49, 58, 59]

Further experiments on the thin film morphology of $E_{17}S_{67}EO_{16}{}^{211}$ were carried out by employing different polymer solution concentrations for the film preparation. In Figure 6.5, the AFM images of films prepared from 5.0 mg/ml 7.5 mg/ml and 10.0 mg/ml polymer solutions are presented. This variation in solution concentration reflects in the final film thickness, since all spinning parameters were kept constant.
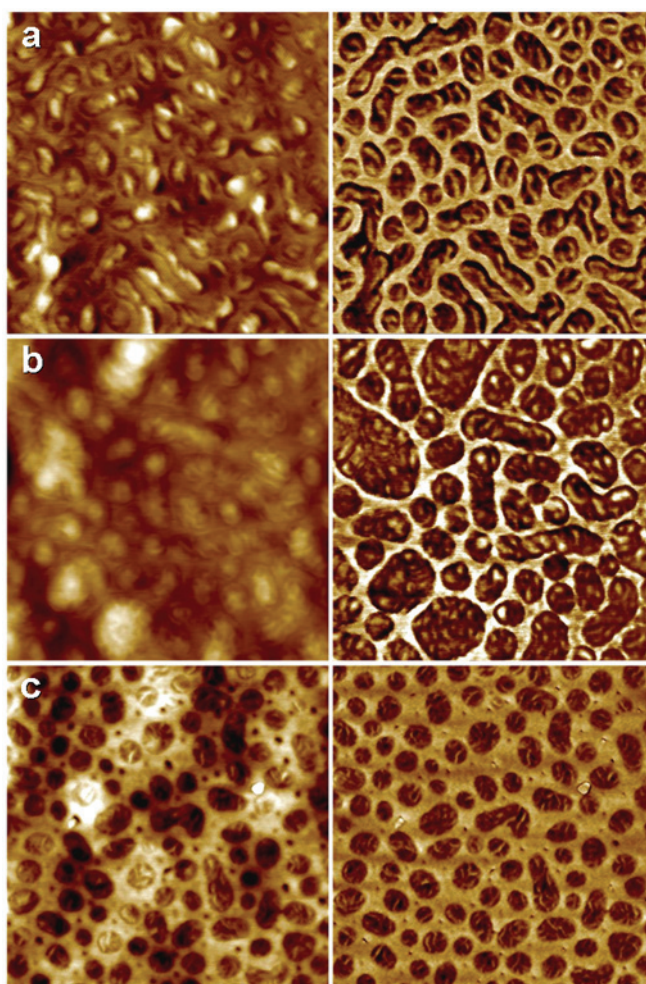
Figure 6.5. AFM height (left) and phase (right) images of $E_{17}S_{67}EO_{16}{}^{211}$ (1 μm · 1 μm, with $z_{max, height}$ = 10 nm, $z_{max, phase}$ = 30 °, tapping softly on the surface) of films prepared by spin coating from (a) 5.0 mg/ml, (b) 7.5 mg/ml and (c) 10.0 mg/ml polymer solutions in toluene.

The results in Figure 6.5 show significant changes of the morphology with the film thickness. The thinnest film, i.e., the film prepared from a 5.0 mg/ml solution presented in Figure 6.5a, shows worm-like domains that are higher in topography than the matrix. Given the triblock terpolymer composition, as well as the previous results, these domains are formed by the PE and the PEO blocks. The two blocks form spherical domains in bulk (Figure 6.1d), but since the film thickness limits one of the dimensions, they are not spherical but stretched to the observed worm-like domains. In the phase image it is possible to observe features inside the domains, which should correspond to the crystalline PE phase, although they are not very well defined.

The film prepared from a 7.5 mg/ml solution (Figure 6.5b) shows a morphology where the domains are even more deformed that in the thinnest film. The presented features correspond to a coalescence of the PE/PEO domains to form bigger ones. The chain dimensions are presented in Table 6.2, calculated for the extended chain and the unperturbed coil of each block. The dimensions presented for the PS block fit with the inter-domain distances observed in the AFM images. The circular, not merged domains also have dimensions in good agreement with the PE and PEO chain dimensions. The merged domains are, on the contrary, too big compared to the chains, and therefore such domains should be interpreted as flat domains on the surface "filled" with end chains of terpolymer chains that lie underneath them.

Table 6.2. All-trans conformation (L') and unperturbed coil ($2<s^2>^{1/2}_{real}$) chain dimensions of the blocks in $E_{17}S_{67}EO_{16}$[211].

Block	L' (nm)	$2<s^2>^{1/2}_{real}$ (nm)
Polyethylene	80.9	16.8
Polystyrene	171.8	29.8
Poly(ethylene oxide)	93.4	13.4

The observed morphology changes drastically for the thickest film, which is shown in Figure 6.5c. The PE/PEO domains form depressions instead of bumps in the height image, the inner-domain structure shown in the phase image corresponds to crystalline lamellae, the size of the domains has decreased and their shape is more spherical. In summary, the morphology is more similar to the bulk morphology observed by TEM than in any other case. It can be assumed that the film thickness obtained with a 10.0 mg/ml polymer solution is enough to allow the formation of spherical domains similar to those formed in bulk. Still, some domains have merged together and the long range order is not as good as in bulk. The merge of the domains observed in different thin films explains the big domains found in Figure 6.3 and 6.4.

Additional information of the morphology is given by using different tapping forces to image the sample surface. The corresponding results are presented in Figure 6.6, with the images obtained by soft (Figure 6.6a) and hard (Figure 6.6b) tapping. While the overall morphology is similar to what has been discussed so far, some interpretations can be introduced.

In the phase image obtained by soft tapping on the surface (Figure 6.6a) it is possible to see the stiff PE lamellae inside the circular domains, surrounded and intercalated by soft PEO and PE amorphous phase (Figure 6.4 is consistent with previous calorimetry results where the PEO block did not crystallize at the temperatures employed in the present experiments). By increasing the tapping force (Figure 6.6b) the matrix is better defined as a stiff material, which supports the assumption that the matrix consists of PS. Also, the stiff PE lamellae inside the domains seem to cover less area than in Figure 6.6a. This could be the effect of some rearrangement caused by the tip that pushes hard towards the substrate. Most likely, the PE lamellae are sunk into the amorphous PEO domains. Some

of the smaller lamellae could also have lost their flat-on orientation and reorient to edge-on.
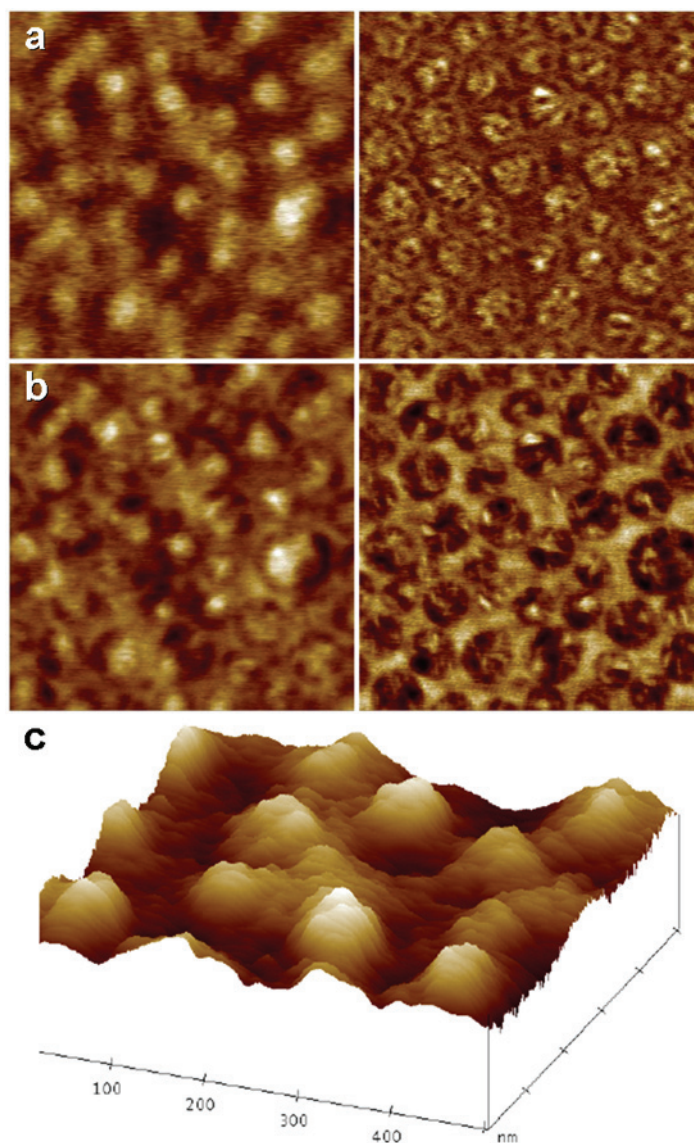
Figure 6.6. AFM height (left) and phase (right) image of $E_{17}S_{67}EO_{16}$[211] (1 μm · 1 μm) obtained by (a) soft tapping and (b) hard tapping on the surface. (c) 3-D representation of a zoom-in area into the height image in (a), with $z_{max, height} = 3$ nm.

A 3-D representation of the topography obtained by soft tapping is presented in Figure 6.6c. The PE/PEO domains are observed as bumps on the surface, which has not always been the case in the previously presented images. This could be an effect of the aging of

the sample, since the long time storage has allowed the PEO crystallization. However, this was not identified in all the aged $E_{17}S_{67}EO_{16}{}^{211}$ samples, and therefore cannot be 100 % attributed to PEO crystallization. As a matter of fact, most of the aged samples of $E_{17}S_{67}EO_{16}{}^{211}$ look unchanged.

6.3.2. Effect of Annealing Procedures on the Morphology

In order to study the effect of the thermal treatment on the morphology of the triblock terpolymer, crystallization of $E_{17}S_{67}EO_{16}{}^{211}$ was carried out at different thermal conditions. The sample was spin-coated from the 10 mg/ml toluene solution, and immediately melted at 200 °C. Further, it was quenched to a T_c and kept there for the crystallization time. In some cases, two different T_cs were used in sequence, in order to crystallize first the polyethylene block and later the poly(ethylene oxide) block. The AFM height and phase images, as well as the conditions used during sample preparation are described in Figure 6.7. In order to gain more insight into the influence of crystallization condition on the microphases, one of these samples (Figure 6.7d) was further submitted to a thermal treatment below T_m of the PE-block, in order to anneal the already existent crystals. The results are shown in Figure 6.7f.

It is evident from Figure 6.7 that some changes in the microphases occur when the sample is subjected to different crystallization programs. In order to quantify these effects, the images were analyzed and the equivalent diameter of the disks was calculated. The disk diameter distribution was then fitted to a Gaussian distribution (results not shown), and the mean disk diameter values were obtained. The results from fittings made to images in Figure 6.7 are represented in Figure 6.8, as disk diameter as a function of the first crystallization temperature used in the thermal treatment. The value corresponding to the sample with further crystal annealing (Figure 6.7f) is plotted for direct comparison.
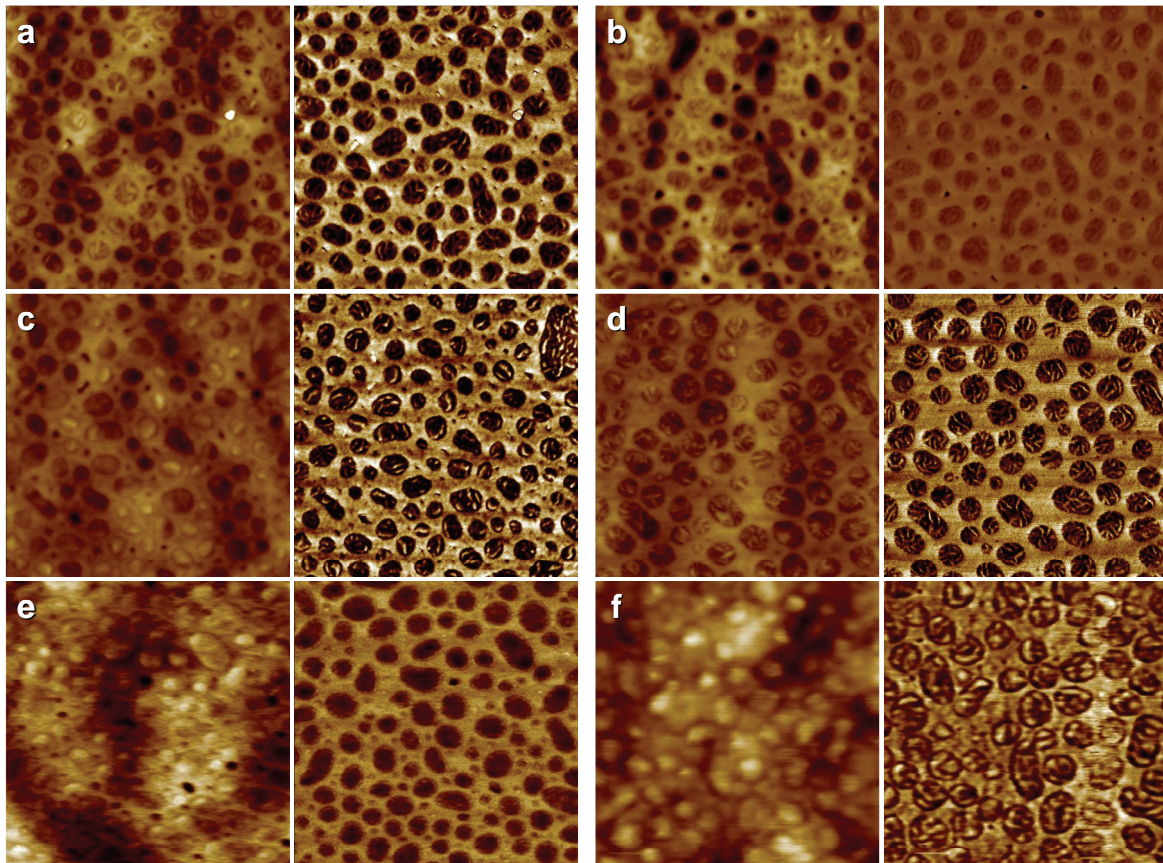
Figure 6.7. AFM height (left) and phase (right) image of $E_{17}S_{67}EO_{16}{}^{211}$ (1 μm · 1 μm, with $z_{max,\,height}$ = 20 nm) melted 60 min at 200 °C and then crystallized with the following procedure: (a) 4205 min at -26 °C, (b) 4030 min at 0 °C, (c) 300 min at 65 °C, followed by 3770 min at -26 °C, (d) 1059 min at 70 °C, followed by 1445 min at 0 °C, (e) 440 min at 80 °C, followed by 840 min at -26 °C, (f) 1059 min at 70 °C and 1445 min at 0 °C, followed by annealing 842 min at 80 °C.

In Figure 6.8, the tendency of in the thermal treatment on the disk diameter can be seen. The sample treated at 65 °C (shown in Figure 6.7c) presented a low disk diameter, which we attribute to the short holding time at the crystallization temperature. For the sample annealed after the crystallization treatment (Figure 6.7f), the diameter shows an increase compared to the non-annealed one. This result is comparable to the increase of lamellar thickness with crystallization temperature and with crystal annealing below T_m. It is fascinating that the actual size of the domain is also affected in the same way. The crystals

are thicker and the density inside the domain is therefore higher at higher crystallization temperatures, from where one would usually assume a smaller domain. However, a higher holding temperature also implies higher mobility of the overall chain, and a consequent more uniform microphase separation arrangement. This increased mobility for long time allows that more short chains come inside the confined domains, making them bigger than before the treatment (the presence of short PEO chains dispersed in the matrix was already revealed by the swelling experiments). These results evidence that the structures obtained at room temperature depend on crystallization and annealing conditions.
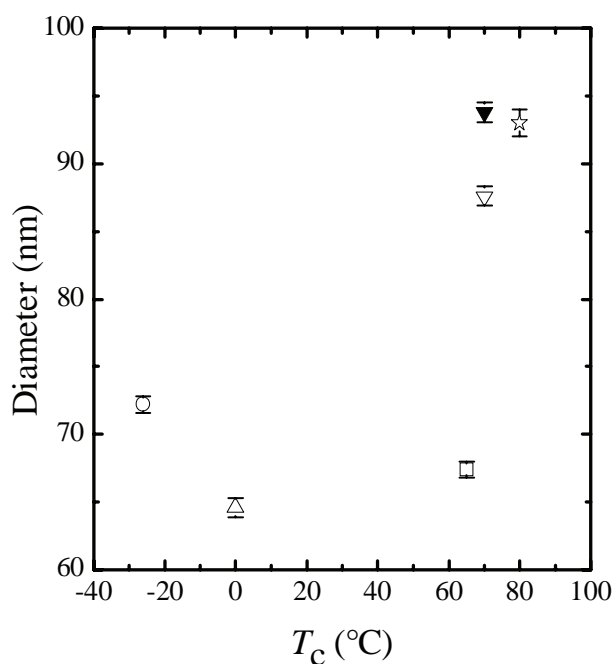
Figure 6.8. Disk diameter distribution for $E_{17}S_{67}EO_{16}{}^{211}$, as a function of the higher crystallization temperature used in the thermal treatment (PE crystallization temperature). The data correspond to the images shown in Figure 6.7, as follows: samples melted 60 min at 200 °C and then crystallized with the following procedure: ○ 4205 min at -26 °C, △ 4030 min at 0 °C, □ 300 min at 65 °C, followed by 3770 min at -26 °C, ▽ 1059 min at 70 °C, followed by 1445 min at 0 °C, ☆ 440 min at 80 °C, followed by 840 min at -26 °C, ▼ 1059 min at 70 °C and 1445 min at 0 °C, followed by annealing 842 min at 80 °C.

Even though theoretically the equilibrium morphology could be reached after very long annealing at high temperatures, in practice this state is very difficult to reach experimentally, due to slow dynamics of the high molecular weights and the risk of degradation of the PEO block. Therefore, the present study focuses mainly on the influence of the particular morphology of a triblock terpolymer system on crystallization. However, many questions regarding the morphology of the molten state remain, such as whether the PE and the PEO would ever segregate and how the phase segregation is in the equilibrium morphology.

The results summarized in Figure 6.8 indicate the possibility to control the dimensions of the spherical crystalline microphases by means of the thermal protocol applied to the sample, as has been previously found in block copolymers by different techniques.[36] The diameter of the spherical microphases can be increased up to 30 % using the same triblock terpolymer. This means that no time-consuming new synthesis is needed in order to vary the spherical size by changing the composition or the molecular weight, opening new possibilities in the control of microphase separation and morphology generation.

The study of the thickness of the crystalline lamellae as a function of the different annealing treatments was not carried out since the error associated to the measurements is not quantifiable. The observed thickness of the crystalline lamellae has been seen to depend on the tapping force (Figure 6.6b), and even when all measurements are taken under "soft tapping" conditions, the force still varies inevitably from sample to sample.

6.3.3. Morphology of Triblock Terpolymers with Different Compositions

The morphology of triblock terpolymers with two other compositions has been studied. These two cases are terpolymers also with similar content of PE and PEO end blocks, where the PS content is decreased (the content of the crystallizable blocks is increased). This change in composition causes two main effects: first, the self-assembled morphology

obtained varies from spherical domains to cylinders and lamellae, and second, the PEO block is able to crystallize at room temperature. The morphology of $B_{29}S_{40}EO_{31}$[168] and its hydrogenated triblock terpolymer is presented in Figure 6.9.
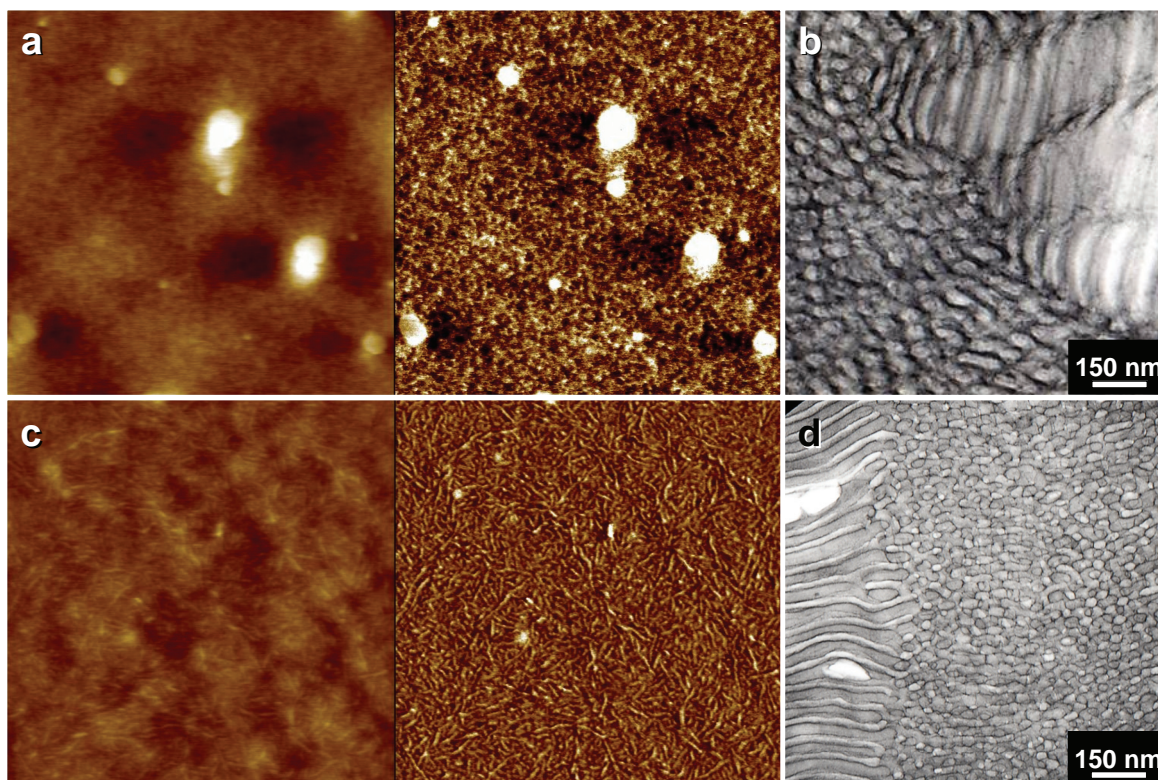
Figure 6.9. AFM height (left) and phase (right) images, 1 µm · 1 µm, with $z_{max, height}$ = 20 nm, and TEM micrographs of ultrathin sections. (a) AFM image and (b) TEM micrograph of $B_{29}S_{40}EO_{31}$[168]. (c) AFM image and (d) TEM micrograph of $E_{29}S_{40}EO_{31}$[170].

The height images corresponding to $B_{29}S_{40}EO_{31}$[168] (Figure 6.9a and 6.9c) show that the film prepared is relatively flat, with z_{max} < 20 nm. From the phase image of the non-hydrogenated terpolymer shown in Figure 6.9a, the dark dispersed polybutadiene domains can be identified, as well as a gray-featured polystyrene matrix. The poly(ethylene oxide) crystals are not evident, which means the block is not preferentially located at the surface but towards the substrate (completely amorphous PEO is not expected based on the calorimetry results that showed T_c = 37.9 °C). The ordered structure observed in bulk by TEM (Figure 6.9b) was not observed in the thin film. Increases of the AFM tapping

strength did not reveal any different features. In the case of the hydrogenated terpolymer ($E_{29}S_{40}EO_{31}^{170}$) displayed in Figure 6.9c, the crystal lamellae are evident, as well as some circular crystalline features that could be interpreted as cylinders, which relates well with the bulk morphology presented in Figure 6.9d.

The thin film morphology results for the third pair of triblock terpolymers studied here, $B_{37}S_{16}EO_{47}^{76}$ and $E_{38}S_{16}EO_{46}^{77}$, are summarized in Figure 6.10. As it has been shown for the previous terpolymers, Figure 6.10a shows the AFM phase image of a thin film of the non-hydrogenated $B_{37}S_{16}EO_{47}^{76}$, where the poly(ethylene oxide) crystalline lamellae were not evident even after increasing the tapping force during the measurement. The bulk morphology (Figure 6.10b) was also not obtained in the thin film.
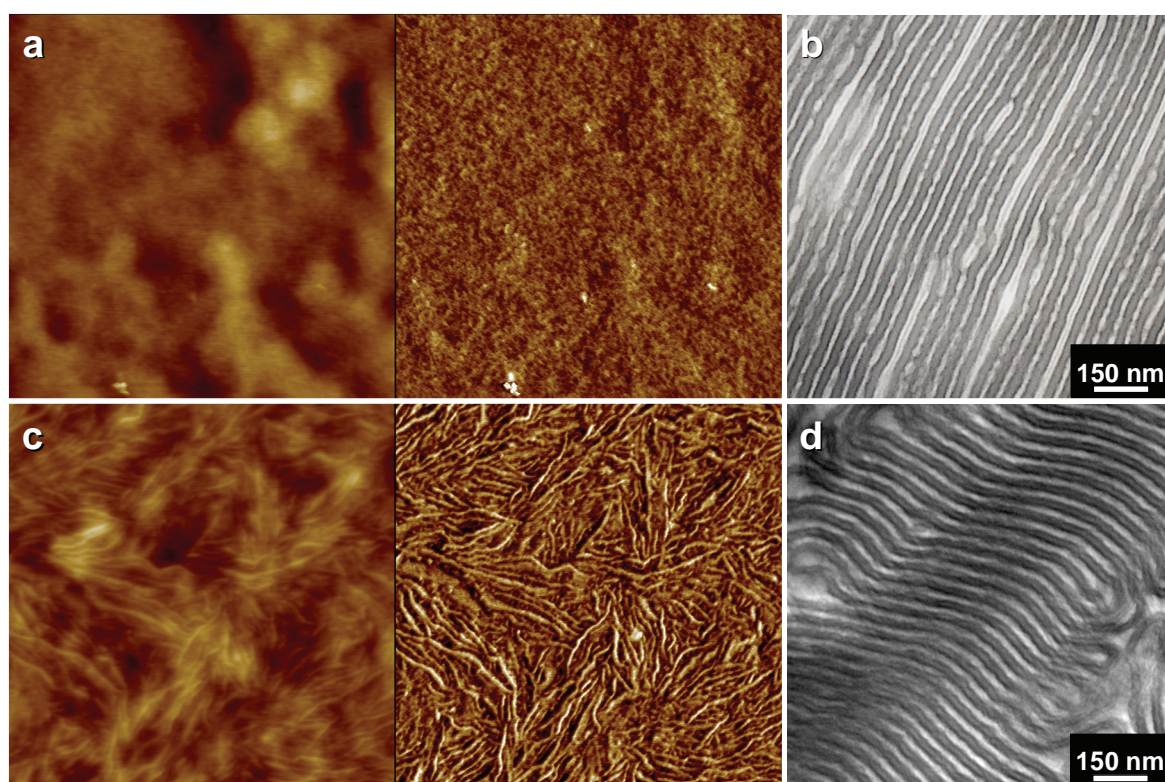
Figure 6.10. AFM height (left) and phase (right) images, 1 µm · 1 µm, with $z_{max,\,height}$ = 20 nm, and TEM micrographs of ultrathin sections. (a) AFM image and (b) TEM micrograph of $B_{37}S_{16}EO_{47}^{76}$. (c) AFM image and (d) TEM micrograph of $E_{38}S_{16}EO_{46}^{77}$.

The thin film morphology of $E_{38}S_{16}EO_{46}^{77}$ shows crystalline lamellae (Figure 6.10c), supposedly of both polyethylene and poly(ethylene oxide) blocks. Compared to the previous results, in this material it is possible to observe more crystalline features than in the others. This is expected since the content of crystallizable blocks (polyethylene and poly(ethylene oxide)) in the triblock terpolymer is around 84 wt %, compared to 60 wt % and 32 wt % from the other two cases. The bulk morphology (Figure 6.10d) has been determined as a clear lamellae morphology, but it is not possible to distinguish the long-range ordered microphases in the AFM images.

The results presented in this section evidence discrepancies between the thin film morphology and the bulk morphology already established by microscopy (TEM) and small angle X-ray scattering (SAXS) (Chapter 4) for the systems with continuous crystalline phases. Variations in polymer solution concentration and tapping force did not provide any information different from the one presented here. Further experiments, such as film preparation from different solvents or onto different substrates could give deeper understanding of the morphology and the influence of crystallization in continuous phases.

6.4. Conclusions

The thin film morphology of $E_{17}S_{67}EO_{16}^{211}$ was studied by atomic force microscopy. The technique provided successful identification and differentiation of polyethylene and poly(ethylene oxide) blocks in the observed morphology. This was possible by studying the surfaces after swelling the poly(ethylene oxide) block with a selective solvent, and during heating the sample beyond its melting temperature. Dispersed spherical domains shared by polyethylene crystals and amorphous poly(ethylene oxide), which are usually segregated, were found for $E_{17}S_{67}EO_{16}^{211}$. The size and shape of those domains varied from worm-like to wide flat domains to spherical ones with the film thickness. The dimensions of the spherical domains could be controlled by adjusting the temperature

program applied to the sample, based on the crystallization of the two blocks. The morphologies of two different compositions with higher content of the crystalline blocks were also studied and gave different results compared to the results of the bulk samples, but further experiments are necessary.

6.5. References

1. Bates, F. S. *Science* **1991,** 251, (4996), 898-905.
2. Lodge, T. P. *Macromolecular Chemistry and Physics* **2003,** 204, (2), 265-273.
3. Hamley, I. W., *The Physics of Block Copolymers*. Oxford University Press: Oxford, 1998.
4. Abetz, V.; Stadler, R. *Macromolecular Symposia* **1997,** 113, 19-26.
5. Bates, F. S. F., Glenn H. *Physics Today* **1999,** 52, (2), 32-38.
6. Bucknall, D. G.; Anderson, H. L. *Science* **2003,** 302, (5652), 1904-1905.
7. Choi, S.; Lee, K. M.; Han, C. D.; Sota, N.; Hashimoto, T. *Macromolecules* **2003,** 36, (3), 793-803.
8. Hamley, I. W. *Nanotechnology* **2003,** 14, (10), R39.
9. Jeong, U.; Lee, H. H.; Yang, H.; Kim, J. K.; Okamoto, S.; Aida, S.; Sakurai, S. *Macromolecules* **2003,** 36, (5), 1685-1693.
10. Jiang, S.; Gopfert, A.; Abetz, V. *Macromolecules* **2003,** 36, (16), 6171-6177.
11. Li, L.; Serero, Y.; Koch, M. H. J.; de Jeu, W. H. *Macromolecules* **2003,** 36, (3), 529-532.
12. Ruzette, A.-V.; Leibler, L. *Nature Materials* **2005,** 4, 19–31.
13. Sota, N.; Sakamoto, N.; Saijo, K.; Hashimoto, T. *Macromolecules* **2003,** 36, (12), 4534-4543.
14. Stupp, S. I.; LeBonheur, V.; Walker, K.; Li, L. S.; Huggins, K. E.; Keser, M.; Amstutz, A. *Science* **1997,** 276, (5311), 384-389.
15. Sundrani, D.; Darling, S. B.; Sibener, S. J. *Nano Lett.* **2004,** 4, (2), 273-276.
16. Whitesides, G.; Mathias, J.; Seto, C. *Science* **1991,** 254, (5036), 1312-1319.
17. Zhu, L.; Cheng, S. Z. D.; Huang, P.; Ge, Q.; Quirk, R. P.; Thomas, E. L.; Lotz, B.; Hsiao, B. S.; Yeh, F.; Liu, L. *Advanced Materials* **2002,** 14, (1), 31-34.
18. Zhu, Y.; Gido, S. P.; Iatrou, H.; Hadjichristidis, N.; Mays, J. W. *Macromolecules* **2003,** 36, (1), 148-152.

19. Bockstaller, M. R.; Lapetnikov, Y.; Margel, S.; Thomas, E. L. *J. Am. Chem. Soc.* **2003,** 125, (18), 5276-5277.

20. Förster, S.; Antonietti, M. *Advanced Materials* **1998,** 10, (3), 195-217.

21. Lazzari, M.; López-Quintela, M. A. *Advanced Materials* **2003,** 15, (19), 1583-1594.

22. Park, C.; Yoon, J.; Thomas, E. L. *Polymer* **2003,** 44, (22), 6725-6760.

23. Aizawa, M.; Buriak, J. M. *J. Am. Chem. Soc.* **2005,** 127, (25), 8932-8933.

24. Cao, D.; Wu, J. *Macromolecules* **2005,** 38, (3), 971-978.

25. Feng, C. L.; Embrechts, A.; Vancso, G. J.; Schonherr, H. *European Polymer Journal* **2006,** 42, (9), 1954-1965.

26. Cheng, J. Y.; Ross, C. A.; Thomas, E. L.; Smith, H. I.; Vancso, G. J. *Applied Physics Letters* **2002,** 81, (19), 3657–3659.

27. Ouk Kim, S.; Solak, H. H.; Stoykovich, M. P.; Ferrier, N. J.; de Pablo, J. J.; Nealey, P. F. *Nature* **2003,** 424, (6947), 411-414.

28. Müller, A. J.; Balsamo, V.; Arnal, M. L., In *Lecture Notes in Physics: Progress in Understanding of Polymer Crystallization*, Reiter, G.; Strobl, G., Eds. Springer: Berlin, 2007; pp 229-259.

29. Chen, H.-L.; Hsiao, S.-C.; Lin, T.-L.; Yamauchi, K.; Hasegawa, H.; Hashimoto, T. *Macromolecules* **2001,** 34, (4), 671-674.

30. Huang, E.; Rockford, L.; Russell, T. P.; Hawker, C. J. *Nature* **1998,** 395, (6704), 757-758.

31. Reiter, G.; Castelein, G.; Sommer, J.-U., Crystallization of Polymers in Thin Films: Model Experiments. In *Lecture Notes in Physics: Polymer Crystallization: Observations, Concepts and Interpretations*, Reiter, G.; Sommer, J.-U., Eds. Springer: Berlin, 2003; Vol. 606, pp 131-152.

32. Zhu, L.; Huang, P.; Chen, W. Y.; Ge, Q.; Quirk, R. P.; Cheng, S. Z. D.; Thomas, E. L.; Lotz, B.; Hsiao, B. S.; Yeh, F.; Liu, L. *Macromolecules* **2002,** 35, (9), 3553-3562.

33. Zhu, L.; Chen, H.-L.; Calhoun, B. H.; Ge, Q.; Quirk, R. P.; Thomas, E. L.; Hsiao, B. S.; Yeh, F.; Lotz, B. *Polymer* **2001,** 42, 5829-5839.

34. Zhu, L.; Chen, Y.; Zhang, A.; Calhoun, B. H.; Chun, M.; Quirk, R. P.; Cheng, S. Z.; Hsiao, B. S.; Yeh, F.; Hashimoto, T. *Physical Review B* **1999,** 60, (14), 10022-10031.

35. Cohen, R. E.; Cheng, P.-L.; Douzinas, K.; Kofinas, P.; Berney, C. V. *Macromolecules* **1990,** 23, 324-327.

36. Lorenzo, A. T.; Arnal, M. L.; Muller, A. J.; Boschetti-de-Fierro, A.; Abetz, V. *European Polymer Journal* **2006,** 42, (3), 516-533.

37. Takeshita, H.; Ishii, N.; Araki, C.; Miya, M.; Takenaka, K.; Shiomi, T. *Journal of Polymer Science Part B: Polymer Physics* **2004,** 42, (22), 4199-4206.

38. Loo, Y.-L.; Register, R. A., Crystallization within block copolymer mesophases. In *Development in block copolymer science and technology*, Hamley, I. W., Ed. John Wiley & Sons, Ltd: 2004; pp 213-243.

39. Floudas, G.; Reiter, G.; Lambert, O.; Dumas, P. *Macromolecules* **1998,** 31, (21), 7279-7290.

40. Jiang, S.; He, C.; An, L.; Chen, X.; Jiang, B. *Macromolecular Chemistry and Physics* **2004,** 205, (16), 2229-2234.

41. Albuerne, J.; Márquez, L.; Müller, A. J.; Raquez, J. M.; Degée, P.; Dubois, P.; Castelletto, V.; Hamley, I. W. *Macromolecules* **2003,** 36, (5), 1633-1644.

42. Müller, A. J.; Albuerne, J.; Esteves, L. M.; Marquez, L.; Raquez, J.-M.; Degée, P.; Dubois, P.; Collins, S.; Hamley, I. W. *Macromolecular Symposia* **2004,** 215, (1), 369-382.

43. Müller, A. J.; Albuerne, J.; Márquez, L.; Raquez, J.-M.; Degée, P.; Dubois, P.; Hobbs, J.; Hamley, I. W. *Faraday Discussions* **2005,** 128, 231-252.

44. Sun, L.; Lui, Y.; Zhu, L.; Hsiao, B. S.; Avila-Orta, C. A. *Polymer* **2004,** 2004, 8181-8193.

45. Hamley, I. W.; Castelletto, V.; Castillo, R. V.; Müller, A. J.; Martin, C. M.; Pollet, E.; Dubois, P. *Macromolecules* **2005,** 38, (2), 463-472.

46. Hamley, I. W.; Parras, P.; Castelletto, V.; Castillo, R. V.; Müller, A. J.; Pollet, E.; Dubois, P.; Martin, C. M. *Macromolecular Chemistry and Physics* **2006,** 207, (11), 941-953.

47. Arnal, M. L.; Balsamo, V.; López-Carrasquero, F.; Contreras, J.; Carrillo, M.; Schmalz, H.; Abetz, V.; Laredo, E.; Müller, A. J. *Macromolecules* **2001,** 34, (23), 7973-7982.

48. Balsamo, V.; Müller, A. J.; Gyldenfeldt, F. v.; Stadler, R. *Macromolecular Chemistry and Physics* **1998,** 199, (6), 1063-1072.

49. Balsamo, V.; Müller, A. J.; Stadler, R. *Macromolecules* **1998,** 31, (22), 7756-7763.

50. Balsamo, V.; Von Gyldenfeldt, F.; Stadler, R. *Macromolecular Chemistry and Physics* **1996,** 197, 3317-3341.

51. Stadler, R.; Auschra, C.; Beckmann, J.; Krappe, U.; Voigt-Martin, I.; Leibler, L. *Macromolecules* **1995,** 28, (9), 3080-3097.

52. Takahashi, K.; Hasegawa, H.; Hashimoto, T.; Bellas, V.; Iatrou, H.; Hadjichristidis, N. *Macromolecules* **2002,** 335, (13), 4859-4861.

53. Loo, Y.-L.; Register, R. A.; Ryan, A. J. *Macromolecules* **2002,** 35, (6), 2365-2374.

54. Magonov, S. N.; Cleveland, J.; Elings, V.; Denley, D.; Whangbo, M.-H. *Surface Science* **1997,** 389, 201-211.

55. Boschetti-de-Fierro, A.; Müller, A. J.; Abetz, V. *Macromolecules* **2007,** 40, (4), 1290-1298.

56. Barton, A. F. M., *CRC Handbook of Polymer Liquid Interaction Parameters and Solubility Parameters*. CRC Press: Boca Raton, 1990; p 768.

57. $\chi = \dfrac{v}{RT}\left(\delta_i - \delta_j\right)^2$, where v is the geometric average of the molar segmental volume calculated from the densities at room temperature (density corrections for the real temperature are neglected), RT is the molar thermal energy at 60 ℃.

58. Lorenzo, A. T.; Arnal, M. L.; Müller, A. J.; Boschetti-de-Fierro, A.; Abetz, V. *Macromolecular Chemistry and Physics* **2006,** 207, (1), 39-49.

59. Müller, A. J.; Balsamo, V.; Arnal, M. L. *Advances in Polymer Science* **2005,** 190, 1-63.

Chapter 7. Crystallization Kinetics of PEO and PE in Different Triblock Terpolymers: Effect of Microdomain Geometry and Confinement

Isothermal crystallization kinetics of poly(ethylene oxide) (PEO) and polyethylene (PE) was studied by differential scanning calorimetry (DSC). The studied polymers were the constituent blocks of various triblock terpolymers. The effect of the geometry of the microdomains was analyzed by studying different compositions of polyethylene-*block*-polystyrene-*block*-poly(ethylene oxide) (PE-*b*-PS-*b*-PEO). It was found that the crystallization rate decreases when the block content decreases for both crystallizable blocks. The effect of the microdomain geometry, confinement or chain tethering on the crystallization of PEO was extensively studied, by comparing pairs of triblock terpolymers with differences either in the other block characteristics (crystalline, glassy, amorphous) or in the location of the other blocks in the terpolymer (end block, middle block, i.e., PE-*b*-PS-*b*-PEO, PS-*b*-PE-*b*-PEO). It was found that the PE crystal is a better nucleation surface than the interphases with the other blocks, but it reduces segmental mobility of its neighbors. A rubbery neighbor block makes crystallization slower than a glassy one. Crystallization goes slower in the middle block than in the end block. For PE block we found that the crystallization rate decreases more strongly with the microdomain geometry reduction than by locating the block as a middle block instead of an end block.

7.1. Introduction

Semi-crystalline block copolymers are materials that attract great interest due to their tailored mechanical properties and various possible morphologies.[1-12] The morphology is

determined by a competition between two factors:[11-19] the block copolymer self-assembly ability,[20] which is based on the interaction among the different blocks and organizes the incompatible blocks into separated microphases, and the crystallization of the crystallizable block(s). The final morphology has been found to be path-dependant, based on whether the crystallization occurs from a homogeneous state or a microphase separated one.[19, 21, 22]

In general, the resultant morphology can be categorized as follows: [2-5, 15-17, 23-25] (a) microphase separation is driven by crystallization when $T_c > T_{ODT} > T_g$, and a lamellar morphology would be created; (b) a lamellar morphology is the result in weakly segregated systems with soft confinement ($T_{ODT} > T_c > T_g$); and (c) in strongly segregated systems with hard confinement, i.e., $T_{ODT} > T_g > T_c$, confined morphologies are formed, such as spheres, cylinders or lamellae.

There has always been interest in the study of polymer crystallization due to the mechanical properties of crystallizable polymers. The crystallization process is, however, far from being well understood, and many discussions have taken place during the last decade.[26-29] The study of crystallization within block copolymer microphases is advantageous mainly for the analysis of the nucleation process due to the nanoscopic scales.

In this chapter the crystallization kinetics of polyethylene (PE) and poly(ethylene oxide) (PEO) as constituent blocks in different triblock terpolymers is studied. The effect of composition, which causes the generation of different morphologies, on crystallization will be investigated. A research of the confinement type is carried out with the study of a wide diversity of triblock terpolymers and topologies. The effects of glassy, rubbery and semi-crystalline blocks as middle blocks or end blocks on the crystallization of the PEO end

block are investigated. The influence of changing the chain topology will also be addressed as the kinetics is calculated on the PE middle block.

7.2. Experimental Part

Anionic polymerization was carried out, as explained in Chapter 4, using solvents and monomers purified according to common procedures described elsewhere.[6, 30] The synthesis of poly(1,4-butadiene)-*block*-polystyrene-*block*-poly(ethylene oxide) (PB-*b*-PS-*b*-PEO) terpolymers was realized by sequential anionic polymerization of butadiene, styrene, and ethylene oxide in benzene with *sec*-BuLi as initiator. Polymerization of ethylene oxide in the presence of a lithium counterion was accomplished by using the strong phosphazene base *t*-BuP$_4$.[2, 31-35] The same procedure was used to synthesize polystyrene-*block*-poly(1,4-butadiene)-*block*-poly(ethylene oxide) (PS-*b*-PB-*b*-PEO) terpolymers. The polymerization of butadiene under the conditions employed leads to a preferential 1,4-addition (Table 7.1), which is essential to get the corresponding "*pseudo* polyethylene*" structure after hydrogenation.

The hydrogenation of the PB-*b*-PS-*b*-PEO terpolymers (precursor) leads to the PE-*b*-PS-*b*-PEO terpolymers. Homogeneous catalytic hydrogenation was carried out with Wilkinson catalyst (Ph$_3$P)$_3$Rh(I)Cl. Further purification in order to eliminate residual Wilkinson catalyst was performed. In the terpolymer notation employed here (A$_x$B$_y$C$_z^m$), the subscript numbers stand for the mass fraction in percent and the superscript indicates the overall number-averaged molecular weight M_n in kg/mol of the block copolymer.

7.2.1. Differential Scanning Calorimetry (DSC)

A Perkin-Elmer PYRIS 1 differential scanning calorimeter in a dry nitrogen atmosphere with a CCA 7 liquid nitrogen cooling device was used. For all measurements a two-point calibration with n-decane and indium was carried out. Samples of 8.0 ± 0.5 mg were

placed in the DSC pans. Standard and isothermal scans, as well as self-nucleation experiments were performed.

Table 7.1. Molecular weight, molecular weight distributions and content of 1,2 units in the polybutadiene block, for the terpolymers employed in the crystallization kinetic studies.

Terpolymer	M_n (Kg/mol)			M_w/M_n[a]
	PB[a] (%1,2[b]) / PE[c]	PS[c]	PEO[c]	
$B_{29}S_{40}EO_{31}{}^{168}$ / $E_{29}S_{40}EO_{31}{}^{170}$	48 (12.9) / 50	67	53	1.03
$B_{17}S_{68}EO_{16}{}^{210}$ / $E_{17}S_{67}EO_{16}{}^{211}$	35 (11.5) / 36	142	33	1.01
$B_{16}S_{40}EO_{44}{}^{143}$ / $E_{16}S_{40}EO_{44}{}^{144}$	22 (14.0) / 23	58	63	1.05
$B_{37}S_{16}EO_{47}{}^{76}$ / $E_{38}S_{16}EO_{46}{}^{77}$	28 (11.8) / 29	13	36	1.03
$S_{30}B_{22}EO_{48}{}^{98}$ / $S_{30}E_{23}EO_{47}{}^{99}$	22 (11.1) / 23	29.5	47	1.01

[a] Determined by SEC in THF calibrated against PB standards. [b] Determined by ^{1}H NMR spectroscopy in CDCl$_3$. [c] Determined by ^{1}H NMR spectroscopy using the molecular weight of the PB precursor obtained by SEC.

7.2.2. Isothermal scans

Two different thermal protocols were employed in order to record the isothermal crystallization of PE in the hydrogenated samples or of PEO block either in the non-hydrogenated or in the hydrogenated terpolymers. In all cases, prior experiments were performed in order to determine the crystallization temperature T_c such that crystallization does not occur during the cooling scan.

Isothermal crystallization of the PE block, and PEO block in non-hydrogenated terpolymers: samples were heated up to 120 °C and hold at the temperature for 3 min in order to erase thermal history. Then they were quenched down to T_c at 80 °C/min, and the isothermal crystallization was followed.

Isothermal crystallization of the PEO block in hydrogenated terpolymers: samples were also heated up to 120 °C and hold at the temperature for 3 min in order to erase thermal history, which was followed by a cooling scan down to –100 °C at 10 °C/min, in order to

induce crystallization in both PE and PEO blocks. Then, a heating scan was performed at 10 °C/min up to 70 °C, and a 75 min isotherm was realized in order to melt completely the PEO block and reach saturation levels of PE crystallization. These conditions were chosen to achieve that all PEO crystals are molten and PE has crystallized to a degree where no further crystallization occurs during the following step. Finally, the sample was cooled down to T_c at 80 °C/min, and the isothermal crystallization was recorded.

Step crystallization: if the crystallization enthalpy is very low, the signal to noise ratio might be too low and the results have high associated errors. In that case, the isothermal crystallization was followed by steps.[8] In the same afore-mentioned way, samples were heated up to 120 °C and hold at the temperature for 3 min in order to erase thermal history. Then, they were quenched down to T_c at 80 °C/min, and the isothermal crystallization was followed during a given time t_c. Finally, the sample was heated from T_c up to 120 °C and the melting enthalpy was determined. The process was repeated for crystallization times varying from 0.1 min to 300 min, until a saturation in the melting enthalpy is reached. The saturation enthalpy was assigned to 100 % relative crystallinity, and the crystallinity degree was calculated for each crystallization time. This allows the creation of a table of crystallinity degree as a function of time.

7.2.3. Self-nucleation (SN) experiments

Self-nucleation measurements were performed in analogy to the procedure described by Fillon et al.[36] The complete thermal treatment has been explained in detail elsewhere.[3, 17] The protocol used can be summarized as follows: 1) Melting of the sample at 120 °C during 5 min in order to erase any previous thermal history. 2) Subsequent cooling at a rate of 10 °C/min to -100 °C, which creates a ''standard'' thermal history. 3) Partial melting by heating at 10 °C/min up to a ''self-nucleation temperature'' T_s. 4) Thermal conditioning at T_s for 5 min. Depending on T_s, the crystalline PE or PEO domains will be

completely molten, only self-nucleated, or self-nucleated and annealed. If T_s is sufficiently high, no self-nuclei or crystal fragments can remain, and the sample is then under so-called Domain I, the complete melting domain. At intermediate T_s values, the sample is almost completely molten, but some small crystal fragments or crystal memory effects remain, which can act as self-nuclei during a subsequent cooling from T_s, and the sample is said to be under Domain II, the self-nucleation domain. Finally, if T_s is too low, the crystals will be only partially molten, and the remaining crystals will undergo annealing during the 5 min at T_s, while the molten crystals will be self-nucleated during the later cooling, and the sample is under Domain III, the self-nucleation and annealing domain. 5) Cooling scan from T_s at 10 °C/min, where the effects of the previous thermal treatment will be reflected on crystallization. 6) Heating scan at 10 °C/min to 120 °C, where the effects of the thermal history will be apparent on the melting signal.

7.3. Results and Discussion

The triblock terpolymer thermal properties were determined by standard DSC scans, as already presented in Chapter 4. It was found that the mentioned properties depend on the molecular weight of the block, and more interestingly on the morphology. That effect is investigated now based on the crystallization kinetics of each crystallizable block. The variety of triblock terpolymers synthesized allow us to carry out a discussion based on different parameters, such as the overall morphology, physical properties of the end block and the middle block and sequence of the blocks in the terpolymer.

7.3.1. Crystallization kinetics of the PEO block

Crystallization kinetics was studied by recording the isothermal crystallization of the samples quenched from the molten state to the given crystallization temperature. An

example of the isothermal crystallization scans that corresponds to $B_{19}S_{34}EO_{47}^{142}$ at different temperatures is presented in Figure 7.1.
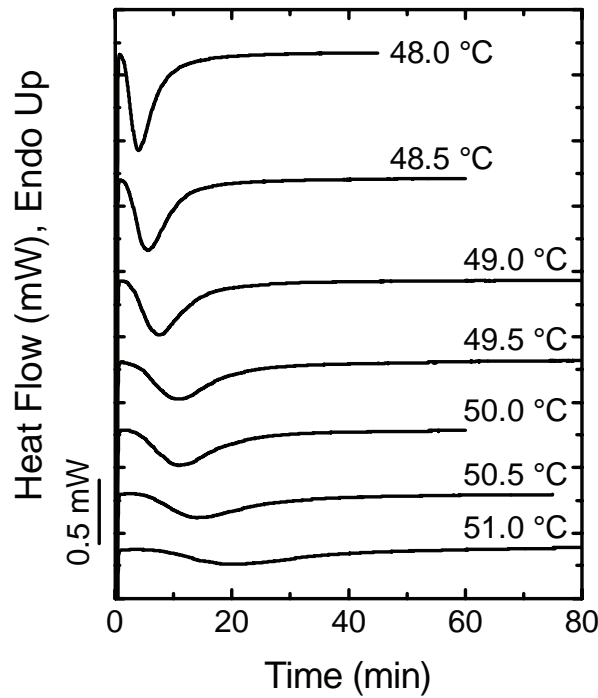
Figure 7.1. DSC isothermal scans for $B_{19}S_{34}EO_{47}^{142}$ at different crystallization temperatures.

The data of the initial stages of crystallization (i.e., for crystallinity degrees between 5 and 35 %) was fitted[37] to the Avrami equation:[38-40]

$$1 - V_c(t) = \exp(-kt^n)$$

(Equation 7.1)

where V_c is the relative volumetric transformed fraction, k is an overall crystallization rate constant for nucleation and growth, and n is the constant known as Avrami index. In the Avrami theory, the Avrami index is an integer number between 1 and 4 which value is considered to consist of two contributions.[9] The first one is related to the nucleation (instantaneous = 0, sporadic = 1), and the second one is related to the dimensionality of the crystal or superstructure (line = 1, disc = 2, sphere = 3). Experimentally, the obtained Avrami indexes are rarely integers, and values lower than 1 have been found in certain systems.[41, 42] There has been a lot of discussions regarding the limitations in the use of the

Avrami equation and its variables.[43] Therefore, the Avrami index will be discussed here only as an indication of nucleation and dimensionality. Our observations are, however, not only based on the Avrami index, but also on previously reported morphological studies, as well as on further thermal experiments such as self-nucleation.

It is appropriate to mention the dependence of the Avrami index on the crystallization temperature.[44] The possibility of instantaneous nucleation decreases when the crystallization temperature increases. In that case, the contribution to the Avrami index increases. However, crystal dimensionality may decrease when the crystallization temperature increases, and the corresponding contribution to the Avrami index decreases. Therefore, the Avrami index as a function of the temperature could increase and later decrease or vice versa, depending on which effect is dominating. In homopolymers, the nucleation is usually the more dominant effect.

It can be seen in equation 1 that the units of the crystallization rate constant k are in reciprocal time units to the power of n (for instance, min^{-n}). Therefore, a comparison among substances with different values of Avrami index n is not suitable. A more convenient parameter to represent the crystallization rate is $1/\tau_{50\%}$, where $\tau_{50\%}$ in the half-crystallization time, i.e., the time at which the crystallization is half of the total relative crystallization.

The crystallization kinetics of the poly(ethylene oxide) block has been studied in different triblock terpolymers. Figure 7.2 shows the values of Avrami index and $1/\tau_{50\%}$ as functions of the crystallization time for $B_{16}S_{68}EO_{16}{}^{210}$, $B_{29}S_{40}EO_{31}{}^{168}$ and $B_{37}S_{16}EO_{47}{}^{76}$, three triblock terpolymers with different compositions and different morphologies. The morphologies have been determined by small angle X-Ray scattering (SAXS), transmission electron microscopy (TEM) and atomic force microscopy (AFM) as presented in Chapters 4, 5 and 6. For the mentioned compositions, morphologies composed of spheres in a polystyrene

matrix, cylinders in a polystyrene matrix and lamellae were found, respectively. An overview of the morphologies found (Chapter 4, Figure 4.3 and 4.4) is presented in Table 7.2 for the sake of simplicity.
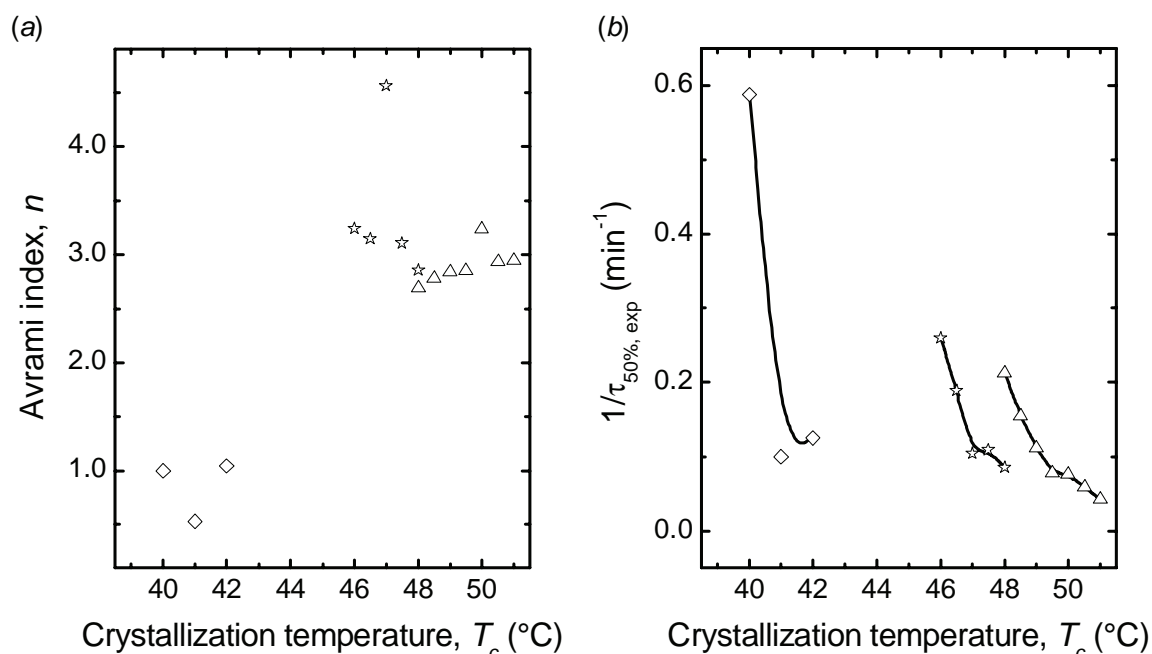
Figure 7.2. Crystallization kinetics parameters for the PEO block in triblock terpolymers with different compositions: $\diamond$ $B_{16}S_{68}EO_{16}{}^{210}$, $\triangle$ $B_{29}S_{40}EO_{31}{}^{168}$ and $\star$ $B_{37}S_{16}EO_{47}{}^{76}$. (a) Avrami index, n, as a function of crystallization temperature, (b) Inverse of experimental crystallization half-time as a function of crystallization temperature.

Table 7.2. Morphologies of the triblock terpolymers, as determined by TEM micrographs and SAXS patterns.

Terpolymer	TEM	SAXS
$B_{29}S_{40}EO_{31}{}^{168}$ / $E_{29}S_{40}EO_{31}{}^{170}$	Connected cylinders	Hexagonally packed cylinders
$B_{16}S_{68}EO_{16}{}^{210}$ / $E_{17}S_{67}EO_{16}{}^{211}$	Spheres	*fcc*-packed spheres
$B_{16}S_{40}EO_{44}{}^{143}$ / $E_{16}S_{40}EO_{44}{}^{144}$	Lamellae / Non-determined	Lamellae / Hexagonally packed cylinders
$B_{37}S_{16}EO_{47}{}^{76}$ / $E_{38}S_{16}EO_{46}{}^{77}$	Lamellae	Lamellae
$S_{30}B_{22}EO_{48}{}^{98}$ / $S_{30}E_{23}EO_{47}{}^{99}$	Cylinders	Hexagonally packed cylinders

The values of Avrami index in Figure 7.2a are similar for the cylindrical and lamellar morphologies ($n = 3$), which indicates that the dimensionality of the crystals growing within lamellae is similar to that growing in cylinders. This effect is probably due to defects in the morphology that allow interconnection of the microphases. The dependence with temperature could indicate a slight difference: while the cylindrical morphology is dominated by nucleation and has a positive slope, the lamellar one has a negative one, which indicates that it is affected by dimensionality and the crystallization is confined to some extend. This indication of lack of confinement in the cylinders is another signal of morphological defects. The Avrami index values obtained for the sphere forming terpolymer is much lower ($n \sim 1$), which is typical for crystallization within isolated domains, where there is sporadic nucleation and virtually infinitely fast growth, this leads to a nucleation controlled first order kinetics.[5, 12, 16] From the results in Figure 7.2b one can see that the crystallization rate for a given crystallization temperature results higher for $B_{29}S_{40}EO_{31}{}^{168}$ than for $B_{37}S_{16}EO_{47}{}^{76}$, but both show a much higher rate than obtained for $B_{16}S_{68}EO_{16}{}^{210}$. This tendency indicates that the crystallization rate decreases when the block content decreases dramatically. The decrease in block content represents in these cases not only a decrease of size of the domains. It also implies an increase in the interfacial area (from sheets or cylinders to spheres).

The previous results establish the effect of the microdomain geometry on the crystallization kinetics. In the following, the effect of the structure of the neighboring blocks will be analyzed. The first of three cases is related to the effect of having a crystallizable block instead of an amorphous block at the other end of the chain. This will be illustrated by comparing $B_{29}S_{40}EO_{31}{}^{168}$ and $E_{29}S_{40}EO_{31}{}^{170}$, which are triblock terpolymers forming PEO cylinders before and after hydrogenation (see Figure 7.3). The results of the Avrami index are presented in Figure 7.3a, where the non-hydrogenated

triblock terpolymer shows higher values than the hydrogenated one, indicating that the crystallization of the PEO block is closer to $n = 2$ when the other end block is crystallized PE. A decrease in Avrami index after hydrogenation was observed in all triblock terpolymers studied here. This decrease could be interpreted as a tendency towards instantaneous nucleation, since it was observed for all the triblock terpolymers studied independent from composition, morphology or block sequence. The nucleation process is generally not purely instantaneous neither sporadic,[42] and therefore one could say that the nucleation process in the hydrogenated terpolymers is "more instantaneous" than the nucleation in non-hydrogenated terpolymers.

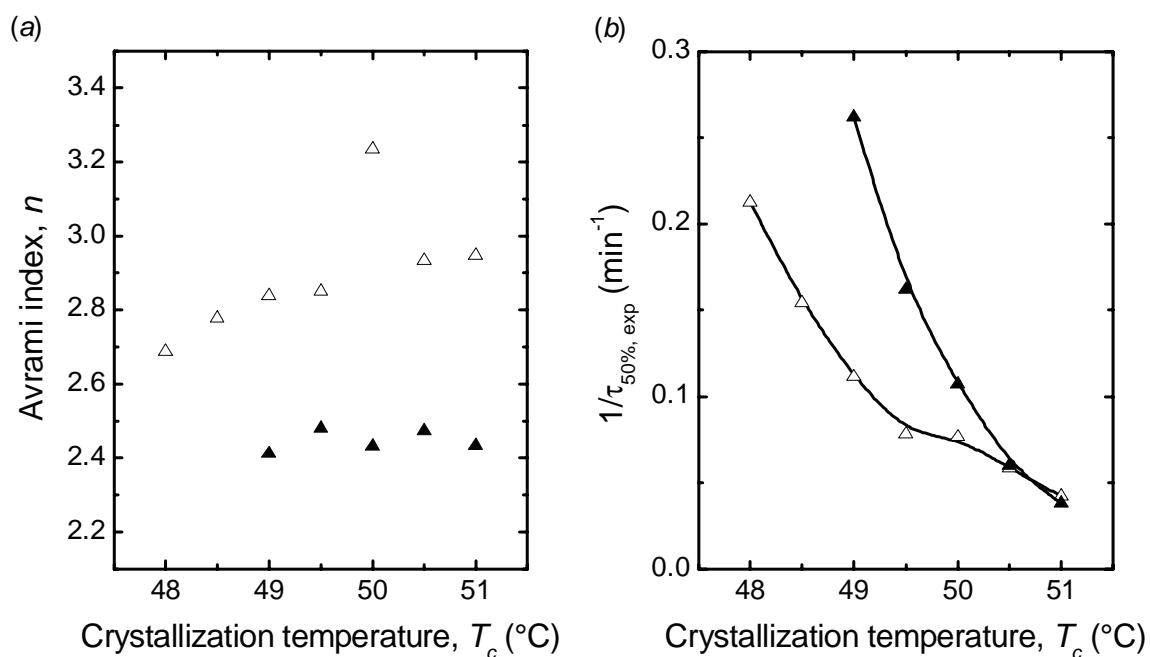**Figure 7.3.** Crystallization kinetics parameters for the PEO block in triblock terpolymers before and after hydrogenation of the PB block: △ $B_{29}S_{40}EO_{31}$[168] and ▲ $E_{29}S_{40}EO_{31}$[170]. (a) Avrami index, n, as a function of crystallization temperature, (b) Inverse of experimental crystallization half-time as a function of crystallization temperature.

Since a more instantaneous nucleation process has been induced by the PE crystals, this means that the PE crystals are nucleating the PEO chains, and the information is somehow transmitted through the PS block. This fact may be possible due to local sub-T_g flow processes at temperatures close to T_g. The increase in local density caused by crystallization generates either voids between the microphases[45] or causes local flow in order to endure volume constriction. Since voids were not observed in the bulk samples, the local flow of the glassy PS chain is assumed. This PE crystallization would lead to a reduction of PS at the interface with PEO and thus the PEO chains have to stretch more away from the PS interface. This local stretching will result in a facilitated crystallization of PEO from that interface. A similar mechanism has been proposed for crystallization in a liquid-phase-separated blend.[46]

The crystallization rate (Figure 7.3b) is slower for the non-hydrogenated terpolymer than for the hydrogenated, i.e., the crystallization of the PEO block is faster in $E_{29}S_{40}EO_{31}^{170}$. The crystallization takes place faster, which is in good agreement with an increase in the nucleation rate. This behavior was also observed in all the triblock terpolymer pairs, independent from composition and morphology.

The second case related to the effect of the physical nature of the surrounding blocks on the crystallization kinetics of the PEO block is illustrated by comparing $E_{16}S_{40}EO_{44}^{144}$ with $S_{43}E_{22}EO_{35}^{112}$, as shown in Figure 7.4. By altering the triblock terpolymer block sequence of the hydrogenated terpolymers, the effect of the PEO chain anchored to the PE semicrystalline phase is investigated. The Avrami index presented in Figure 7.4a decrease with the crystallization temperature, which indicates that the dimensionality of the crystals is relevant and there is some confinement. Slightly lower Avrami index values and lower crystallization rates were found for $S_{43}E_{22}EO_{35}^{112}$, where the PE block is next to the PEO crystallizable chain. The PE block is a semicrystalline phase with a crystallinity degree

around 30 %. Therefore, the crystallizable PEO phase is likely surrounded by a rubbery PE phase, and this decreases the crystallization rate of the PEO block. The effect of a rubbery neighbor block will be further analyzed with the following example.
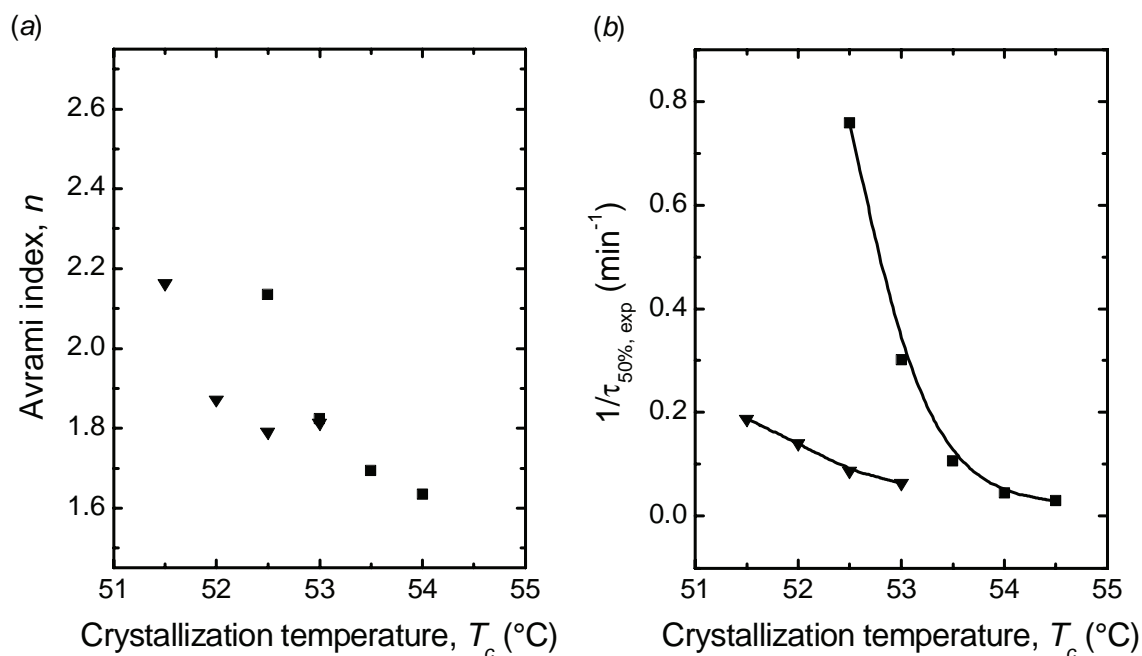

Figure 7.4. Crystallization kinetics parameters for the PEO block in triblock terpolymers with similar compositions but different block sequence: ■ $E_{16}S_{40}EO_{44}$[144] and ▼ $S_{43}E_{22}EO_{35}$[112]. (a) Avrami index, n, as a function of crystallization temperature, (b) Inverse of experimental crystallization half-time as a function of crystallization temperature.

The third and last case of the environment effect on crystallization of PEO considers the classic soft-hard confinement effect. Two comparisons will be described. First, a comparison between $E_{16}S_{40}EO_{44}$[143] and $E_{19}EP_{40}EO_{41}$[138] is done in Figure 7.5. The $E_{19}EP_{40}EO_{41}$[138] is a polyethylene-*block*-poly(ethylene-*alt*-propylene)-*block*-poly(ethylene oxide) triblock terpolymer obtained from the catalytic hydrogenation of polybutadiene-*block*-polyisoprene-*block*-poly(ethylene oxide), synthesized by sequential anionic polymerization.[47] In both cases the morphology consists of PEO cylinders in either a PS or

a PEP matrix, while the PE crystals are distributed in the matrix as axialites, as also reported elsewhere.[47] Later, the block sequence alternation will have a different meaning in the non-hydrogenated triblock terpolymer, since the glassy PS neighbor is substituted by a rubbery one. This last case of comparison (illustrated in Figure 7.6) is not based on a substitution of exclusively the middle block. However, due to the large differences between the two middle blocks, its discussion results simpler and more accurate when associated to the soft-hard confinement case.
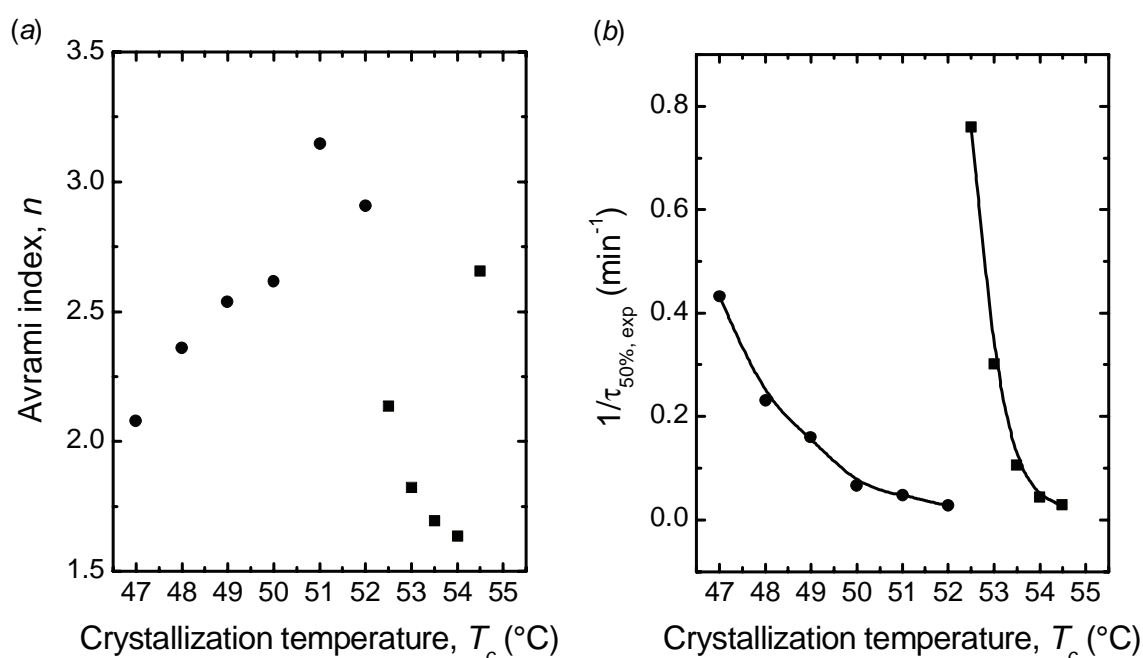

Figure 7.5. Crystallization kinetics parameters for the PEO block in triblock terpolymers with similar compositions but different middle block: ■ $E_{16}S_{40}EO_{44}$[143] and ● $E_{19}EP_{40}EO_{41}$[138]. (a) Avrami index, n, as a function of crystallization temperature, (b) Inverse of experimental crystallization half-time as a function of crystallization temperature.

The values of Avrami index presented in Figure 7.5a are higher for the terpolymer with the rubbery PEP middle block, where also the confinement effect is not dictating a decrease of the Avrami index with the crystallization temperature, as in the case of the glassy PS middle block. This indicates, as expected, that a rubbery matrix causes less confinement

than a glassy one. The crystallization rate shown in Figure 7.5b is slower for the PEO in the terpolymer with rubbery middle block. That means that the crystallization of the PEO is slowed down due to the high mobility of the rubbery middle block, as was also observed in Figure 7.4b. In related works, the crystallization kinetics of poly(*p*-dioxanone)-*block*-poly(ε-caprolactone) diblock copolymers were investigated, in the temperature range were the polycaprolactone block was molten, the isothermal crystallization kinetics of the poly(*p*-dioxanone) block was greatly depressed as compared to that of an equivalent homopolymer since the topological restrictions imposed by the highly mobile covalently bonded poly(caprolactone) chains increase the energy barrier for secondary nucleation.[10, 48, 49] Similar results where the crystallization rate of a crystallizable block is slowed down by a covalently bonded rubbery neighbor have been reported by Ueda et al. and by Shiomi et al.[50, 51]
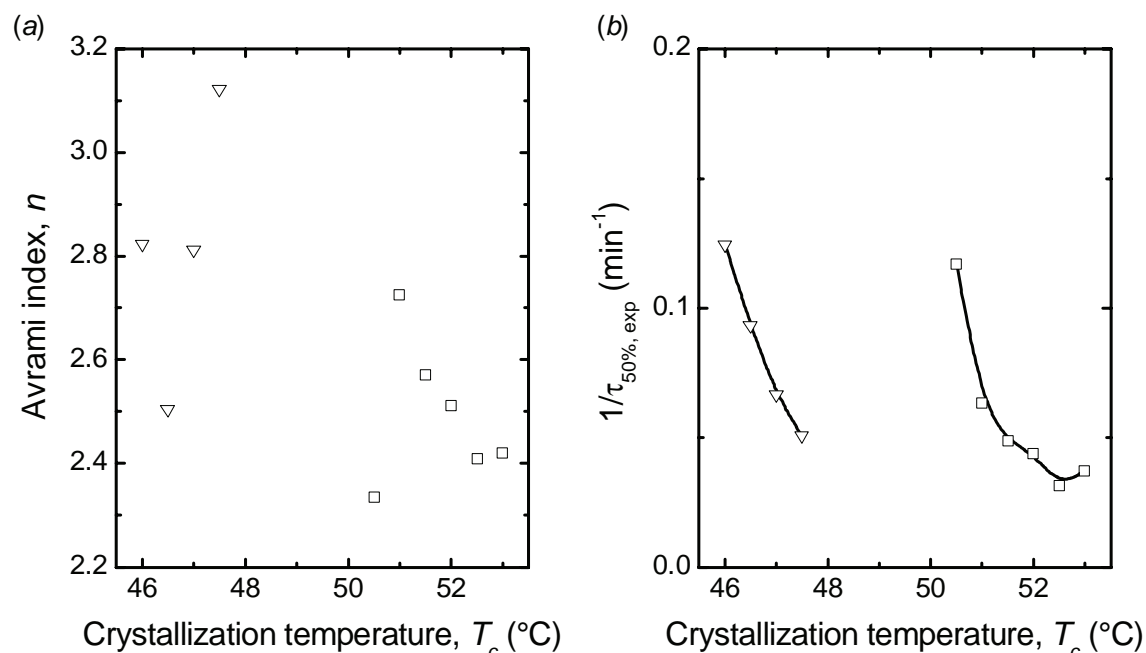

Figure 7.6. Crystallization kinetics parameters for the PEO block in triblock terpolymers with similar compositions but different block sequence: □ $B_{16}S_{40}EO_{44}$[143] and ▽ $S_{43}B_{21}EO_{36}$[111]. (a) Avrami index, *n*, as a function of crystallization temperature, (b)

Inverse of experimental crystallization half-time as a function of crystallization temperature.

The behavior of the Avrami index with temperature shown in Figure 7.6a for $B_{16}S_{40}EO_{44}$[143] and $S_{43}B_{21}EO_{36}$[111] is similar to the one observed in Figure 7.5a. The Avrami index increases with temperature when the rubbery PB is the middle block, and the values are higher than those corresponding to the glassy PS middle block. Also, the inverse of crystallization half time is lower when the PB is in the middle block position (Figure 7.6b), which is due to the same effect mentioned for $E_{19}EP_{40}EO_{41}$[138], i.e., high mobility of the neighbor block slows down the attachment of the chain segments to the growing nuclei and therefore decreases the crystallization rate.

It is interesting that in both Figure 7.5 and 7.6 the rubbery block (PEP and PB respectively) has a higher effect on the crystallization rate of the PEO block than a neighboring glassy block like PS. This trend may depend on how much higher is the crystallization temperature than the T_g of the rubbery block, since reverse trends have been recently been observed in different systems. Müller et al.[52] have recently investigated the crystallization of the PE block within diblock copolymers containing different neighboring blocks. A glassy block of polystyrene (PS), a rubbery block of poly (*D,L*-lactide) (PDLA), a semicrystalline block of poly (*L*-lactide) (PLLA) and a miscible block of poly(ethylene-*alt*-propylene) (PEP) were used to asses the influence of the degree of confinement and miscibility on the crystallization kinetics of PE. PEP had the largest effect on the crystallization kinetics of the PE block in view of its miscibility. For the strongly segregated systems larger restrictions were imposed by vitreous PS due to hard confinement as compared with the soft confinement of the rubbery PDLA block. A nucleation effect of previously crystallized PLLA on the PE block was detected which offset its depression of the crystallization kinetics of PE. Since the T_g of PDLA is 55 °C

and the crystallization temperatures for the PE block employed were only 30 to 40 °C above this value, the mobility of the PDLA chains may not be as large as those of PB at these temperatures.

7.3.2. Crystallization kinetics of the PE block

The crystallization kinetics of the PE block was also investigated. The effect of the morphology, as well as the position of the crystallizable block (i.e., middle or end block resulting in differences in chain tethering) is presented in Figure 7.7. The morphology effect on crystallization kinetics of PE has been also studied on diblock copolymer systems, and is reported in a literature contribution.[53]
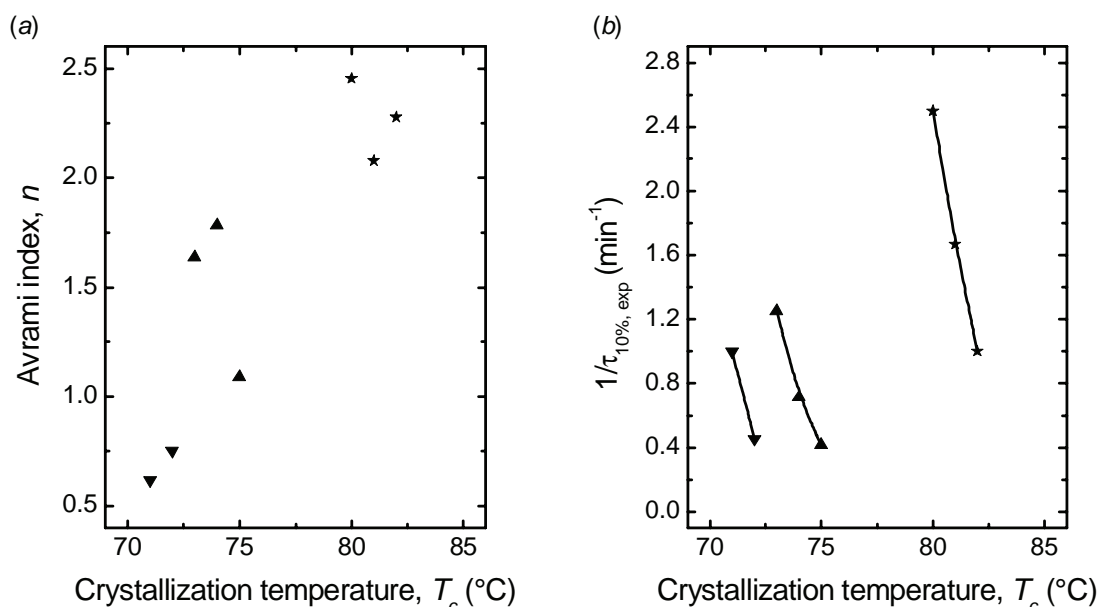

Figure 7.7. Crystallization kinetics parameters for the PE block in triblock terpolymers with different compositions: ▲ $E_{29}S_{40}EO_{31}^{170}$, ★ $E_{38}S_{16}EO_{46}^{77}$ and ▼ $S_{43}E_{22}EO_{35}^{112}$ (a) Avrami index, n, as a function of crystallization temperature, (b) Inverse of experimental time at 10% of crystallization as a function of crystallization temperature.

The Avrami index values presented in Figure 7.7a seem to depend on the morphology: the lamellae forming terpolymer, i.e., $E_{38}S_{16}EO_{46}^{77}$, has the higher values (between 2.0 and 2.5), followed by the terpolymer arranged in cylindrical microphases ($n \sim 1.0 – 2.0$), i.e.,

$E_{29}S_{40}EO_{31}^{170}$. There is also a marked difference between $E_{29}S_{40}EO_{31}^{170}$ and $S_{43}E_{22}EO_{35}^{112}$, where the latter shows much lower values (between 0.5 and 0.8). This result is a consequence of the huge mobility loss that the PE chain suffers as a middle block when the chain is tethered at both ends, albeit the morphology generated in both cases is the same (a TEM micrograph corresponding to $S_{43}E_{22}EO_{35}^{112}$ can be found as complementary material).

The rate of crystallization of the PE block is illustrated in Figure 7.7b as $1/\tau_{10\%}$. This value is more reliable than $1/\tau_{50\%}$, since the experiments were carried out with the step crystallization technique. The limitation of the technique is the large experimental times and consequently there are only few measurements at times close to 50 % of crystallization, compared to the measurements during the initial stages. The results are in good agreement with the interpretation given to the Avrami index data. The crystallization rate decreases when the block sequence is changed from the end to the middle, clearly due to the loss of mobility by chain tethering at both ends. However, the decrease in crystallization rate when going from a lamellar morphology to a cylindrical one is much higher than the decrease observed due to alternation in block sequence. This result proves that the confinement of the crystallization in a microphase with higher interfacial area implies not only a decrease of chain mobility and diffusion, but more importantly a decrease in nucleation rate (since heterogeneous nucleation is less probable as MD size decreases).[5]

7.3.3. Self-nucleation experiments

In order to study the crystallization within the terpolymer with the lowest content in crystallizable blocks, self-nucleation experiments were done on $B_{16}S_{68}EO_{16}^{210}$ and $E_{17}S_{67}EO_{16}^{211}$. The aim of the experiments was to determine whether the crystallization is totally confined inside the spherical microphases. Figure 7.8 and 7.9 show the cooling and

heating scans for the PEO block in the non-hydrogenated and the hydrogenated triblock terpolymers, respectively. Studies were also performed on the PE block, and the cooling scans and subsequent heating scans are presented in Figure 7.10. In Figure 7.11 the domain definitions are presented for both terpolymers.
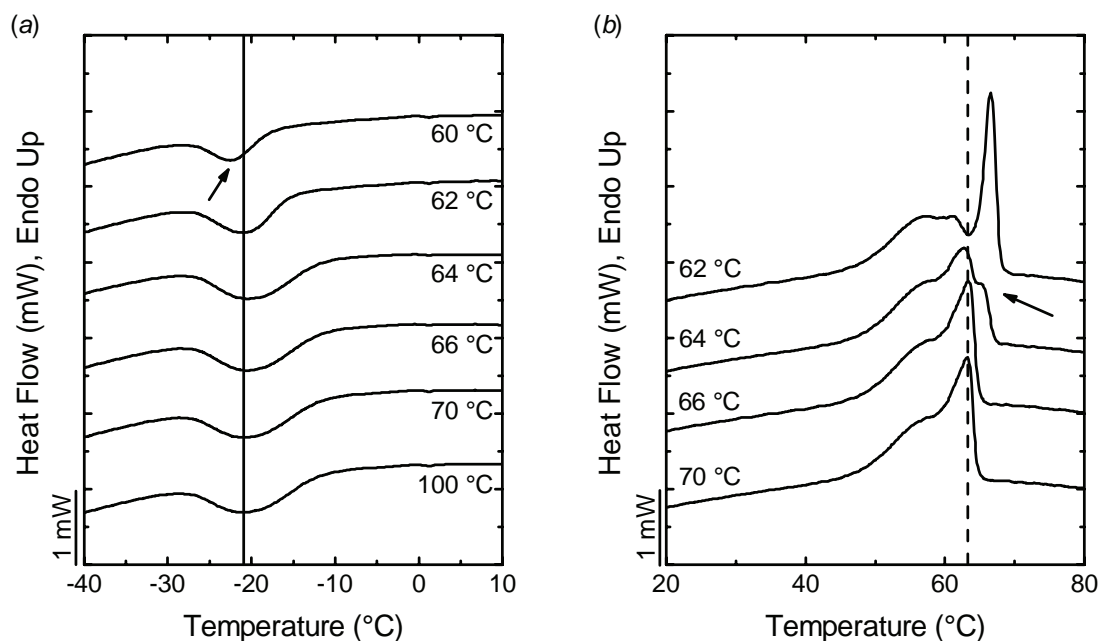

Figure 7.8. Self-nucleation experiments of the PEO block in $B_{16}S_{68}EO_{16}^{210}$: (a) cooling scans at 10 °C/min after 5 min at indicated T_s, (b) subsequent heating scans at 10 °C/min. Arrows indicate: (a) shift of crystallization peak to lower temperature, and (b) melting peak of annealed crystals.

In both cooling DSC scans presented in Figure 7.8a and 7.9a the exotherms that appear at very low temperatures (peak crystallization temperatures of approximately -20 °C and -30 °C respectively) are due to the crystallization of confined PEO spheres. It is now well known that when a polymer is confined in a large number of microphase domains (MD), if the density of MD is much larger than the available heterogeneities in the system, the nucleation mechanism changes from heterogeneous to superficial and/or homogeneous.[5, 17]
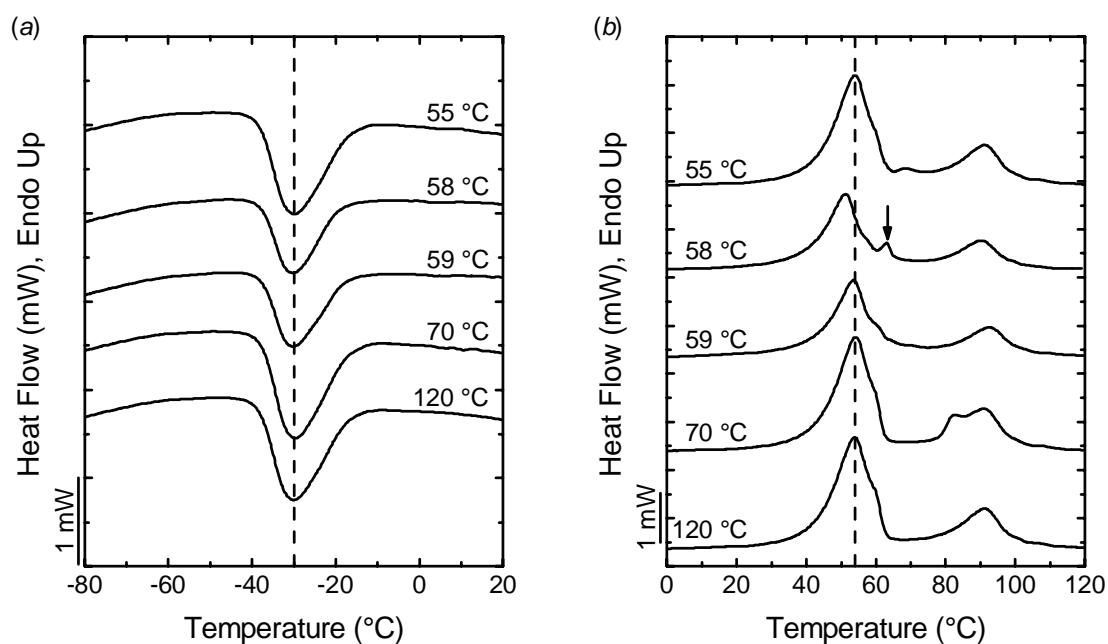
Figure 7.9. Self-nucleation experiments of the PEO block in $E_{17}S_{67}EO_{16}$[211]: (a) cooling scans at 10 °C/min after 5 min at indicated T_s, (b) subsequent heating scans at 10 °C/min. Arrow indicates melting peak of annealed crystals.

In the cooling scans presented in Figure 7.8a for $B_{16}S_{68}EO_{16}$[210], the crystallization peaks observed in the standard scan ($T_s = 100$ °C) showed no shifts to lower temperatures for T_s > 60 °C. This indicates that no self-nucleation occurs at higher temperatures. The heating scans presented in Figure 7.8b show the appearance of a high temperature melting signal at $T_s = 64$ °C, corresponding to the crystals annealed at T_s. This temperature marks the transition from Domain I to Domain III$_A$, a domain of exclusive annealing where no self-nucleation takes place. Self-nucleation is detected at 60 °C as indicated by the decrease in the crystallization peak temperature. This corresponds to the transition to Domain III$_{SA}$, where both self-nucleation and annealing take place. Since there is no T_s where only self-nucleation occurs, the Domain II is absent. This behavior is commonly assigned to a crystallization induced by simultaneous nucleation at the interfaces instead of sporadic nucleation from heterogeneities.[5]

The results of the PEO block in the hydrogenated terpolymer, $E_{17}S_{67}EO_{16}$[211] (Figure 7.9), demonstrate no major variations after hydrogenation. Since no shift was observed in the crystallization peak temperature signal, there is no domain where self-nucleation takes place (Domain II or Domain III$_{SA}$). The annealing of the crystals is evident at $T_s = 58$ °C, which is the transition from Domain I or complete melting domain to Domain III$_A$ or annealing domain. As in the non-hydrogenated triblock terpolymer case, the absence of Domain II or self-nucleation domain is evident.

The study of the self-nucleation behavior of the polyethylene block in $E_{17}S_{67}EO_{16}$[211] is presented in Figure 7.10. Similar to the case of the poly(ethylene oxide) block in the same triblock terpolymer, no shift was observed in the crystallization temperature when T_s was decreased. Only the annealing of the crystals could be evidenced, as indicated by the arrow in Figure 7.10b, at $T_s = 96$ °C. These and the previously discussed results are summarized in Figure 7.11. For all the studied cases, transitions from Domain I to Domain III$_A$ where observed. The absence of the self-nucleation domain (Domain II) indicates instantaneous nucleation, which usually is a sign that the crystallization occurs confined into the microphases.[9,16] Based on the morphology determination it can be assumed that isolated PEO or PE/PEO spheres are distributed in the PS matrix and crystallization occurs (almost) exclusively inside them. These results are consistent with the crystallization kinetics results, corresponding to a first order kinetics, i.e., Avrami index close to 1, as was observed in Figure 7.2a.
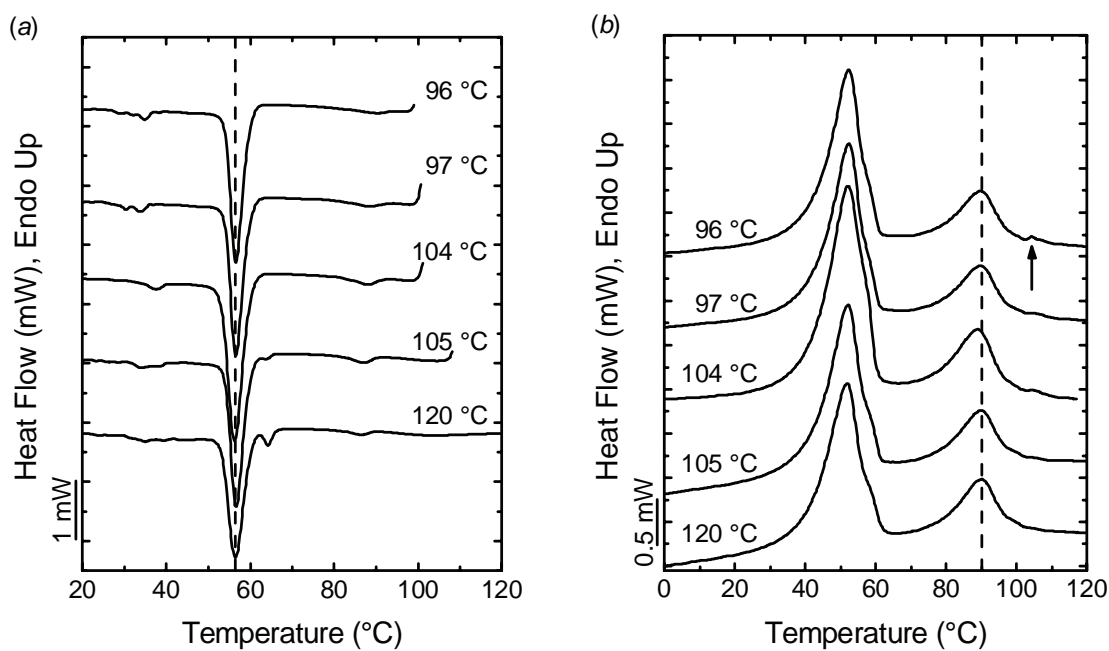
Figure 7.10. Self-nucleation experiments of the PE block in $E_{17}S_{67}EO_{16}^{211}$: a) cooling scans at 10 °C/min after 5 min at indicated T_s, b) subsequent heating scans at 10 °C/min. Arrow indicates melting peak of annealed crystals.
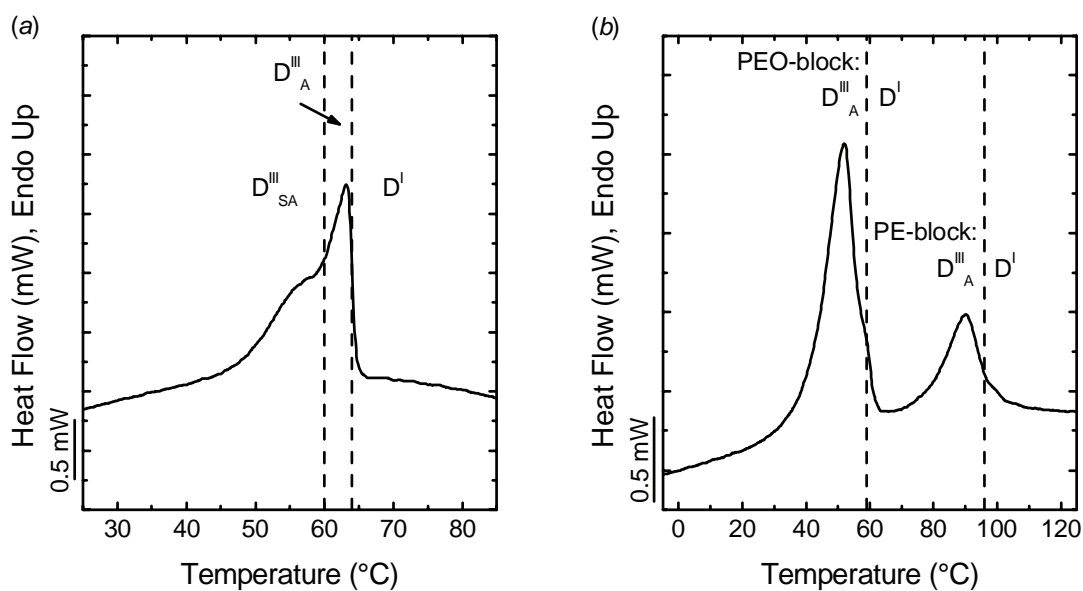

Figure 7.11. Self-nucleation domains definition for PE and PEO blocks in (a) $B_{16}S_{68}EO_{16}^{210}$ and (b) $E_{17}S_{67}EO_{16}^{211}$, represented on the heating scan at 10 °C/min.

7.4.   Conclusions

Due to the wide compositional range and variety of triblock terpolymers in this work, the crystallization kinetics of PEO and PE blocks has been studied as a function of mainly two parameters: microphase geometry and microphase surroundings.   For the case of the microphase geometry, it was found that the crystallization rate decreases with the block content, i.e., from lamellae via cylinders to spheres.   The Avrami index was found to be very similar for lamellae and cylinders, due to the high connectivity among these microdomains.   Avrami indices close to 1 were found for the PEO spheres, indicating first order nucleation controlled kinetics.   These results were consistent with the self-nucleation experiments carried out, where the Domain II was absent for all the blocks forming spheres.

The surroundings were analyzed elaborating different comparisons.   It was found that a second crystalline block as the PE increases the crystallization rate of the PEO block, compared to the amorphous PB.   This leads to the conclusion that PE crystals are a better nucleation surface for PEO than the interfaces with either PB or PS.   However, if the PE block is a direct neighbor of the PEO block, the crystallization rate decreases slightly due to its anchoring effect.   The crystallization rate decreases in soft confinements, which is attributed to a decrease in the segmental alignment to the nuclei caused by the high mobility of the rubbery neighbor block.

The crystallization kinetics of the PE block revealed a high importance of the microphase geometry.   The lowest crystallization rate was found when the PE was the middle block and formed cylinders.   A higher rate was observed for the end block forming cylinders, and a remarkably higher rate was shown for the lamellae forming PE at the end block position.   The effect of restricting the microphase geometry decreases the crystallization rate more than the mobility restrictions given by chain tethering at both ends.   This implies that the

restrictions of the microdomain geometry do not only limit the diffusion phase of crystallization to a higher extent but also affect the nucleation stage of crystallization, since the probability of heterogeneous nucleation decreases with an increase in MD density.

7.5. References

1. Hamley, I. W., *The Physics of Block Copolymers*. Oxford University Press: Oxford, 1998.

2. Zhu, L.; Chen, H.-L.; Calhoun, B. H.; Ge, Q.; Quirk, R. P.; Thomas, E. L.; Hsiao, B. S.; Yeh, F.; Lotz, B. *Polymer* **2001,** 42, 5829-5839.

3. Schmalz, H.; Müller, A. J.; Abetz, V. *Macromolecular Chemistry and Physics* **2003,** 204, 111-124.

4. Sun, L.; Lui, Y.; Zhu, L.; Hsiao, B. S.; Avila-Orta, C. A. *Polymer* **2004,** 2004, 8181-8193.

5. Müller, A. J.; Balsamo, V.; Arnal, M. L. *Advances in Polymer Science* **2005,** 190, 1-63.

6. Schmalz, H.; Böker, A.; Lange, R.; Krausch, G.; Abetz, V. *Macromolecules* **2001,** 34, 8720-8729.

7. Chen, H.-L.; Hsiao, S.-C.; Lin, T.-L.; Yamauchi, K.; Hasegawa, H.; Hashimoto, T. *Macromolecules* **2001,** 34, (4), 671-674.

8. Li, L.; Serero, Y.; Koch, M. H. J.; de Jeu, W. H. *Macromolecules* **2003,** 36, (3), 529-532.

9. Balsamo, V.; Urdaneta, N.; Pérez, L.; Carrizales, P.; Abetz, V.; Müller, A. J. *European Polymer Journal* **2004,** 40, 1033-1049.

10. Müller, A. J.; Balsamo, V.; Arnal, M. L., In *Lecture Notes in Physics: Progress in Understanding of Polymer Crystallization*, Reiter, G.; Strobl, G., Eds. Springer: Berlin, 2007; pp 229-259.

11. Hamley, I. W.; Fairclough, J. P. A.; Bates, F. S.; Ryan, A. J. *Polymer* **1998,** 39, (6-7), 1429-1437.

12. Loo, Y.-L.; Register, R. A., Crystallization within block copolymer mesophases. In *Development in block copolymer science and technology*, Hamley, I. W., Ed. John Wiley & Sons, Ltd: 2004; pp 213-243.

13. Ryan, A. J.; Hamley, I. W.; Bras, W.; Bates, F. S. *Macromolecules* **1995,** 28, 3860-3868.

14. Hamley, I. W. *Advances in Polymer Science* **1999,** 148, 113-137.

15. Loo, Y.-L.; Register, R. A.; Ryan, A. J.; Dee, G. T. *Macromolecules* **2001,** 34, 8968-8977.

16. Loo, Y.-L.; Register, R. A.; Ryan, A. J. *Macromolecules* **2002,** 35, (6), 2365-2374.

17. Müller, A. J.; Balsamo, V.; Arnal, M. L.; Jakob, T.; Schmalz, H.; Abetz, V. *Macromolecules* **2002,** 35, (8), 3048-3058.

18. Floudas, G.; Vazaiou, B.; Schipper, F.; Ulrich, R.; Wiesner, U.; Iatrou, H.; Hadjichristidis, N. *Macromolecules* **2001,** 34, 2947-2957.

19. Rangarajan, P.; Register, R. A.; Adamson, D. H.; Fetters, L. J.; Bras, W.; Naylor, S.; Ryan, A. J. *Macromolecules* **1995,** 28, 1422-1428.

20. Bates, F. S. F., Glenn H. *Physics Today* **1999,** 52, (2), 32-38.

21. Séguéla, R.; Prud'homme, J. *POlymer* **1989,** 30, (8), 1446-1455.

22. Cohen, R. E.; Cheng, P.-L.; Douzinas, K.; Kofinas, P.; Berney, C. V. *Macromolecules* **1990,** 23, 324-327.

23. Sun, L.; Zhu, L.; Ge, Q.; Quirk, R. P.; Xue, C.; Cheng, S. Z. D.; Hsiao, B. S.; Avila-Orta, C. A.; Sics, I.; Cantino, M. E. *Polymer* **2004,** 45, (9), 2931-2939.

24. Zhu, L.; Cheng, S. Z. D.; Huang, P.; Ge, Q.; Quirk, R. P.; Thomas, E. L.; Lotz, B.; Hsiao, B. S.; Yeh, F.; Liu, L. *Advanced Materials* **2002,** 14, (1), 31-34.

25. Zhu, L.; Mimnaugh, B. R.; Ge, Q.; Quirk, R. P.; Cheng, S. Z. D.; Thomas, E. L.; Lotz, B.; Hsiao, B. S.; Yeh, F.; Liu, L. *Polymer* **2001,** 42, 9121-9131.

26. Heck, B.; Hugel, T.; Iijima, M.; Strobl, G. *Polymer* **2000,** 41, 8839-8848.

27. Strobl, G. *The European Physical Journal E - Soft Matter* **2000,** V3, (2), 165-183.

28. Muthukumar, M. *The European Physical Journal E - Soft Matter* **2000,** 3, 199-202.

29. Muthukumar, M.; Welch, P. *Polymer* **2000,** 41, (25), 8833-8837.

30. Schmalz, H.; Abetz, V.; Lange, R.; Soliman, M. *Macromolecules* **2001,** 34, 795-800.

31. Esswein, B.; Molenberg, A.; Möller, M. *Macromol. Symp.* **1996,** 107, (331-340).

32. Esswein, B.; Möller, M. *Angew. Chem.* **1996,** 108, 703-705.

33. Esswein, B.; Steidl, N. M.; Möller, M. *Macromol. Rapid Commun.* **1996,** 17, 143-148.

34. Floudas, G.; Vazaiou, B.; Schipper, F.; Ulrich, R.; Wiesner, U.; Iatrou, H.; Hadjichristidis, N. *Macromolecules* **2001,** 34, 2947-2957.

35. Förster, S.; Krämer, E. *Macromolecules* **1999,** 32, 2783-2785.

36. Fillon, B.; Wittmann, J. C.; Lotz, B.; Thierry, A. *Journal of Polymer Science Part B: Polymer Physics* **1993,** 31, 1383-1393.

37. Lorenzo, A. T.; Arnal, M. L.; Albuerne, J.; Müller, A. J. *Polymer Testing* **2007,** 26, 222-231.

38. Avrami, M. *Journal of Chemical Physics* **1939,** 7, 1103-1112.

39. Avrami, M. *Journal of Chemical Physics* **1940,** 8, 212-224.

40. Avrami, M. *Journal of Chemical Physics* **1941,** 9, 177-184.

41. Lotz, B.; Kovacs, A. J. *Polym Prepr Am Chem Soc Div Polym Chem* **1969,** 10, 820-825.

42. Gedde, U. W., *Polymer Physics*. Chapman & Hall: London, 1995; p 298.

43. Piorkowska, E.; Galeski, A.; Haudin, J.-M. *Progress in Polymer Science* **2006,** 31, (6), 549-575.

44. Mandelkern, L., *Crystallization of Polymers*. 2nd ed.; Cambridge University Press: Cambridge, 2002; Vol. 1, p 550.

45. Opitz, R.; Lambreva, D. M.; de Jeu, W. H. *Macromolecules* **2002,** 35, (18), 6930-6936.

46. Zhang, X.; Wang, Z.; Dong, X.; Wang, D.; Han, C. C. *The Journal of Chemical Physics* **2006,** 125, (2), 024907-10.

47. Schmalz, H.; Knoll, A.; Müller, A. J.; Abetz, V. *Macromolecules* **2002,** 35, (27), 10004-10013.

48. Albuerne, J.; Márquez, L.; Müller, A. J.; Raquez, J. M.; Degée, P.; Dubois, P.; Castelletto, V.; Hamley, I. W. *Macromolecules* **2003,** 36, (5), 1633-1644.

49. Müller, A. J.; Albuerne, J.; Márquez, L.; Raquez, J.-M.; Degée, P.; Dubois, P.; Hobbs, J.; Hamley, I. W. *Faraday Discussions* **2005,** 128, 231-252.

50. Ueda, M.; Sakurai, K.; Okamoto, S.; Lohse, D. J.; MacKnight, W. J.; Shinkai, S.; Sakurai, S.; Nomura, S. *Polymer* **2003,** 44, (22), 6995-7005.

51. Shiomi, T.; Takeshita, H.; Kawaguchi, H.; Nagai, M.; Takenaka, K.; Miya, M. *Macromolecules* **2002,** 35, (21), 8056-8065.

52. Müller, A. J.; Lorenzo, A. T.; Castillo, R. V.; Arnal, M. L.; Boschetti-de-Fierro, A.; Abetz, V. *Macromolecular Symposia* **2007,** submitted.

53. Lorenzo, A. T.; Arnal, M. L.; Müller, A. J.; Boschetti-de-Fierro, A.; Abetz, V. *Macromolecules* **2007,** accepted.
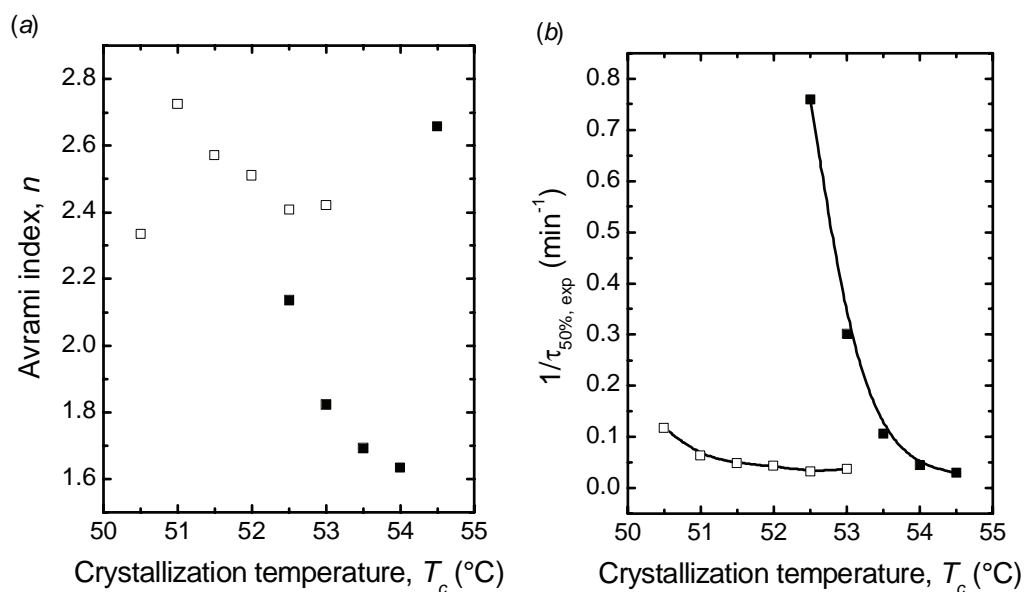
7.6. Appendix

Figure 7.A. Crystallization kinetics parameters for the PEO block in triblock terpolymers before and after hydrogenation of the PB block: $\square$ $B_{16}S_{40}EO_{44}$[143] and $\blacksquare$ $E_{16}S_{40}EO_{44}$[143]. (a) Avrami index, n, as a function of crystallization temperature, (b) Inverse of experimental crystallization half-time as a function of crystallization temperature.
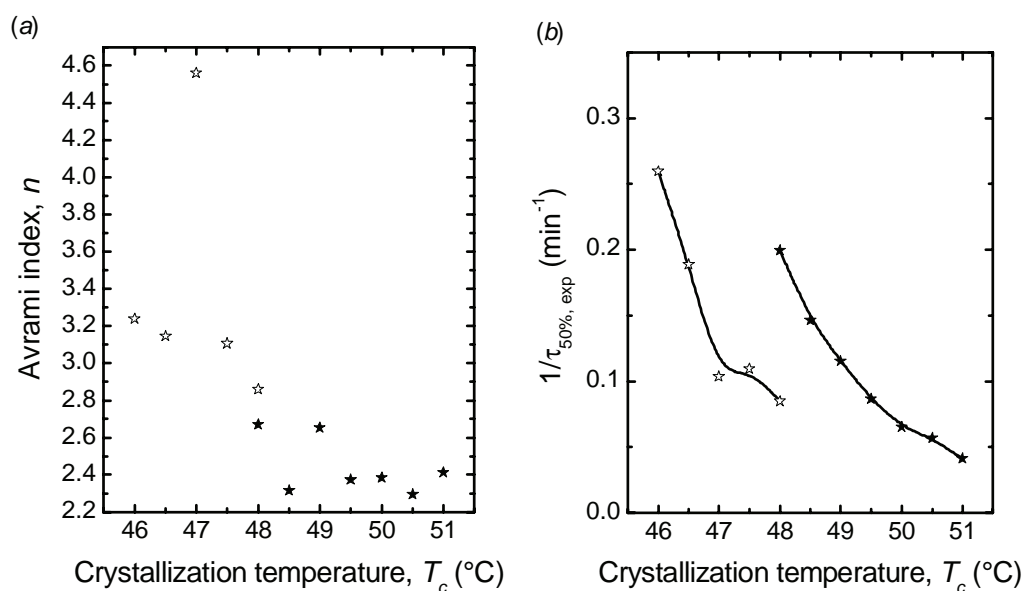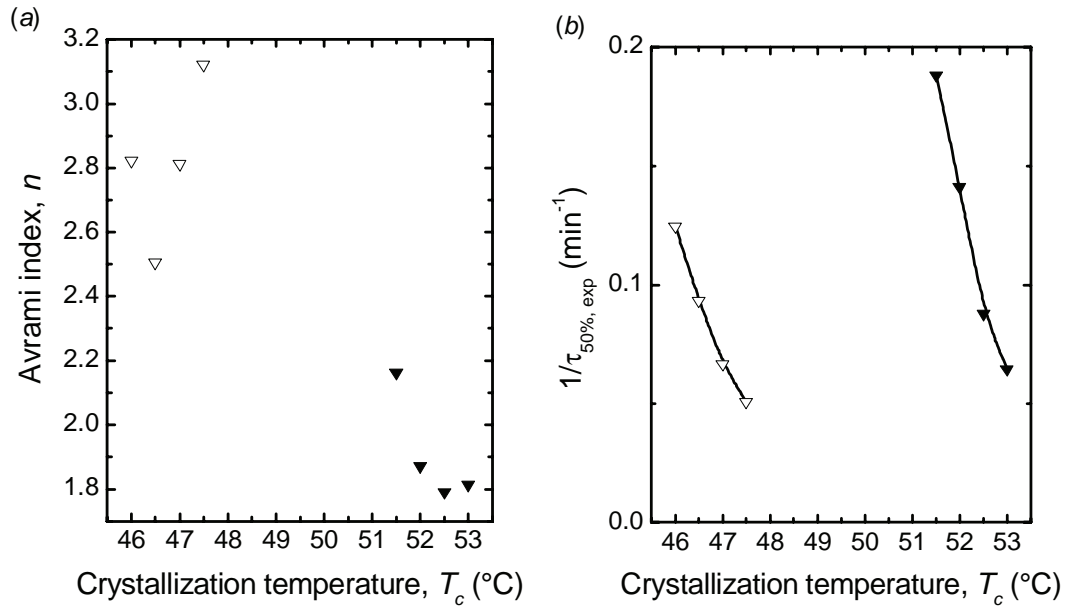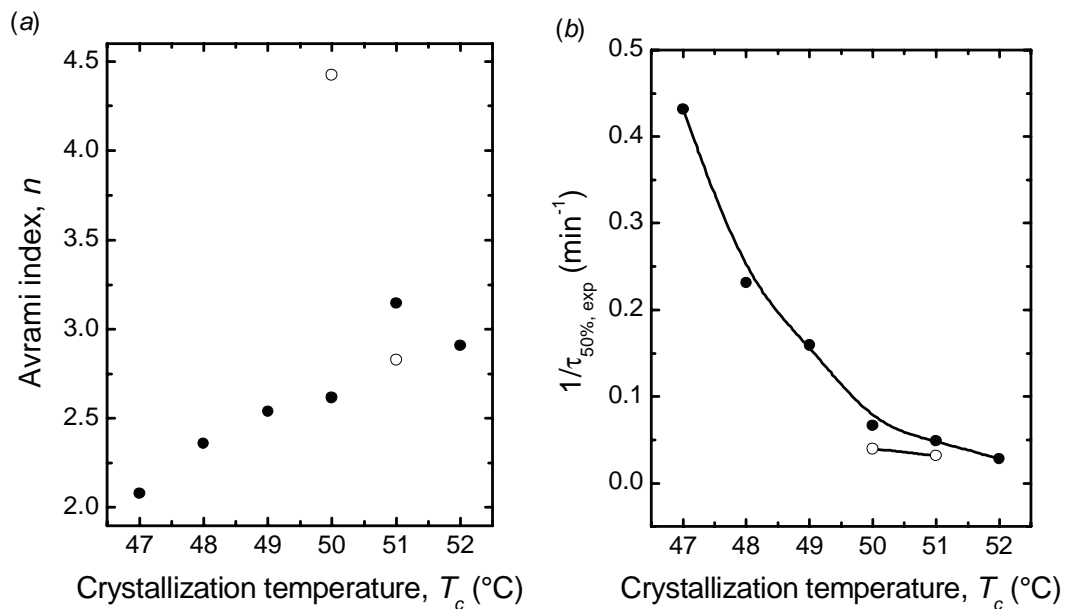

Figure 7.B. Crystallization kinetics parameters for the PEO block in triblock terpolymers before and after hydrogenation of the PB block: $\stackrel{\wedge}{\not\subset}$ $B_{37}S_{16}EO_{47}$[76] and $\bigstar$ $E_{38}S_{16}EO_{46}$[77]. (a) Avrami index, n, as a function of crystallization temperature, (b) Inverse of experimental crystallization half-time as a function of crystallization temperature.

Figure 7.C. Crystallization kinetics parameters for the PEO block in triblock terpolymers before and after hydrogenation of the PB block: $\triangledown$ $S_{43}B_{21}EO_{36}$[111] and $\blacktriangledown$ $S_{43}E_{22}EO_{35}$[112]. (a) Avrami index, n, as a function of crystallization temperature, (b) Inverse of experimental crystallization half-time as a function of crystallization temperature.
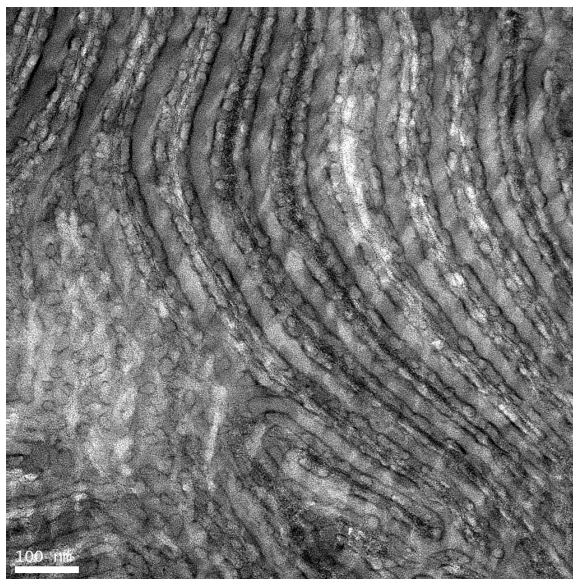

Figure 7.D. Crystallization kinetics parameters for the PEO block in triblock terpolymers before and after hydrogenation of the PB block: $\bigcirc$ $B_{19}I_{39}EO_{42}$[135] and $\bullet$ $E_{19}EP_{40}EO_{41}$[138]. (a) Avrami index, n, as a function of crystallization temperature, (b) Inverse of experimental crystallization half-time as a function of crystallization temperature.

Figure 7.E. TEM micrograph for $S_{43}E_{22}EO_{35}{}^{112}$. Ultrathin sections were obtained from films cast from toluene solutions at 70 °C, and stained with RuO_4 vapor

Chapter 8. Summary

8.1.   Summary

The main motivation of the present work was to study the competition between microphase separation and crystallization in crystallizable block copolymers, as well as to contribute to the understanding of the crystallization process in polymers by following the crystallization kinetics in a confined microphase. For this purpose, sequential living anionic polymerization has been employed in order to synthesize novel polybutadiene-*block*-polystyrene-*block*-poly(ethylene   oxide)   (PB-*b*-PS-*b*-PEO)   linear   triblock terpolymers where the PEO is able to crystallize. Due to the preferential 1,4 addition achieved under the used conditions during the 1,3 butadiene polymerization, the further catalytic hydrogenation lead to polyethylene-*block*-polystyrene-*block*-poly(ethylene oxide) (PE-*b*-PS-*b*-PEO), a triblock terpolymer with two crystallizable blocks.

The morphology in bulk of the different triblock terpolymer compositions was studied by transmission electron microscopy (TEM) and small angle X-ray scattering (SAXS). It was found that the morphologies of non-hydrogenated and hydrogenated pairs did not change in any of the studied compositions but one, a fact that indicated the templating influence of the poly(ethylene oxide) during the sequential microphase separation that takes place during the film formation from solution. Consequently, in hydrogenated triblock terpolymers, the generated morphology was determined by the compromise between the segregation of the poly(ethylene oxide) block and the crystallization of the polyethylene block.

The thermal properties of the triblock terpolymers were effectively compared using a novel approach in order to consider the effect of the molecular weight as well as the influence of the block confinement. This consisted in a 2D map of degree of polymerization vs.

volume fraction, where the thermal properties T_c, T_m and α_c of the PE and PEO blocks were graded with intensity. It was found that low crystallization temperatures are possible for blocks with high molecular weight due to the high segregation strength. The thermal properties of the PE block were found to depend more on the PEO volume fraction than on its own, which confirms the PEO block template effect during the morphology generation. Additionally, bulk morphology was also studied with small angle X-ray scattering under a thermal protocol, in order to further detect the effect of crystallization on the morphology formation. While a non-hydrogenated triblock terpolymer showed lamellar behavior below and above the melting temperature of PEO, its hydrogenated analogue showed a poorly ordered lamellar morphology at room temperature, and a cylindrical morphology is developed upon melting of the PEO block and remains in the molten state. This difference was attributed to a slight increase of the interaction parameters with the PE block compared to those with the PB block, as well as to the composition of the terpolymer, which locates the system very close to the boundary between these two morphologies.

Thin film morphology was investigated by atomic force microscopy (AFM), especially for a hydrogenated triblock terpolymer with low content of the two crystallizable end blocks. The technique allowed imaging of the polymer surface under different conditions, such as after water treatment and during a thermal protocol. The end blocks were found to share spherical domains, which shape and size could be controlled by the film thickness and the thermal history given to the sample.

Crystallization kinetics of both PEO and PE blocks in different triblock terpolymers was studied by differential scanning calorimetry (DSC) using different thermal protocols and the data were fitted to the Avrami equation. The crystallization rate was found to decrease with the content of the crystallizable block, while the Avrami index was found to be very similar for systems with connected morphologies (cylinders and lamellae) and was close to

1 for the system with the lowest content of PEO block. This system was found to have confined domains of the end blocks, both before and after hydrogenation, as determined by self-nucleation experiments. The crystallization rate of the PEO block was found to be increased by a second semicrystalline block (PE), compared to an amorphous block (PB). It was slightly decreased if the crystallizable block (PE) was the middle block instead of the end block. It was also decreased when the confinement was a soft and rubbery poly(ethylene-*alt*-propylene) block (PEP) instead of a glassy block (PS).

The results of the crystallization kinetics of the PE block lead to the conclusion that the geometric restrictions in microdomains do not only affect the diffusion but also the nucleation stage of the crystallization. This was evident because changing from a lamellar to a cylindrical morphology caused a higher decrease in crystallization rate than including mobility restrictions due to changing from end block to the middle block position, where both chain ends are fixed at domain boundaries.

8.2. Zusammenfassung

Die wesentliche Motivation der vorliegenden Arbeit war die Untersuchung des Wechselspiels/Konkurrenz zwischen Mikrophasenseparation und Kristallisation in Blockcopolymeren, sowie einen Beitrag zum Verständnis des Kristallisationsprozesses von Polymeren zu leisten, indem die Kinetik der Kristallisation innerhalb einer räumlich eingeschränkten Mikrophase verfolgt wurde. Neuartige Polybutadien-*block*-Polystyrol-*block*-Polyethylenoxid (PB-*b*-PS-*b*-PEO) Dreiblockterpolymere mit linearer Topologie wurden hierzu mit Hilfe der lebenden anionischen Polymerisation hergestellt. Da unter den gegebenen Bedingungen bei der 1,3-Butadien-Polymerisation vorzugsweise eine 1,4-Verknüpfung erhalten wird, führt die katalytische Hydrierung dieser Makromoleküle zu einem Polyethylen-*block*-Polystyrol-*block*-Polyethylenoxid (PE-*b*-PS-*b*-PEO) Dreiblockterpolymer mit zwei kristallisierbaren Blöcken.

Die Morphologie beider Dreiblocktermopolymere mit unterschiedlichen Zusammensetzungen wurde mit Hilfe der Transmissionselektronenmikroskopie (TEM) und Röntgenkleinwinkelstreuung (SAXS) untersucht. Hierbei stellte sich heraus, dass eine Hydrierung keinen Wechsel der Morphologie gegenüber dem nichthydrierten Polymer verursachte. Dies wurde dahingehend gedeutet, dass während der sequentiellen Mikrophasenseparation aus Lösung die Polyethylenoxid-Phase den Verlauf der anschließenden Phasenbildung diktiert (Templat-Effekt). Im Falle der hydrierten Dreiblockterpolymere resultierte die Morphologie aus dem Wechselspiel zwischen Segregation des Polyethylenoxidblocks und der Kristallisation des Polyethylenblocks.

Die thermischen Eigenschaften der Dreiblockterpolymere wurden mit Hilfe eines neuartigen Ansatzes auf die Abhängigkeit sowohl vom Molekulargewicht als auch von den räumlichen Einschränkungen untersucht. Dies führte zu einer Darstellung, bei welcher der Polymerisationsgrad und der Volumenanteil eine Ebene aufspannen und der die thermischen Eigenschaften T_c, T_m and α_c der PE und PEO Blöcke jeweils mit der Farbintensität in der dritten Dimension korreliert werden. Hierbei offenbarte sich, dass niedrige Kristallisationstemperaturen im Falle von Blöcken mit hohem Molekulargewicht aufgrund starker Segregation gefunden werden. Die thermischen Eigenschaften der PE Blöcke hängen demnach mehr von dem PEO Volumenanteil ab als von ihrem eigenen, was den dirigierenden Effekt des PEOs während der Morphologiebildung bestätigt.

Weiterhin wurde die Festphasen-Morphologie temperaturabhängig mit Röntgenkleinwinkelstreuung untersucht, um weiterhin den Effekt der Kristallisation auf die Morphologie-Bildung zu untersuchen. Während ein nichthydriertes Dreiblockterpolymer sowohl unterhalb als auch oberhalb des Schmelzpunktes von PEO eine lamellare Morphologie aufwies, zeigte das hydrierte Analogon bei niedrigen Temperaturen eine nur schlecht ausgeprägte lamellare Fernordnung, die sich jedoch beim

150

Überschreiten des Schmelzpunktes der PEO-Phase in eine Zylinder-Morphologie umwandelte. Dieser Unterschied kann durch eine geringe Zunahme des Wechselwirkungsparameters mit dem PE-Block gegenüber dem des PB-Blocks und der Tatsache, dass sich das untersuchte System aufgrund der Zusammensetzung nahe an der Phasengrenze beider Morphologien befindet, erklärt werden.

Die Dünnfilm-Morphologie wurde mit Rasterkraftmikroskopie (AFM) für die hydrierten Dreiblockterpolymere mit geringem Anteil an teilkristallinen Endblöcken untersucht. Diese Technik erlaubt die Abbildung von Polymeroberflächen unter verschiedenen Bedingungen, wie zum Beispiel, Vorbehandlung mit Wasser oder in Abhängigkeit von der Temperatur. Die endständigen Blöcke teilen sich hierbei eine sphärische Domäne, deren Form und Größe durch die Filmdicke und die thermische Vorbehandlung der Probe beeinflusst werden können.

Die Kristallisationskinetik der PEO und PE Blöcke der verschiedenen Dreiblockterpolymere wurde mit Hilfe der differentiellen Wärmeflußkalorimetrie (DSC) (verschiedene Verfahrung) untersucht, wobei die Daten nach der Avrami-Gleichung angepasst wurden. Die Geschwindigkeit der Kristallisation nahm mit dem Gehalt des kristallisierbaren Blocks ab, wobei der Avrami-Index eine große Ähnlichkeit zu Systemen, bei denen sich die unterschiedlichen Domänen miteinander verbinden können, aufweist. Bei niedrigem PEO-Gehalt war der Avrami-Index nahe bei 1. Bei dieser Zusammensetzung befanden sich die Endblöcke innerhalb einer räumlich beschränkten Domäne – sowohl vor als auch nach der Hydrierung – wie durch Selbstnukleierungsexperimente nachgewiesen werden konnte. Die Kristallisationsgeschwindigkeit des PEO Blocks wurde durch die Anwesenheit eines zweiten teilkristallinen Blocks (PE) im Vergleich zu einem nichtkristallinen Block (PB) erhöht. Allerdings wurde diese Geschwindigkeit leicht herabgesetzt, falls der

kristallisierbare Block nicht am Ende sondern in der Mitte des Dreiblockterpolymers angeordnet war. Weiterhin führte das Vorliegen eines gummiartigen Blocks wie Poly(ethylen-*alt*-propylen) (PEP) anstelle eines glasartigen Blocks (PS) zu einer verminderten Kristallisationsgeschwindigkeit.

Die Ergebnisse der Kristallisationskinetik des PE Blocks lassen den Schluss zu, dass geometrische Einschränkungen innerhalb der Mikrodomänen den Kristallisationsprozess nicht nur im Diffusions- sondern auch im Nukleierungsstadium beeinflussen. Diese Erkenntnis folgt aus der Beobachtung, dass der Wechsel von einer lamellaren zu einer zylindrischen Morphologie eine stärkere Verlangsamung der Kristallisationsgeschwindigkeit mit sich bringt, als sie durch Mobilitätseinschränkungen aufgrund einer Änderung der Blocksequenz (Endblock wird zum Mittelblock) hervorgerufen werden kann.

Chapter 9. Acknowledgements

List of Publications

1. Lorenzo, A. T., Arnal, M. L., Müller, A. J., Boschetti-de-Fierro, A. and Abetz, V., "High Speed SSA Thermal Fractionation and Limitations to the Determination of Lamellar Sizes and Their Distributions", *Macromolecular Chemistry and Physics* **2006** 207 (1) 39-49.

2. Müller, A. J., Lorenzo, A. T., Arnal, M. L., Boschetti-de-Fierro, A. and Abetz, V., "Self-Nucleation Behavior of the Polyethylene Block as Function of the Confinement Degree in Polyethylene-b-Polystyrene Diblock Copolymers", *Macromolecular Symposia* **2006** 240 (1) 114-122.

3. Lorenzo, A. T., Arnal, M. L., Muller, A. J., Boschetti-de-Fierro, A. and Abetz, V., "Confinement Effects on the Crystallization and SSA Thermal Fractionation of the PE Block within PE-b-PS Diblock Copolymers", *European Polymer Journal* **2006** 42 (3) 516-533.

4. Müller, A. J., Lorenzo, A. T., Castillo, R. V., Arnal, M. L., Boschetti-de-Fierro, A. and Abetz, V., "Crystallization Kinetics of Homogeneous and Melt Segregated PE Containing Diblock Copolymers", *Macromolecular Symposia* **2006** 245/246 154-160.

5. Albuerne, J., Boschetti-de-Fierro, A., Simon, P. F. W. and Abetz, V., "Modification of Polymeric Surfaces for the Improvement of Thermoplastic Composites", *Polymer Preprints (American Chemical Society, Division of Polymer Chemistry)* **2006** 47 (2) 557-558.

6. Boschetti-de-Fierro, A., Müller, A. J. and Abetz, V., "Synthesis and Characterization of Novel Linear PB-b-PS-b-PEO and PE-b-PS-b-PEO Triblock Terpolymers", *Macromolecules* **2007** 40 (4) 1290-1298.

7. Lutter, S., Tiersch, B., Koetz, J., Boschetti-de-Fierro, A. and Abetz, V., "Covalently Closed Microemulsions in Presence of Triblock Terpolymers", *Journal of Colloid and Interface Science* **2007** In Press, Accepted Manuscript.

8. Lorenzo, A. T., Arnal, M. L., Müller, A. J., Boschetti-de-Fierro, A. and Abetz, V., "Nucleation and Isothermal Crystallization of the Polyethylene Block within Diblock Copolymers with Different Segregation Strengths", **2007** submitted.

9. Boschetti-de-Fierro, A., Spindler, L., Reiter, G., Olmos, D., Magonov, S. and Abetz, V., "Thin Film Morphology in Triblock Terpolymers with One and Two Crystallizable Blocks", **2007** submitted.

10. Boschetti-de-Fierro, A., Lorenzo, A. T., Müller, A. J. and Abetz, V., "Crystallization Kinetics of PEO and PE in Different Triblock Terpolymers: Effect of Crystal Geometry and Confinement", **2007** submitted.

11. Boschetti-de-Fierro, A., Fierro, D., Albuerne, J., Funari, S. S. and Abetz, V., "Thermal Monitoring of Morphology in Triblock Terpolymers with Crystallizable Blocks", **2007** submitted.